DISSERTATION

submitted to the

Combined Faculty of Natural Sciences and Mathematics
of Heidelberg University, Germany

for the degree of

Doctor of Natural Sciences

Put forward by

Lukas Corell

born in: Frankenthal (Pfalz)
Oral examination: 30.06.2021

Quantum Dynamics from the
Functional Renormalisation Group
with a Temporal Regulator

Referees: Prof. Dr. Jan Martin Pawlowski
Prof. Dr. Thomas Gasenzer

Quantendynamik mit der funktionalen Renormierungsgruppe unter Verwendung eines zeitlichen Regulators

Diese Arbeit beschäftigt sich mit der Entwicklung einer Methode zur Berechnung der Zeitentwicklung von Korrelationsfunktionen. Dazu werden Verfahren aus der funktionalen Renormierungsgruppe (fRG) verwendet, wobei die Besonderheit ein zeitlicher Regulator ist. Durch diese Wahl werden Quantenfluktuationen basierend auf einer Zeitskala unterdrückt, welche in Kausalitätseigenschaften für Korrelationsfunktionen resultieren. Aufgrund dieser Eigenschaften ist es immer möglich Flussgleichungen analytisch zu integrieren. Insbesondere folgt daraus eine exakte Ein-Loop-Gleichung für den inversen Propagator. Zusätzlich zu diesen formalen Ergebnissen wird die Methode in der ϕ^3-Theorie angewendet, wobei der dynamische Propagator betrachtet wird. Schon in der verwendeten einfachen Trunkierung finden sich Hinweise auf eine selbstähnliche Zeitentwicklung. In einem gesonderten Teil wird die Yang-Mills-Theorie in drei Dimensionen im Gleichgewicht betrachtet. Die vereinfachte Numerik im Vergleich zu Rechnungen außerhalb des Gleichgewichts, ermöglicht es diese Theorie mit Fokus auf unterschiedliche Trunkierungen zu untersuchen. Dabei ist ersichtlich, dass Trunkierungen mit Bedacht gewählt werden müssen, damit unterschiedliche Rechnungen scheinbar konvergieren.

Quantum Dynamics from the Functional Renormalisation Group with a Temporal Regulator

In this work, a framework for the computation of the time evolution of correlation functions is developed. For that purpose, techniques from the functional renormalisation group (fRG) are used, with the unique feature of a temporal regulator. This specific choice of regulator suppresses quantum fluctuations based on a time scale and yields causal properties for correlation functions. As a consequence, flow equations can always be integrated analytically, which in turn allows for the derivation of a one-loop exact functional relation for the inverse propagator. In addition to this formal result, the method is applied to the ϕ^3-theory, where the dynamics of the propagator is investigated. In this setup, the system is prepared far-from-equilibrium and the time evolution of the propagator is computed. Even in the simple truncation that is employed, there are already hints at a self-similar time evolution. In a separate part, three-dimensional Yang-Mills theory is examined in equilibrium. Due to the simpler computation as opposed to non-equilibrium scenarios, it is possible to investigate this theory in view of different truncations. This study reveals that truncations have to be chosen carefully in order to achieve apparent convergence.

Contents

Chapter 1

Introduction

<div style="text-align: right">**1**</div>

The investigation of quantum systems can be approached in a wide variety of ways. In quantum field theory, the probably most naive approach is perturbation theory. Starting from a set of classical propagators and vertices, diagrams for full quantities can be calculated and, therefore, corrections to propagators and vertices are obtained. While the general idea is simple, selecting a consistent set of diagrams is not. Furthermore, not every theory can be described perturbatively across the full energy range. The prime example is quantum chromodynamics (QCD). For low energies, the coupling of the gauge sector, which is described by Yang-Mills theory, becomes too large in order to be used as the parameter of a perturbative expansion. This problem gives rise to the development of non-perturbative methods. Among these methods, there are roughly two categories: lattice quantum field theory and functional methods. In lattice field theory, the problem of computing diagrams is completely eliminated. In its simplest form, correlation functions are computed as the weighted average over field configurations. Consequently, there is no restriction on the order of corrections. This approach, however, only directly works in the imaginary-time formalism, i.e. in Euclidean space, and for zero chemical potential. Otherwise the probabilistic interpretation is not possible. However, more involved methods exist or are in development. Functional methods, on the other hand, rely again on the computation of diagrams. Contrary to perturbation theory, however, those diagrams are not entirely built from classical propagators and vertices. Depending on the method, some or all vertices are fully dressed quantities. Consequently, calculated corrections can include any order of the coupling and, hence, are not perturbative. Functional methods that are relevant in this work are the functional renormalisation group (fRG), Dyson-Schwinger equations (DSEs) and the 2PI effective action formalism. An additional distinction can be made for those methods. While DSEs and the 2PI effective action formalism provide a systematic approximation for n-point functions, they do not encode

any recipe for computations. They just provide a system of coupled equations that have to be solved iteratively. Such a non-linear system strongly depends on the (numeric) initial conditions in order to converge. On the contrary, the fRG is built such that it provides a system of coupled differential equations that allow for the interpolation from an initial action to the effective action. Even though the numerics in the fRG should be more stable, it does not reveal more about the quality of the resulting correlation functions than the other methods. A separate examination using various approximations is necessary.

When it comes to the study of the dynamics of quantum systems, not all of the aforementioned methods are equally suitable. For example, quantum field theory on the lattice heavily relies on Euclidean space. As a consequence, analytic continuation of the results is required in order to obtain real-time properties in Minkowski space. Having said that, functional methods can be formulated in either metric. Hence, they are better candidates for the investigation of quantum dynamics. Admittedly, out-of-equilibrium computations, where the time evolution of correlation functions is of interest, yield additional challenges. Conservation laws, for example, play a crucial role. A violation of conservation laws propagates with time and can cause secularities, which eventually leads to the breakdown of the approach. As a matter of fact, this makes the fRG with a cutoff in momentum space not feasible because such a cutoff modifies local conservation laws. While this is also true in equilibrium, those modifications are well-captured within modified symmetry identities.

1.1. Motivation

The motivation of this work can be divided into a motivation for developing a new method, and the question why to look at quantum dynamics altogether.

For gauge theories, the incentive for a new method is already partly justified above. In that case, an fRG approach in momentum space breaks gauge invariance. In view of avoiding secularities, finding a gauge invariant regularisation is therefore of great interest. In this work, regularisation is achieved by suppressing quantum fluctuations based on a time cutoff. For a local regulator, the action is manifestly gauge invariant.

While this problem motivates the method for gauge theories, this work predominantly deals with scalar field theories. In this context, a major concern is energy conservation. Similarly to the above case, secularities can arise in non-conserving approximations. One way to obtain evidently conserving approximations is to work in the 2PI effective action formalism. However, in

comparison to an fRG approach, only the dynamics of the propagator can be examined. Additionally, non-classical initial conditions are not directly implemented in that approach. Therefore, a system can not be arbitrarily prepared.

The fRG, on the other hand, allows for a wide variety of approximations for all orders of correlation function. This freedom comes at the cost that energy conservation is not apparent. But the locality of flow equations strongly hints at this property. The t-fRG, which is further developed in this work, also allows the inclusion of non-classical initial correlation functions.

Lastly, there also exist approaches like classical statistical simulations or (vertex-resummed) kinetic theory. Although well justified, they suffer from the problem that they are not applicable to the full range of time evolution. They rather only work in overlapping ranges. For example, classical statistical simulations are well suited for high occupation numbers. But since particles are redistributed over time, occupation numbers eventually get too small and quantum corrections have to be included. An approach that is valid for all occupancies and, consequently, for all times, is favourable.

The possibility to compute the time evolution for correlation functions without a restriction on the valid time range, and arbitrary initial conditions, permits the study of out-of-equilibrium scenarios. While a system that is prepared out of equilibrium will inevitably reach equilibrium, two cases can be distinguished. A system close to equilibrium will directly flow towards equilibrium. Regardless of the relaxation time, the dynamics of the system is of little interest. On the other hand, a system far from equilibrium can undergo a very interesting behaviour. Instead of directly flowing to equilibrium, it can reach a so-called non-thermal fixed point. In that regime, the time evolution is describes by self-similar dynamics. The details of a system are essentially forgotten, and time evolution is described by a set of scaling exponents. Seemingly unrelated systems can share the same exponents and, therefore, follow the same dynamics. Consequently, a classification is possible, which leads to far-from-equilibrium universality classes. So far, universality is not investigated that well, which partly fuels the development in this thesis. Another motivation is the theoretical study of heavy ion collisions, where a framework that is capable of describing far-from-equilibrium dynamics for gauge theories is required. In that context, the inclusion of non-classical initial correlators is an extra benefit as it allows for a system to be initially prepared such that it resembles experiments.

1.2. Publications

The compilation of this thesis was performed solely by the author. The results presented throughout the work have been obtained with collaborator, and most of the research is either published or available as preprint. Text and figures that originate from these article are not marked explicitly, but the comments in the following list indicate where they are incorporated in this dissertation.

[1] **Correlation functions of three-dimensional Yang-Mills theory from the FRG**
Lukas Corell, Anton K. Cyrol, Mario Mitter, Jan M. Pawlowski, Nils Strodthoff
Published: SciPost Phys. 5.6 (2018)
DOI: 10.21468/SciPostPhys.5.6.066
E-Print: arXiv:1803.10092 [hep-ph] (2018)
Comment: This article is printed nearly unmodified in chapter 6 and appendix D.

[2] **Flowing with the Temporal Renormalisation Group**
Lukas Corell, Anton K. Cyrol, Markus Heller, Jan M. Pawlowski
E-Print: arXiv:1910.09369 [hep-th] (2019)
Comment: Content from this article is used throughout the thesis, with the results presented in chapter 4 and appendix C.3.

1.3. Outline

This thesis is structured as follows. In chapter 2, the basics required for this work are introduced. This includes an introduction to the Schwinger-Keldysh real-time formalism in section 2.1 as well as a brief discussion of functional methods in section 2.2. The methods include the functional renormalisation group (fRG), Dyson-Schwinger equations (DSEs) and Φ-derivable approximations. The chapter is also used to fix the notation and conventions for the rest of the work.

Chapter 3 is the centrepiece where the method of the temporal functional renormalisation group (t-fRG) is developed. The key aspects of the approach, where the emphasis is on causality, is subsequently showcased in a formal discussion for the inverse propagator. As a unique feature of the t-fRG, an exact one-loop functional relation for the inverse propagator is derived in section 3.5.3. In section 3.6, two possible approaches towards solving time evolution equations are presented. The chapter concludes with a brief discussion in initial conditions and renormalisation in section 3.7.

In chapter 4, the t-fRG is applied in the ϕ^3-theory, where the dynamics of the propagator is considered. Results contain the time evolution of the dispersion relation as well as the occupation number. The latter are further analysed for a self-similar time evolution. As a consistency check, the results are investigated in view of energy conservation. For that purpose an expression for the total energy is derived solely in terms of the propagator in section 4.3.

In chapter 5 a scalar theory with quartic interactions is discussed. The previous considerations of initial conditions and renormalisation are exemplified using the tadpole diagram in section 5.2. It follows the derivation of two different truncations for the dynamical four-point vertex in section 5.3. These include a one-loop vertex correction as well as the s-channel resummation. Lastly, the t-fRG approach is generalised to an N-component scalar field theory in section 5.3.3 where the s-channel resummation leads to a $1/N$ expansion.

In chapter 6, Yang-Mills theory is examined in three space-time dimensions using the fRG. This investigation in equilibrium is completely self-contained and presents truncations that are yet out of reach in the t-fRG approach. The fRG results are compared to results from Dyson-Schwinger equations and the lattice.

Finally, the dissertation is concluded in chapter 7 and possible future applications are discussed.

Appendix A provides the derivation of DSEs in the ϕ^3-theory that are referred to throughout the work. Appendices B and C contain details for dealing with equations on the closed time path, as well as numerical details. In appendix D, details of fRG computations in Yang-Mills theory are provided, including a numerical verification of regulator independence.

In this preliminary chapter, some basics for the understanding of this work are presented. It starts with the introduction of the Schwinger-Keldysh formalism, which serves as the formalism used throughout this thesis. In this context, the closed time path and correlation functions are considered. Subsequently, functional methods that are based on the path integral approach are briefly discussed. Although the essential method for this work is the functional renormalisation group, it is worthwhile to also have a basic knowledge of other frameworks. Since they are not mutually exclusive, they can be simultaneously employed for diagrammatic discussions. For that purpose, Dyson-Schwinger equations and Φ-derivable approximations are presented. The latter is particularly useful for the discussion of conserving approximations.

2.1. Schwinger-Keldysh formalism

In the context of non-equilibrium phenomena, it is instructive to employ a real-time formalism. That way, the occurring time is indeed the physical time and therefore time evolution is most descriptive. Throughout this work, the Schwinger-Keldysh formalism, which was developed in [3–7], is used. In this section, the formalism is introduced in terms of operator expectation values. This approach gives a good intuition concerning the different arising correlation functions. Furthermore, a generating functional for non-equilibrium correlation functions is provided, although a treatment within functional methods, e.g. the functional renormalisation group, is deferred to section 2.2. To further clarify the occurring correlation functions, they are discussed by means of one-point and two-point functions.
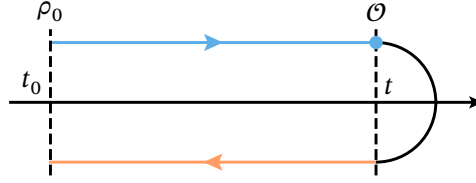
2.1.1. Closed time path

At the heart of the Schwinger-Keldysh formalism lies the concept of a time path that runs from an initial time to a finite or infinite time, and then back again. This path is suitably named *closed time path (CTP)* and is clearly motivated by examining operator expectation values. The computation of operator expectation values requires all information on the state of a quantum system at the time in question. The quantity that does contain all this information is the *density matrix* $\rho(t)$. Usually, the density matrix is known at some initial time t_0 at which the system is prepared. It could very well describe a system in thermal equilibrium, where $\rho_0 = \rho(t_0) \propto e^{-\beta H}$, with the inverse temperature β and the Hamiltonian H. Generally, it describes any system and, in particular, interesting ones far from equilibrium. The time evolution of the density matrix is governed by the *unitary time evolution operator U*. Hence, the density matrix at an arbitrary time is given by

$$\rho(t) = U(t, t_0)\,\rho(t_0)\,U(t_0, t)\,. \tag{2.1}$$

The expectation value of any operator $\mathcal{O}$ at time t is given as the trace over the density matrix at that time and the operator. Utilising the time evolution from equation (2.1) and exploiting the invariance of the trace under cyclic permutations, the expectation value reads

$$\langle \mathcal{O} \rangle(t) = \text{Tr}\left[U(t_0, t)\,\mathcal{O}\,U(t, t_0)\,\rho(t_0) \right]\,. \tag{2.2}$$

This form is very illustrative when reading the argument of the trace from right to left: The initial density matrix is evolved in time from t_0 to t where the operator $\mathcal{O}$ is inserted. Subsequently, there is a time evolution back to the initial time. This operator ordering, which starts and ends at the same time, directly suggests the term *closed time path*. This time path consists of a *forward* and *backward branch*. The time contour is denoted by $\mathcal{C}$ and the forward and backward branches by $\mathcal{C}^+$ and $\mathcal{C}^-$, respectively. A graphical representation of the closed time path for the expectation value of $\mathcal{O}(t)$ is shown in figure 2.1. In the current form, the closed time path runs exactly up to the time of the operator. However, this path can be arbitrarily extended beyond that time by using the unitarity of the time evolution operator. For an extension up to infinity, unity in the form of $U(t, \infty)\,U(\infty, t) = \mathbb{1}$ is inserted into the trace in equation (2.2). Since care has to be taken in view of operator ordering, the next two sections deal with the one-point function and two-point function separately. Understanding the latter directly allows generalisation to higher-order n-point functions.

Figure 2.1. Closed time path for the computation of the time-dependent expectation value of the operator $\mathcal{O}$, see equation (2.2). ρ_0 is the density matrix at the initial time t_0. Note that the time path does not extend further than where the operator is inserted.
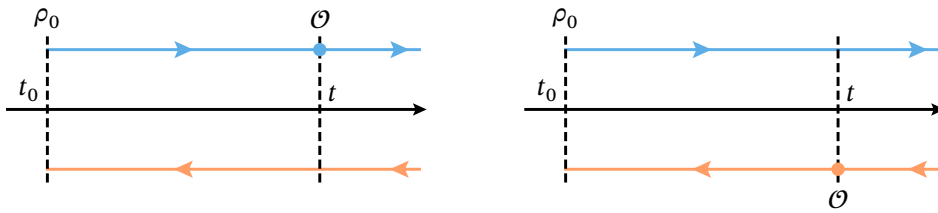
Figure 2.2. Graphical representation of equation (2.3). The closed time path is extended beyond the operator insertion to compute the expectation value of a single operator. The placement of the operator on either branch is equivalent and both diagrams represent the same expectation value.

2.1.2. One-point functions

The extension of the closed time path to infinity for the expectation value of a single operator is straightforward because no care has to be taken with regard to operator ordering. Unity in the form of $U(t, \infty)\, U(\infty, t) = \mathbb{1}$ can be inserted either to the left or the right of the operator in equation (2.2). Visually, these cases correspond to the operator being inserted on the forward and backward branch, respectively, as depicted in figure 2.2. The corresponding equation for the operator insertion on the forward branch is given as

$$\langle \mathcal{O} \rangle(t) = \mathrm{Tr}\left[U(t_0, \infty)\, U(\infty, t)\, \mathcal{O}\, U(t, t_0)\, \rho(t_0) \right]. \tag{2.3}$$

Although there are seemingly two expectation values depending on which branch the operator is located, they are identical. As a consequence, the one-point function is uniquely defined.
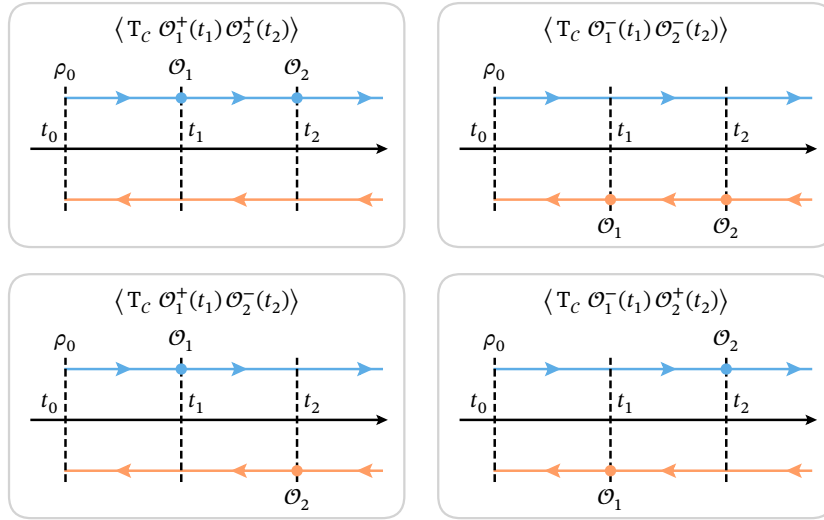
2.1.3. Two-point functions

For two-point functions, i.e. the expectation value of two operators, there is no unique way of extending the closed time path. Given two operators at different or equal times, the extension of the contour could be inserted before, between or after them. Another way to think of this is to first consider the closed time path and then insert the operators. In doing so, it is clear that the placement of the operators is crucial. This is incorporated into the formalism by considering contour-time-ordered correlation functions. This time-ordering on the closed time path is best understood as walking along the path in the direction of the arrow in figure 2.1. Thus, time-ordering on the forward branch is the usual time-ordering, while on the backward branch, it is anti-time-ordering. In particular, this means that every time on the backward part of the contour is considered later than any time on the forward part. The contour-time-ordering operator is denoted by T_C. Just by counting, it is clear that there are four distinct two-point functions. To be specific, both operators can be inserted on the same branch (two possibilities) or each on a different branch (two possibilities), see figure 2.3. If both operators are identical, the two-point functions are related. In section 2.1.4, the relation is clarified for the expectation values of two field operators, that is the propagator. To further clarify the extension of the time contour, it is convenient to mark the operators to indicate if they should be inserted on the forward ($+$) or backward ($-$) branch. Apart from this distinction, the operator itself remains unchanged. As an example, consider the case where both operators are inserted on the forward branch. Given an operator $\mathcal{O}_1$ at time t_1 and $\mathcal{O}_2$ at t_2 with $t_1 < t_2$, the time-ordered expectation value is

$$\left\langle \mathrm{T}_C\, \mathcal{O}_1^+(t_1)\, \mathcal{O}_2^+(t_2) \right\rangle = \mathrm{Tr}\left[U(t_0, \infty)\, U(\infty, t_2)\, \mathcal{O}_2\, U(t_2, t_1)\, \mathcal{O}_1\, U(t_1, t_0)\, \rho(t_0) \right], \quad (2.4)$$

This equation is depicted in the top left panel in figure 2.3. The same figure also shows the remaining three cases, which are obtained analogously. Explicitly writing out those expectation values, it is apparent that the contour-time-ordering as described above is indeed correct. For the sake of brevity, the exemplary correlation function has only been considered for $t_1 < t_2$. In general, a distinction of cases is required, see section 2.1.4.

2.1.4. Propagator

The most ubiquitous two-point function is the propagator, that is the connected part of the contour-time-ordered expectation value of two field operators. It is worthwhile to explicitly work out the propagator in order to find a good

Figure 2.3. Graphical representation of a two-point function where the closed time path is extended beyond both operator insertions. The different placements of the operators lead to four distinct correlation functions.

representation, also in regard to numerical computations, see chapter 4. In section 2.1.2 it was established, that one-point functions are unique and therefore the macroscopic field, i.e. the expectation value of a single field operator φ, reads

$$\phi(x) = \langle \varphi(x) \rangle. \tag{2.5}$$

Due to the uniqueness of the mean field it is irrelevant that the argument is actually on the time contour. This changes for the propagator where four cases are distinguished. It is defined on the closed time path as

$$G(x, y) = \langle T_C \, \varphi(x)\varphi(y) \rangle - \phi(x)\phi(y). \tag{2.6}$$

Previously, operators were marked with '+' and '−' superscripts according to their position on the closed time path. Following this convention, the propagator is denoted similarly. In this notation, the first and second superscript correspond to the first and second argument, respectively. Keeping the contour-time-ordering in mind, the ++-component of the propagator is given as

$$G^{++}(x, y) + \phi(x)\phi(y) = \langle \varphi(x)\varphi(y) \rangle \, \theta(x^0 - y^0) + \langle \varphi(y)\varphi(x) \rangle \, \theta(y^0 - x^0). \tag{2.7}$$

Explicitly writing out the remaining components, it is clear that not all propagators are independent. In fact, only two of them are necessary to express the others. For example, the propagators with arguments on different branches, i.e. G^{+-} and G^{-+}, can be used to express the others. A convenient way is to use linear combinations of G^{+-} and G^{-+} which results in two real functions [8, 9]. The first one is the *spectral function*

$$\rho(x,y) = i\left(G^{-+}(x,y) - G^{+-}(x,y)\right) = i\left\langle\left[\varphi(x),\varphi(y)\right]\right\rangle, \tag{2.8}$$

where $[\cdot,\cdot]$ denotes the commutator, and the second one is the *statistical two-point function* or *statistical propagator*

$$F(x,y) = \frac{1}{2}\left(G^{-+}(x,y) + G^{+-}(x,y)\right) = \frac{1}{2}\left\langle\left\{\varphi(x),\varphi(y)\right\}\right\rangle - \phi(x)\phi(y), \tag{2.9}$$

where $\{\cdot,\cdot\}$ denotes the anti-commutator. Due to the definitions, the spectral function and statistical propagator are odd and even functions, respectively. The former contains the equal-time commutation relations [9]

$$\rho(x,y)\big|_{x^0=y^0} = 0,$$

$$\partial_{x^0}\rho(x,y)\big|_{x^0=y^0} = \delta(\mathbf{x}-\mathbf{y}). \tag{2.10}$$

Inserting the spectral function (2.8) and statistical propagator (2.9) into the propagator (2.7) and the remaining components, reduces the representation to the two degrees of freedom that are necessary out of equilibrium. Yet, the propagators are not defined on the time contour, but rather on the real time axis for one specific case of operator placement. On the closed time path, the propagator can be written as

$$G(x,y) = F(x,y) - \frac{i}{2}\rho(x,y)\,\mathrm{sgn}_C(x^0 - y^0), \tag{2.11}$$

where the contour-sign function sgn_C is introduced. It is defined analogously to the regular sign function, except that the time arguments are considered on the closed time path. This means, with both arguments on the forward branch, it is just the regular sign function, while it has an overall minus sign on the backward branch. In particular, for the first argument on the forward and the second one on the backward branch the function evaluates to -1, and with the arguments swapped to 1. This form of the propagator is particularly useful, since it consists of two real functions that are defined on the real time axis and the only function that is defined on the time contour is the contour-sign function. This simplifies equations, especially those containing integrals over the contour. Some useful identities for integrals on the time contour are derived in appendix B.

2.1.5. Generating functional

After introducing the closed time path, contour-time-ordering and non-equilibrium correlations functions, it is possible to define a generating functional of correlation functions. Although functional methods are covered in section 2.2, providing this functional here concludes the introduction of the Schwinger-Keldysh formalism. Additionally, the form of the generating functional provided here is utilised again in chapter 3.

The only remaining ingredient in order to define a generating functional is the notion of integration along the closed time path. This integration follows again the direction of the time contour as already mentioned for the understanding of contour-time-ordering. Let f be a function defined on the contour, and the functions f^+ and f^- on the real time axis, where the superscripts again indicate where the time argument is placed. The integration can then be written as

$$\int_C \mathrm{d}x^0 \, f(x^0) = \int_{t_0}^{\infty} \mathrm{d}x^0 \left\{ f^+(x^0) - f^-(x^0) \right\}. \tag{2.12}$$

In this notation, the initial time t_0 on the left hand side is understood implicitly as it is typically unambiguous. On the right hand side the sign of the second term stems from the reversed direction of integration on the backward branch. Another notation used throughout this work is the integral that incorporates also spatial dimensions. A general integral over space-time in $1 + d$ dimensions is then denoted by

$$\int_{C(x)} = \int_C \mathrm{d}x^0 \int_{\mathbb{R}^d} \mathrm{d}^d\mathbf{x}. \tag{2.13}$$

With the understanding of the integration along the closed time path, the definition of a generating functional for non-equilibrium correlation functions is straightforward. In its simplest form it contains only a linear source term and can be written as the trace

$$Z[J;\rho] = \mathrm{Tr}\left[\rho(t_0) \, \mathrm{T}_C \exp\left\{ \mathrm{i} \int_{C(x)} \varphi(x) J(x) \right\} \right], \tag{2.14}$$

where J denotes the source and T_C is the contour-time-ordering operator. In this definition, the time contour in the source term extends to infinity. Correlation functions are obtained as functional derivatives with respect to the source

$$\langle \varphi(x_1) \cdots \varphi(x_n) \rangle = (-\mathrm{i})^n \left. \frac{\delta^n Z[J;\rho]}{\delta J(x_1) \cdots \delta J(x_n)} \right|_{J=0}. \tag{2.15}$$

Alternatively, generating functionals can be defined in the path integral formalism. In section 2.2, that approach is used in the context of functional methods.

2.2. Functional methods

So far, the Schwinger-Keldysh formalism was introduced where correlation functions were given as operator expectation values. While this is certainly enough to understand the basics of correlation functions out of equilibrium, computations require a systematic approach on how to approximate them. To achieve this, functional methods are employed in this work, with the focus on the *functional renormalisation group (fRG)* as a basis to develop the framework of the *temporal functional renormalisation group (t-fRG)* in chapter 3. Despite this focus, it is instructive to also look at other functional methods like *Dyson-Schwinger equations* and Φ-*derivable approximations*. In particular, Dyson-Schwinger equations are employed in the computation of the total energy in section 4.3.

2.2.1. Generating functionals

In equation (2.14) a generating functional for contour-time-ordered correlation functions was given in the form of a trace which included a linear source term. Another way for such a functional is given in the path integral approach, see [9]. It is quite similar to the path integral in equilibrium, except that the closed time path has to be considered. In this formalism the generating functional is

$$Z[J,R] = \int_{\varphi^+(t_0)}^{\varphi^-(t_0)} [\mathrm{d}\varphi]\, \exp\left\{ \mathrm{i}\left[S[\varphi] + \int_{C(x)} J(x)\,\varphi(x) + \frac{1}{2}\int_{C(x,y)} \varphi(x)\,R(x,y)\,\varphi(y) \right]\right\}, \quad (2.16)$$

where $S[\varphi]$ denotes the classical action. The measure $[\mathrm{d}\varphi]$ excludes integration over $\mathrm{d}\varphi^{\pm}(t_0)$ which is fixed by the initial conditions, and J and R are linear and bilinear sources, respectively. The usage of exactly those two sources, as opposed to just a linear source term or anything up to an n-linear source term, is merely motivated by what is necessary for this work. Like in the equilibrium case, a generating functional of connected correlation functions with the same dependence on the sources can be defined as

$$W[J,R] = -\mathrm{i}\ln Z[J,R]. \quad (2.17)$$

Before going on with the definition of effective actions, it is instructive to discuss the derivation of correlation functions to fix the notation.

2.2.2. Correlation functions

Contour-time-ordered correlation functions can be derived as functional derivatives of the generating functionals with respect to one of the sources. While utilising the linear source term gives access to any n-point function, derivatives with respect to the bilinear term only allow the derivation of $2m$-point functions with m a positive integer. The first case, for any connected n-point function, reads

$$\langle\varphi(x_1)\cdots\varphi(x_n)\rangle_{J,R}^{\text{conn.}} = (-\mathrm{i})^{n-1}\frac{\delta^n W[J,R]}{\delta J(x_1)\cdots\delta J(x_n)}\,. \tag{2.18}$$

Note that the functional derivatives are not evaluated at vanishing sources. The dependence on the sources is deliberately kept and is indicated by subscripts for clarity. Although it seems tedious to carry the sources as subscripts, it has the advantage to make the derivation of some relations in the next section more apparent. And by introducing the bilinear source term, the flow equation of the one-particle irreducible (1PI) effective action is easily obtained. The source-dependent macroscopic field, i.e. one-point function, is given as

$$\phi_{J,R}(x) \coloneqq \langle\varphi(x)\rangle_{J,R} = \frac{\delta W[J,R]}{\delta J(x)}\,, \tag{2.19}$$

and the propagator, that is the connected two-point function, is

$$G_{J,R}(x,y) \coloneqq \langle\varphi(x)\,\varphi(y)\rangle_{J,R} - \phi_{J,R}(x)\,\phi_{J,R}(y) = -\mathrm{i}\frac{\delta^2 W[J,R]}{\delta J(x)\,\delta J(y)}\,. \tag{2.20}$$

In view of correlation functions derived from functional derivatives with respect to the bilinear source, a general form is not as useful. However, for the propagator, this approach is quite handy. It produces both the connected and disconnected part and the propagator can be defined equivalently as

$$\frac{1}{2}\Big[G_{J,R}(x,y) + \phi_{J,R}(x)\,\phi_{J,R}(y)\Big] \coloneqq \frac{\delta^2 W[J,R]}{\delta R(x,y)}\,. \tag{2.21}$$

Higher-order correlation functions can be derived in a similar way.

2.2.3. Effective actions

In addition to generating functionals for (connected) correlation functions, effective actions are further functionals of great importance. They are the

Legendre transforms of generating functionals of connected correlation functions in the source terms. Most generally, for up to n-linear source terms, the Legendre transform in each source results in the *n-particle irreducible (nPI) effective action*. Since those effective actions have a dependence on up to n-point functions they allow for the derivation of the *quantum equations of motion* for those correlation functions. This section deals exclusively with the 1PI and 2PI effective action. The former is essential in the framework of the functional renormalisation group, see e.g. [10], and will be referred to simply as effective action. The latter is fundamental for Φ-derivable approximations, also known as 2PI effective action formalism, see e.g. [9, 11].

1PI effective action

The effective action Γ, which generates the 1PI correlation functions, is the Legendre transform of equation (2.17) in the linear source. Therefore, it is a functional of the macroscopic field. Also keeping the bilinear source R, the effective action is

$$\Gamma_R[\phi] = W[J_{\phi,R}, R] - \int_{C(x)} \phi(x) J_{\phi,R}(x). \qquad (2.22)$$

The dependence of the source J on both the mean field ϕ and source R is given by the definition of the mean field in equation (2.19). Knowing all dependencies, finding the quantum equation of motion for the macroscopic field is just a matter of applying the chain rule in the variation of the effective action with respect to the macroscopic field

$$\frac{\delta\Gamma_R[\phi]}{\delta\phi(x)} = \int_{C(y)} \frac{\delta W[J_{\phi,R}, R]}{\delta J_{\phi,R}(y)} \frac{\delta J_{\phi,R}(y)}{\delta\phi(x)} - \int_{C(y)} \phi(y) \frac{\delta J_{\phi,R}(y)}{\delta\phi(x)} - J_{\phi,R}(x). \qquad (2.23)$$

The first and second term on the right hand side cancel due to equation (2.19). For non-vanishing sources, the quantum equation of motion is

$$\frac{\delta\Gamma_R[\phi]}{\delta\phi(x)} = -J_{\phi,R}(x). \qquad (2.24)$$

Higher-order functional derivatives of the effective action with respect to the field result in the 1PI n-point functions

$$\Gamma_R^{(n)}[\phi](x_1, \ldots, x_n) = \frac{\delta^n \Gamma_R[\phi]}{\delta\phi(x_1) \cdots \delta\phi(x_n)}. \qquad (2.25)$$

For $n > 2$ those are vertex functions, and the case $n = 2$ should be treated separately. Using the definitions of the 1PI correlation functions (2.25), the propagator (2.20) and the macroscopic field (2.19), as well as the equation of motion (2.24), it follows that the two-point function is related to the propagator by

$$\int_{C(z)} \Gamma_R^{(2)}[\phi](x,z)\, G_R[\phi](z,y) = \mathrm{i}\, \delta_C(x-y)\,. \tag{2.26}$$

Therefore, it is the inverse of the propagator. It is important that in position space this is an integral equation. This inverse problem is further discussed in section 3.6. On the other hand, in momentum space (using time and spatial translation invariance in equilibrium) the 1PI two-point function is just the reciprocal of the propagator. This simpler relation in momentum space is a major advantage for numerical computations. In chapter 6, this is used in the context of the fRG in equilibrium for Yang-Mills theory.

2PI effective action

The 2PI effective action is the Legendre transform with respect to both the linear and bilinear source. Equivalently, it is the Legendre transform of the 1PI effective action (2.22) with respect to the bilinear source

$$\Gamma^{(2\mathrm{PI})}[\phi, G] = \Gamma_R[\phi] - \int_{C(x,y)} \frac{\delta \Gamma_R[\phi]}{\delta R(x,y)}\, R(x,y) \tag{2.27}$$

The functional derivative of the 1PI effective action with respect to the bilinear source can be evaluated by applying the chain rule. It follows

$$\frac{\delta \Gamma_R[\phi]}{\delta R(x,y)} = \frac{\delta W[J_{\phi,R}, R]}{\delta R(x,y)} + \int_{C(z)} \frac{\delta W[J_{\phi,R}, R]}{\delta J_{\phi,R}(z)} \frac{\delta J_{\phi,R}(z)}{\delta R(x,y)} - \int_{C(z)} \phi(z) \frac{\delta J_{\phi,R}(z)}{\delta R(x,y)}\,, \tag{2.28}$$

where the second and third term on the right hand side cancel due to equation (2.19). The first term is the two-point function defined in equation (2.21). Therefore, the 2PI effective action, which is a functional of the macroscopic field and the propagator, is given as

$$\Gamma^{(2\mathrm{PI})}[\phi, G] = \Gamma_R[\phi] - \frac{1}{2} \int_{C(x,y)} \Big[G(x,y) + \phi(x)\, \phi(y) \Big] R(x,y)\,. \tag{2.29}$$

Using equation (2.24), the quantum equations of motion for the macroscopic field and propagator are obtained as

$$\frac{\delta \Gamma^{(2\mathrm{PI})}[\phi, G]}{\delta \phi(x)} = -J(x) - \int_{C(y)} R(x, y) \, \phi(y) \,,$$

$$\frac{\delta \Gamma^{(2\mathrm{PI})}[\phi, G]}{\delta G(x, y)} = -\frac{1}{2} R(x, y) \,. \tag{2.30}$$

As a final remark, it is worthwhile to note that the 2PI effective action coincides with the 1PI effective action if it is evaluated at $G = G_{\mathrm{EoM}}[\phi]$, which is the solution to the equation of motion (2.30) for $R = 0$. For a non-vanishing bilinear source, both effective actions can also be related if the modified effective action (2.31) is considered.

2.2.4. Functional renormalisation group

The central functional method for this work is the functional renormalisation group (fRG). It is based on the *Wilsonian approach to renormalisation* [12], where degrees of freedom are successively integrated-out. The functional approach was developed in [13]. By introducing a scale-dependent bilinear source, the so-called regulator, quantum fluctuations are suppressed depending on the scale. The derivative of the effective action with respect to the scale then leads to a differential equation. This is the *flow equation of the effective action* and allows for the interpolation from some initial action to the full effective action. The shape of the regulator in this equation is not unique, but should rather be chosen to suit the use case. In any case, it has to make sure that all quantum fluctuations at the initial scale are suppressed so that the initial action is just an input. On the other hand, the regulator has to vanish at the final scale. In this work, different regulators are used in the context of the temporal functional renormalisation group in chapter 3 and equilibrium Yang-Mills theory in chapter 6.

In the following, the regulator is denoted by R_s, where s is the introduced scale. All quantities that depend on the regulator are also indicated by the scale. Depending on the problem, it has a different meaning. For example, in equilibrium, a momentum scale is reasonable.

Modified effective action

As already mentioned above, at the initial scale, the regulator has to suppress all quantum fluctuations. For any valid regulator, this means that the scale-

dependent effective action is initially given by the sum of the initial (input) action and the quadratic regulator term. It is then reasonable to define a modified version of the effective action where the regulator term is subtracted. Starting from its definition in equation (2.22), this leads to the modified effective action

$$\Gamma_s[\phi] \to \Gamma_s[\phi] - \frac{1}{2} \int_{C(x,y)} \phi(x) \, R_s(x,y) \, \phi(y) \,. \tag{2.31}$$

Both definitions coincide for a vanishing regulator. This directly leads to a constraint on the regulator shape. At the final scale the regulator has to approach zero. Only then, the flow equation can be used to interpolate towards the full quantum effective action. This modification of the effective action of course impacts some of the properties derived in section 2.2.3. First of all, the relation between the 1PI two-point function and propagator now includes the regulator

$$\int_{C(z)} \left[\Gamma_s^{(2)}[\phi] + R_s \right](x,z) \, G_s[\phi](z,y) = \mathrm{i} \, \delta_C(x-y) \,. \tag{2.32}$$

Secondly, the variation of the modified effective action with respect to the regulator is given by equation (2.28). Also using equation (2.21), the derivative is now just the propagator

$$\frac{\delta \Gamma_s[\phi]}{\delta R_s(x,y)} = \frac{1}{2} G_s[\phi](x,y) \,. \tag{2.33}$$

The second term was cancelled by the modification to the effective action.

Flow equation

The flow equation of the effective action is the partial derivative with respect to the scale. Hence, with an appropriate regulator it allows integrating from some initial condition, e.g. the classical action, to the full effective action. With the modified effective action (2.31) and its variation with respect to the regulator from equation (2.33), the flow equation is

$$\partial_s \Gamma_s[\phi] = \int_{C(x,y)} \frac{\delta \Gamma_s[\phi]}{\delta R_s(x,y)} \partial_s R_s(x,y) = \frac{1}{2} \int_{C(x,y)} G_s[\phi](x,y) \, \partial_s R_s(x,y) \,, \tag{2.34}$$

which is also referred to as the *Wetterich equation* [13]. It has an inherent one-loop structure, as do the flow equations for 1PI n-point functions. The latter are given by functional derivatives with respect to the field as in equation (2.25).

Due to the fact that the Wetterich equation contains a two-point function, i.e. the propagator, on the right hand side, the flow equation for an n-point function depends on up to $(n+2)$-point functions. This leads to an infinite hierarchy of coupled (integro-) differential equations and a truncation has to be applied. Typically, multiple different truncations are required to look for and achieve *apparent convergence*. In chapter 6, this procedure is applied and presented in the context of three-dimensional Yang-Mills theory in equilibrium.

Flow equation in equilibrium

For computations in equilibrium, it is beneficial to formulate the flow equation in momentum space. Since the goal is to integrate-out momentum shells, the scale parameter in the regulator is also a momentum scale and is denoted by k. Using translation invariance in both time and space the flow equation is given as

$$\partial_t \Gamma_k[\phi] = \frac{1}{2} \int_p G_k[\phi](p)\, \partial_t R_k(p)\,.$$ (2.35)

The occurring RG time is defined as $t = \ln(k/k_0)$ for a fixed k_0, which leads to the partial derivative $\partial_t = k\, \partial_k$.

2.2.5. Dyson-Schwinger equations

Another approach to systematically obtain approximations for non-perturbative computations, is the use of Dyson-Schwinger equations, see e.g. [14]. As for the functional renormalisation group, Dyson-Schwinger equations are all derived from one master equation through functional derivatives with respect to the mean field. In this section, this master equation will be briefly derived. One way is to start with a vanishing functional integral, i.e. one where the integrand is a total derivative. In this context, only a linear source term included, and the integral to start with is

$$\int_{\varphi^+(t_0)}^{\varphi^-(t_0)} [\mathrm{d}\varphi] \frac{\delta}{\delta\varphi} \exp\left\{ \mathrm{i} \left[S[\varphi] + \int_{C(x)} J(x)\,\varphi(x) \right] \right\} = 0\,.$$ (2.36)

The functional derivative can be executed and, subsequently, the fields in the functional in front of the exponential function are replaced by derivatives with respect to the source. That way, this functional does not depend on the field

and can be pulled out of the integral. The remaining integral is then just the generating functional $Z[J]$ and the equation becomes

$$\left(\frac{\delta S[\varphi]}{\delta \varphi(x)}\bigg|_{\varphi=-i\frac{\delta}{\delta J}} + J(x)\right) Z[J] = 0 \,. \tag{2.37}$$

After replacing the functional $Z[J]$ by $e^{iW[J]}$ and multiplying its inverse from the left, the equation reads

$$\frac{\delta S[\varphi]}{\delta \varphi(x)}\bigg|_{\varphi=\frac{\delta W[J]}{\delta J}-i\frac{\delta}{\delta J}} = -J(x) \,. \tag{2.38}$$

The functional derivative is now evaluated at $\varphi = \frac{\delta W[J]}{\delta J} - i\frac{\delta}{\delta J}$, where the first term is just the mean field. Since the goal is to derive Dyson-Schwinger equations for 1PI correlation function, the derivative with respect to the source has to be rewritten in terms of the mean field. Exploiting the chain rule for functional derivatives, and using both the definition of the macroscopic field (2.19) and the propagator (2.20), the derivative is

$$-i\frac{\delta}{\delta J(x)} = \int_{C(z)} G(x,z)\frac{\delta}{\delta \phi(z)} = G \cdot \frac{\delta}{\delta \phi} \,. \tag{2.39}$$

In this equation, a condensed notation was introduced on the right hand side. Finally, the source in equation (2.38) is given by the quantum equation of motion (2.24). The result is the Dyson-Schwinger equation for the effective action

$$\frac{\delta \Gamma[\phi]}{\delta \phi(x)} = \frac{\delta S[\varphi]}{\delta \varphi(x)}\bigg|_{\varphi=\phi+G\cdot\frac{\delta}{\delta \phi}} \,. \tag{2.40}$$

Dyson-Schwinger equations for n-point functions are again obtained from the master equation (2.40) as functional derivative with respect to the field. See appendix A for an example in the ϕ^3-theory.

Structure of Dyson-Schwinger equations

To better understand the structure of the master equation, it is convenient to use a vertex expansion of the classical action. For a theory with up to m-point interactions, the expansion can be written as

$$S[\varphi] = \sum_{n=2}^{m} \frac{1}{n!} \int_{C(z_1,\dots,z_n)} S^{(n)}(z_1,\dots,z_n)\,\varphi(z_1)\cdots\varphi(z_n) \,. \tag{2.41}$$

Plugging this expansion into the master equation (2.40), there is a term which is schematically

$$S^{(m)} \times \left[\phi + G \cdot \frac{\delta}{\delta\phi}\right]^{m-2} \times \phi. \qquad (2.42)$$

It is clear that the diagram with the highest order correlation function comes from this term. It contains the most functional derivatives with respect to the mean field, and each increases the order of a correlation function by one. To get the highest n-point function, all functional derivatives have to successively hit the propagator, then the three-point function it generates, and so on. The resulting diagram then has the form

$$S^{(m)} \times G^{m-1} \times \Gamma^{(m-1)}. \qquad (2.43)$$

Therefore it consists of the classical m-point function, and all legs but one are connected with a propagator to the 1PI $(m-1)$-point function. This examination concludes that the Dyson-Schwinger equation for the effective action contains up to $(m-1)$-point functions, where m is given by the highest order tree-level vertex. Furthermore, the Dyson-Schwinger equation for an n-point function includes up to $(n+m-2)$-point functions. Similarly to the flow equations in the fRG, this leads to an infinite tower of coupled equations, and a truncation is necessary. But contrary to the flow equations, Dyson-Schwinger equations in general do not have a one-loop structure.

Self-energy and Dyson equation

The vertex expansion of the classical action (2.41) allows for the derivation of Dyson-Schwinger equations without explicitly specifying the interaction terms. In addition, this expansion reveals that the Dyson-Schwinger equation for any 1PI n-point contains the classical vertex and a set of diagrams

$$\Gamma^{(n)}(x_1, \dots, x_n) = S^{(n)}(x_1, \dots, x_n) + \text{diagrams}. \qquad (2.44)$$

Consequently, Dyson-Schwinger equations relate classical vertices to 1PI vertices. A particularly important DSE is for the inverse propagator. It is also referred to as *gap equation* and reads

$$\Gamma^{(2)}(x_1, x_2) = S^{(2)}(x_1, x_2) - i\Sigma(x_1, x_2), \qquad (2.45)$$

where the *self-energy* Σ is implicitly defined. The self-energy contains all diagrams of the Dyson-Schwinger equation for the inverse propagator, excluding
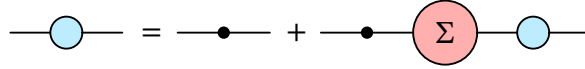
Figure 2.4. Diagrammatic representation of the Dyson equation. The black dot denotes the free propagator and the blue circle the dressed one. The large red circle is the self-energy.

the classical inverse propagator. Using that the 1PI two-point function is the inverse of the full propagator, and analogously for the classical quantities, the equation for the inverse propagator can be transformed to an equation for the propagator

$$G(x_1, x_2) = G_0(x_1, x_2) + \int_{C(z_1, z_2)} G_0(x_1, z_2) \, \Sigma(z_1, z_2) \, G(z_2, x_2). \qquad (2.46)$$

Here, G_0 denotes the free propagator, and the equation is the well-known Dyson equation, see figure 2.4 for a diagrammatic representation. This equation is particularly useful for computations out-of-equilibrium, where the inverse propagator is not simply the reciprocal of the propagator. Essentially, the Dyson series is an alternative way to compute the inverse in a given approximation, that is for a given self-energy.

2.2.6. Φ-derivable approximations

In the last section, the self-energy was defined in the framework of Dyson-Schwinger equations where it is a result of the chosen truncation. Since there is essentially no restriction on how to truncate the set of equations, not all approximations are conserving. This is a crucial aspect regarding non-equilibrium computations where, in particular, energy conservation is of utmost importance. Another approach is to demand a self-energy that ensures a conserving approximation. Symmetry considerations, see e.g. [15], lead to the observation that any self-energy of the form

$$\Sigma[\phi, G](x, y) = 2i \frac{\delta \Phi[\phi, G]}{\delta G(x, y)} \qquad (2.47)$$

is a conserving approximation, as long as the functional Φ obeys the symmetry that corresponds to the conserved quantity. Since the self-energy is a sum of *one-particle irreducible* diagrams, the Φ-functional only contains *two-particle*

irreducible diagrams. This functional constitutes the difference of the full and one-loop 2PI effective action, see e.g. [8, 9, 16]. Up to an irrelevant constant, the 2PI effective action can be written as

$$\Gamma^{(2\mathrm{PI})}[\phi, G] = S[\phi] + \frac{\mathrm{i}}{2} \mathrm{Tr}_C\left\{\ln G^{-1}\right\} + \frac{\mathrm{i}}{2} \mathrm{Tr}_C\left\{G_0[\phi]^{-1} G\right\} + \Phi[\phi, G], \qquad (2.48)$$

where $G_0[\phi]$ denotes the free propagator. Plugging equation (2.48) into the quantum equation of motion (2.30), directly leads to

$$\Gamma^{(2)}(x_1, x_2) = S^{(2)}(x_1, x_2) + R(x_1, x_2) - \mathrm{i}\Sigma(x_1, x_2). \qquad (2.49)$$

Therefore, the self-energy defined here is equivalent to the one in the DSE framework if a modified classical action with $S^{(2)} \to S^{(2)} + R$ is considered.

Temporal functional renormalisation group

This chapter is the centrepiece in view of the formal development of the *temporal functional renormalisation group (t-fRG)*. The method was originally proposed in [17, 18] and is introduced and further developed here. As the name suggests, the underlying framework is the functional renormalisation group (fRG), which has been introduced in section 2.2.4. In the fRG, the general idea is to suppress quantum fluctuations based on some scale, and successively adding them to the computation by moving said scale. In equilibrium, the choice of which fluctuations are suppressed is based on a momentum scale, see chapter 6. In the t-fRG, however, the goal is to obtain the time evolution of correlation functions. This non-equilibrium scenario requires a different kind parameter. The notion of causality, which plays a fundamental role in the t-fRG, dictates that this parameter is a time. In particular, quantum fluctuations are *completely* suppressed after the cutoff time. Time evolution is then governed by moving this cutoff to later times.

The idea of a complete suppression of fluctuations is introduced in two steps. At first, the suppression is implemented solely in terms of a finite closed time path in section 3.1. There, a generating functional of correlation functions is provided, which is a modification to the generating functional on the infinite closed time path from section 2.1. In this approach, properties of the cutoff-dependent correlation functions are directly evident. Subsequently, in section 3.2, an equivalent generating functional based on the path integral and a regulator is given. Implementing the finite closed time path by means of a regulator, allows for the utilisation of techniques from the fRG, ultimately providing the flow equation of the effective action in section 3.3. As causality is so fundamental in this method, it is further discussed in section 3.4. The provided causal properties are then used in section 3.5 to show that flows can

always be integrated analytically. In particular, in section 3.5.3, a one-loop exact functional relation for the propagator is derived. Following this formal discussion, multiple ways are provided on how to obtain time evolution equations in section 3.6. An approach that is inspired by the momentum-space fRG is discarded in favour of two methods that better incorporate causal arguments. Those methods rely heavily on the previous result of integrated flows, and proved feasible in a numeric setup.

The chapter is concluded with the inclusion of non-classical initial conditions into the formalism. The freedom of choosing any reasonable condition is then used to discuss equilibrium initial conditions as well as renormalisation

3.1. Finite closed time path

In the introduction to the Schwinger-Keldysh formalism, the closed time path was intentionally extended to infinity. This has the benefit of a simple notation, e.g. in the generating functional. However, this extension is essentially unity, as is obvious from the construction. In other words, for fixed times it is exactly known how far the contour has to extend. Namely, up to the largest occurring time. Anything after that time is extraneous. This argument can be utilised to analyse the impact of a finite time path on correlation functions. In this scenario, the extent of the contour is fixed to a cutoff time τ, while the time arguments of correlation functions are arbitrary. The generating functional (2.14) is only slightly modified by restricting the integral in the source term to the finite closed time path

$$Z_\tau[J;\rho] = \text{Tr}\left[\rho(t_0)\,\text{T}_C \exp\left\{\text{i}\int_{C(x)<\tau}\varphi(x)\,J(x)\right\}\right]. \tag{3.1}$$

The regularised correlation functions derived from this generating functional inevitably depend on the cutoff time. Despite that, they are still given by functional derivatives

$$\langle\varphi(x_1)\cdots\varphi(x_n)\rangle_\tau = (-\text{i})^n\,\frac{\delta^n Z_\tau[J;\rho]}{\delta J(x_1)\cdots\delta J(x_n)}\bigg|_{J=0}. \tag{3.2}$$

It is important that the dependence on the cutoff is well understood: the cutoff time can be interpreted as a parameter that merely switches correlation functions of the fully interacting theory on and off. As long as all times of the correlation functions are smaller than the cutoff time, the correlation functions
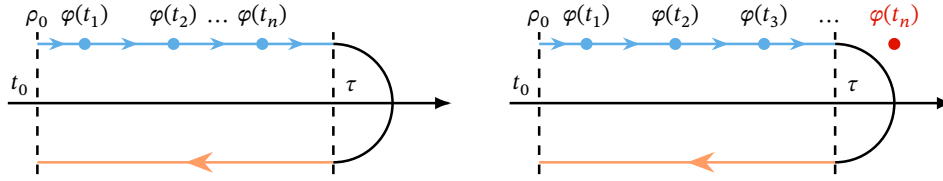
Figure 3.1. Regularised correlation functions. • *Left*: All times are smaller than the cutoff time τ. It is equivalent to the correlation of the fully interacting theory. • *Right*: (At least) one time is larger than the cutoff time τ. Due to causality, it is identically zero.

are equivalent to the ones of the fully interacting theory. The left panel of figure 3.1 illustrates such a scenario. In this case, the regularisation has no impact at all. The remaining cases all contain at least one time that is larger than the cutoff time. Since a functional derivative containing such a time vanishes, the correlation function does as well. The right panel of figure 3.1 represents this case. Therefore, the τ-dependence of the regularised correlation functions boils down to a jump from zero to the full correlation function at the cutoff time. This relation can be summarised as

$$\big\langle \varphi(x_1) \cdots \varphi(x_n) \big\rangle_\tau = \begin{cases} \big\langle \varphi(x_1) \cdots \varphi(x_n) \big\rangle & \text{for } x_1, \dots, x_n < \tau \\ 0 & \text{otherwise.} \end{cases} \tag{3.3}$$

The interpretation of this relation becomes clear by considering the functional in equation (3.1). It only sums over fluctuations up to the cutoff time. Therefore, all information earlier than this time is included and all n-point functions that only have earlier time arguments are full correlation functions. In fact, this is a direct consequence of causality. Likewise, causality entails that quantum fluctuations from the future can not mix with the past. Thinking about the cutoff time as the present, it is obvious that correlation functions with at least one time later than the cutoff time have to vanish identically. The concept of causality and the property of the regularised n-point functions, which are either of the fully interacting theory or vanishing, are key aspects of the temporal functional renormalisation group. In particular, they are indispensable for the analytic integration of flow equations and, correspondingly, the derivation of one-loop exact equations.

3.2. Temporal regulator

Moving the cutoff from an initial to later times, exactly governs the time evolution of correlation functions. In order to implement this moving of the cutoff by the flow equation as it is done in the fRG, it is essential that a suitable regulator is equivalent to the formulation using a finite closed time path. More precisely, the regulator should result in the same property for regularised correlation functions as in equation (3.3). Using the path integral formalism from section 2.2, the generating functional for regularised correlation functions is written as

$$
Z_\tau[J] = \int_{\varphi^+(t_0)}^{\varphi^-(t_0)} [\mathrm{d}\varphi] \, \exp\left\{ \mathrm{i}\left[S[\varphi] + \int_{C(x)} J(x)\,\varphi(x) + \frac{1}{2}\int_{C(x,y)} \varphi(x)\, R_\tau(x,y)\,\varphi(y) \right] \right\}, \quad (3.4)
$$

where the cutoff time is denoted by τ. When looking for an appropriate class of regulators that lead to the given properties, it is directly evident that only *sharp* regulators are suitable. Otherwise, no jump can occur in the correlations functions. Moreover, to achieve that the regularised correlation functions are either zero or the full non-regularised one, it is crucial that the regulator is either *zero* or *infinite*. Regions where the regulator is infinite are necessary to completely suppress all fluctuations and assure causality. On the other hand, zero-values of the regulator ensure that full, i.e. cutoff-independent correlation functions appear in the regularised ones. Any relaxation of one of these constraints directly leads to breaking the given properties. It is clear that these constraints do not uniquely determine the regulator, but rather lead to a class of regulators. Nevertheless, a particularly simple and useful choice is given by the local regulator

$$
-\mathrm{i}R_\tau(x,y) = r(x^0)\,\delta_C(x-y) \tag{3.5}
$$

where r denotes the shape function, which has been chosen to only depend on the time argument. The δ_C-distribution on the closed time path is defined analogously to its counterpart on the real time axis, such that

$$
\int_{C(y)} \delta_C(x-y)f(y) = f(x). \tag{3.6}
$$

This makes the regulator local in both time and space, which is expected to be crucial for gauge theories. The regulator term can only be gauge invariant for a local regulator. In particular, regulators that contain spatial or time derivatives,

which is the case in momentum space, always break gauge invariance. The regulator shape function that is suitable for the local regulator is

$$
r_\tau(x^0) = \begin{cases} \infty & \text{if } x^0 > \tau \\ 0 & \text{otherwise.} \end{cases}
$$
(3.7)

To clarify that this regulator truly acts as intended, it is convenient to consider the functional integral as a sum over all possible field configurations. If such a configuration has support only for times smaller than the cutoff, the regulator term is vanishing. For any other configuration, i.e. ones containing $\varphi(x^0) \neq 0$ for any $x^0 > \tau$, the regulator leads to a vanishing integrand. Therefore, only the former contribute to the functional integral. Introducing the measure $[\mathrm{d}\varphi]_{\mathrm{reg},\tau}$, which only includes the relevant field configurations, the generating functional can also be written as

$$
Z_\tau[J] = \int_{\varphi^+(t_0)}^{\varphi^-(t_0)} [\mathrm{d}\varphi]_{\mathrm{reg},\tau} \, \exp\left\{ \mathrm{i}\left[S[\varphi] + \int_{C(x)<\tau} J(x)\,\varphi(x) \right] \right\}.
$$
(3.8)

where it is sufficient that the integral of the linear source term is limited to times smaller than the cutoff time. Integration beyond that time is vanishing. This form resembles the generating functional given in equation (3.1) and the same arguments hold concerning the properties of regularised correlation functions.

3.3. Flow equation

After establishing, that a properly chosen temporal regulator implements exactly the same suppression of quantum fluctuations as a finite closed time path, the well-known flow equation (2.34) from the fRG can be used. With an adapted notation, this equation reads

$$
\partial_\tau \Gamma_\tau[\phi] = \frac{1}{2} \int_{C(x,y)} G_\tau[\phi](x,y)\,\partial_\tau R_\tau(x,y).
$$
(3.9)

Note that the regulator in the t-fRG has to be regarded as a distribution that has to be regularised in the derivation of the flow equation. Flow equations for 1PI n-point functions are given by functional derivatives with respect to the background field ϕ

$$
\partial_\tau \Gamma_\tau^{(n)}[\phi](x_1,\ldots,x_n) = \frac{\delta^n}{\delta\phi(x_1)\cdots\delta\phi(x_n)} \, \partial_\tau \Gamma_\tau[\phi].
$$
(3.10)

In the derivation of flow equations also appear functional derivatives of the field-dependent propagator. From its relation to the 1PI two-point function, see equation (2.32), follows that the derivative is

$$\frac{\delta}{\delta\phi(y)} G_\tau[\phi](x_1, x_2) = \mathrm{i} \int_{C(z_1, z_2)} G_\tau[\phi](x_1, z_1) \, \Gamma^{(3)}[\phi](z_1, y, z_2) \, G_\tau[\phi](z_2, x_2). \quad (3.11)$$

The structure of the flow equations in the t-fRG do not differ from their fRG-counterpart in momentum space (equilibrium). They lead to an infinite hierarchy of coupled differential equations. Additionally, they share the fact that there is no flow equation for the propagator, but rather the inverse propagator. Therefore, solving the (truncated) set of equations requires to solve an inverse problem. A naive approach, analogously to equilibrium computations, is discussed in section 3.6.1. As it turns out, the aspect of causality and implied properties, allows for a more elegant way to solve these equations. The next sections provide the key results necessary for this approach, which is subsequently discussed in section 3.6.2.

3.4. Causality

The properties of regularised correlation functions that have been discussed so far, are a direct consequence of causality. Since this is an outstanding feature of the temporal regulator, it is further discussed here and additional properties in this framework are established. Causality in view of correlation functions basically expresses that an n-point function does not depend on information later than its latest time argument. Setting the cutoff time to exactly this latest time argument, this reasoning can be directly transferred to the flow equation. The previously introduced regulators, all implement causality. A particular important consequence of the present cutoff procedure, and therefore causality, is that the regularised propagator G_τ is strictly zero if at least one time argument exceeds the cutoff time. In turn, for vanishing or constant backgrounds ϕ_c it is the fully interacting propagator $G \equiv G_{\tau=\infty}$. Consequently the regularised propagator can be written as

$$G_\tau(x, y) = G(x, y) \, \theta(\tau - x^0) \, \theta(\tau - y^0). \quad (3.12)$$

This equation entails the important property that the full propagator for vanishing or constant fields ϕ_c only depends on the full cutoff-independent two-point function $\Gamma^{(2)}[\phi_c]$. The cutoff-independent n-point functions are defined in the

limit where the regulator vanishes. In the t-fRG, this corresponds to $\tau = \infty$. In the following, those correlation functions are denoted without the τ-subscript

$$\Gamma^{(n)}[\phi] \equiv \Gamma^{(n)}_{\tau=\infty}[\phi]. \tag{3.13}$$

The surprising property of equation (3.12) is deeply rooted in the *locality* and *causality* of the present cutoff procedure. Furthermore, it is linked to the functional optimisation of the fRG, compare [10]. There, it has been shown that optimised fRG flows have a related property: for optimal cutoffs, the regulator variation of the two-point function perpendicular to the direction of the optimised flow vanishes: $\delta_\perp \Gamma^{(2)}_k = 0$. The *local* temporal regularisation discussed in the present work shares this property.

A useful alternative representation of equation (3.12) is given by the relation between the propagator and the 1PI two-point function in equation (2.32). However, due to equation (3.12), the occurring two-point function is the cutoff-independent one. Therefore, the propagator can be written as

$$G_\tau(x, y) = \left[\frac{\mathrm{i}}{\Gamma^{(2)} + R_\tau} \right](x, y). \tag{3.14}$$

The causal structure extends to all 1PI n-point functions $\Gamma^{(n)}_\tau$: they are fully dressed as long as all their time arguments are smaller than or equal to τ, and the initial ones otherwise. Hence, $\Gamma^{(n)}_\tau[\phi_c]$ for constant backgrounds ϕ_c with $n \geq 2$ can be written as

$$\Gamma^{(n)}_\tau(x_1, \ldots, x_n) = \Gamma^{(n)}_{t_0}(x_1, \ldots, x_n) + \Delta\Gamma^{(n)}(x_1, \ldots, x_n) \prod_{i=1}^{n} \theta(\tau - x_i^0), \tag{3.15}$$

where $\Delta\Gamma^{(n)}$ constitutes the difference of the full and initial n-point function

$$\Delta\Gamma^{(n)} = \Gamma^{(n)} - \Gamma^{(n)}_{t_0}. \tag{3.16}$$

For more details see appendix B of [18]. This structure of the 1PI n-point functions is preserved by the flow equation and make this approach manifestly causal. Note that the $\Delta\Gamma^{(n)}$ in general contain θ- and δ-distributions and, therefore, are distributions themselves. This intricacy is dealt with for integrated flows in section 3.5, and more explicitly for the dynamic vertex in the ϕ^4-theory in section 5.3.

The causality constraints of the present temporal fRG also lead to another very important identity that is peculiar to this approach. As in any fRG approach, the

τ-derivative of the regulator only appears in the form $G_\tau \cdot \partial_\tau R_\tau \cdot G_\tau$. In the t-fRG, however, for constant background, this term is simply given by the τ-derivative of the propagator

$$\partial_\tau G_\tau(x, y) = \mathrm{i} \int_{C(z_1, z_2)} G_\tau(x, z_1) \, \partial_\tau R_\tau(z_1, z_2) \, G_\tau(z_2, y) \,. \tag{3.17}$$

This identity follows readily from the τ-derivative of equation (3.12) using the representation in equation (3.14). In contrast to standard flows with momentum cutoffs, the term proportional to $\partial_\tau \Gamma_\tau^{(2)}$ is absent. Equation (3.17) has important implications on the general structure of the temporal flow equations and is crucial for the approach.

3.5. Integrated flows

The causality of the flow equation has the remarkable consequence that the time flow can always be integrated analytically. In particular, the properties of the propagator in equation (3.12) and the higher-order 1PI correlation functions in equation (3.15), are indispensable. Additionally, the relation of the τ-derivative of the regulator in equation (3.17) is crucial for the approach. Generally, the flow of any n-point function schematically reads

$$\mathrm{Flow}\left[\Gamma_\tau^{(n)}\right] = \mathrm{Diagrams}\left[\left\{G_\tau, \partial_\tau R_\tau, \Gamma_\tau^{(3)}, \ldots, \Gamma_\tau^{(n+2)}\right\}\right], \tag{3.18}$$

where the right hand side represents a sum of diagrams that are build up from τ-dependent correlation functions and the τ-derivative of the regulator in the set. The causality preserving regulator can be replaced by the τ-derivative of the propagator using equation (3.17), since it always appears in the form $G_\tau \cdot \partial_\tau R_\tau \cdot G_\tau$. Therefore, the regulator is completely eliminated from the flow, which now has the form

$$\mathrm{Flow}\left[\Gamma_\tau^{(n)}\right] = \mathrm{Diagrams}\left[\left\{\partial_\tau G_\tau, G_\tau, \Gamma_\tau^{(3)}, \ldots, \Gamma_\tau^{(n+2)}\right\}\right]. \tag{3.19}$$

At this point, only correlation functions or their τ-derivative appear in the diagrams. The n-point functions can always be split into a τ-independent function and θ-distributions as in equation (3.12) or indicated by equation (3.15). The derivative of the propagator directly follows as

$$\partial_\tau G_\tau(x, y) = G(x, y)\left[\delta(\tau - x^0)\theta(\tau - y^0) + \theta(\tau - x^0)\delta(\tau - y^0)\right]. \tag{3.20}$$

Each diagram now also contains a τ-independent part which consists of the full correlation functions. This part is obviously irrelevant in the τ-integration to obtain the integrated flow. The remaining part consists exclusively of θ- and δ-distributions. Integrating the latter part can always be done analytically and gives a non-trivial prefactor. As a consequence, each diagram and, hence, any flow can be integrated analytically. Keeping initial conditions in mind, the integrated flow can be written as

$$\Gamma^{(n)} = \Gamma^{(n)}_{t_0} + \text{Diagrams}\left[\left\{\#, G, \Gamma^{(3)}, \dots, \Gamma^{(n+2)}\right\}\right], \tag{3.21}$$

where $\#$ denotes the non-trivial prefactor for each individual diagram. The diagrams in this equation have a one-loop structure just like the flow equation. Furthermore, they contain only fully dressed correlation functions. This striking result is only possible due to causality. In momentum space, even a sharp regulator does not result in one-loop equations. An example for this procedure is given within a general discussion for the propagator in section 3.5.3. It is further applied in the context of ϕ^3-theory in chapter 4, and ϕ^4-theory in chapter 5.

3.5.1. Vanishing diagrams

In the process of integrating flow equations, there are certain diagrams that can be argued to be vanishing due to causality by comparing distributions of the external arguments on both sides of the equation. Those are all diagrams that contain n-point functions with $n > 2$ that are either non-local or (partially) local. In the latter case, occurring δ-distributions are not connecting internal and external points. This section provides a clean calculation demonstrating that such diagrams are always zero.

In the flow of any n-point function, there are always multiple diagrams, which only differ in where the regulator is inserted. In the t-fRG, this corresponds to where the τ-derivative of the propagator is. Therefore, the flow equation of any n-point function contains integrals of the form

$$\partial_\tau \Gamma^{(n)}_\tau(x_1, \dots, x_n) = \int_{C(z_1, \dots, z_{2m})} \partial_\tau\big[G_\tau(z_1, z_2)\cdots G_\tau(z_{2m-1}, z_{2m})\big] f_\tau(x_1, \dots x_n; z_1, \dots z_{2m}),$$

$$\tag{3.22}$$

where the positive integer m and f_τ are specific to the diagram. In general, the right hand includes a sum over distinct diagrams. Since the propagators are all internal, their arguments z_i for $i = 1 \dots 2m$ are all integration variables. The

distribution f_τ represents all vertices within a certain diagram. It takes all, both internal and external, points as arguments. It is indeed to be understood as distribution, since it contains δ- and θ-distributions. The local structure of the included correlation functions is crucial, and the following assumption is made.

Assumption: The δ-distributions included in f_τ either have only external or internal points in their argument. Contributions of the form $\delta_C(x_i - z_j)$ for $i = 1 \ldots n$ and $j = 1 \ldots 2m$ are not allowed. That way, (partially) local vertices do not connect internal and external points.

The remaining distributions are θ-distributions to an arbitrary power for every external and internal point, which is an expression of causality. For the internal points, those distributions would only result in an overall factor and are ignored in the following. Without loss of generality, the case without any δ-distribution is used, and the θ-distributions are to the power of one. It is also sufficient to consider external points with $x_1^0 > x_2^0 > \cdots > x_n^0$. Completely separating all distributions leads to

$$\partial_\tau \Gamma_\tau^{(n)}(x_1, \ldots, x_n) \propto \int_{C(z_1, \ldots, z_{2m})} G(z_1, z_2) \cdots G(z_{2m-1}, z_{2m}) f(x_1, \ldots x_n; z_1, \ldots z_{2m})$$
$$\times \left(\prod_{i=1}^{n} \theta(\tau - x_i^0) \right) \partial_\tau \left(\prod_{i=1}^{2m} \theta(\tau - z_i^0) \right), \quad (3.23)$$

where f is understood to be f_τ without the θ-distributions. The aforementioned argument that this integral vanishes, involves comparing distributions on both sides of the equation. On the left hand side, there has to be a term, apart from exponents, that has the form

$$\partial_\tau \left(\prod_{i=1}^{2m} \theta(\tau - x_i^0) \right), \quad (3.24)$$

and therefore contains one δ-distribution. On the right hand side a similar term exists, but is not a derivative with respect to τ. Hence, there is no δ-distribution to match the left hand side. At this point, the assumption that no (partially) local vertex connects intern and external point is crucial. Otherwise the missing δ-distribution could arise. If the distributions on either side of the equation do not match, the only possible solution is a vanishing flow. While this argument is certainly valid, the vanishing of the flow can be shown rigorously. For the sake of a shorter notation, the function

$$I(\mathbf{x}; \mathbf{z}) = G(z_1, z_2) \cdots G(z_{2m-1}, z_{2m}) f(x_1, \ldots x_n; z_1, \ldots z_{2m}) \quad (3.25)$$

contains all functions of the integrand. The time-contour integrals are now denoted by $C(\mathbf{z}) = C(z_1, \dots, z_{2m})$. With the restriction to $x_1^0 > x_2^0 > \cdots > x_n^0$, the integrated flow is obtained by the τ-integration of the flow equation just in the neighbourhood of x_1^0

$$\Gamma^{(n)}(x_1, \dots, x_n) \propto \lim_{\varepsilon \to 0_+} \int_{x_1^0 - \varepsilon}^{x_1^0 + \varepsilon} d\tau \int_{C(\mathbf{z})} I(\mathbf{x}; \mathbf{z}) \left(\prod_{i=1}^{n} \theta(\tau - x_i^0) \right) \partial_\tau \left(\prod_{i=1}^{2m} \theta(\tau - z_i^0) \right).$$

(3.26)

Integration by parts is convenient for the τ-integration. To this end, the part containing a total derivative in the integral is denoted by $\Gamma_A^{(n)}$, and the remaining part by $\Gamma_B^{(n)}$. The integration of the former is straightforward and gives

$$\Gamma_A^{(n)}(x_1, \dots, x_n) = \lim_{\varepsilon \to 0_+} \int_{C(\mathbf{z})} I(\mathbf{x}; \mathbf{z}) \left\{ \left(\prod_{i=1}^{2m} \theta(x_1^0 - x_i^0 + \varepsilon) \right) \left(\prod_{i=1}^{n} \theta(x_1^0 - z_i^0 + \varepsilon) \right) \right.$$

$$\left. - \left(\prod_{i=1}^{2m} \theta(x_1^0 - x_i^0 - \varepsilon) \right) \left(\prod_{i=1}^{n} \theta(x_1^0 - z_i^0 - \varepsilon) \right) \right\}. \quad (3.27)$$

Due to the choice of x_1^0 being the largest external time, the first product of θ-distributions in the first line is unity, the second product just restricts the integrals to times smaller than $x_1^0 + \varepsilon$. In the second line, the first product contains $\theta(x_1^0 - x_1^0 - \varepsilon) = 0$ and therefore the second term is zero. Performing the limit after the integration gives

$$\Gamma_A^{(n)}(x_1, \dots, x_n) = \int_{C(\mathbf{z}) < x_1^0} I(\mathbf{x}; \mathbf{z}).$$

(3.28)

The second term is given by

$$\Gamma_B^{(n)}(x_1, \dots, x_n) = - \lim_{\varepsilon \to 0_+} \int_{x_1 - \epsilon}^{x_1 + \epsilon} d\tau \int_{C(\mathbf{z})} I(\mathbf{x}; \mathbf{z}) \left(\prod_{i=1}^{n} \theta(\tau - z_i^0) \right) \partial_\tau \left(\prod_{i=1}^{2m} \theta(\tau - x_i^0) \right).$$

(3.29)

The τ-derivative leads to a sum of $2m$ terms. Of those terms, only the one where the derivative hits the θ-distribution that has x_1 in its argument has a

contribution. This term is proportional to $\partial_\tau \theta(\tau - x_1^0) = \delta(\tau - x_1^0)$, and after the τ-integration, the remaining product is

$$\prod_{i=2}^{2m} \theta(x_1^0 - x_i^0) = 1 \, . \tag{3.30}$$

If the derivative with respect to τ would have hit any other θ-distribution, this remaining product would have at least one vanishing factor. The θ-distributions with internal points in their argument again restrict the integrals to times smaller than x_1^0, and the result is

$$\Gamma_{\mathrm{B}}^{(n)}(x_1, \dots, x_n) = - \int_{C(\mathbf{z}) < x_1^0} I(\mathbf{x}; \mathbf{z}) \, . \tag{3.31}$$

It is evident, that both parts of the integration differ only by an overall sign and, therefore, the integrated flow vanishes:

$$\Gamma^{(n)}(x_1, \dots, x_n) = \Gamma_{\mathrm{A}}^{(n)}(x_1, \dots, x_n) + \Gamma_{\mathrm{B}}^{(n)}(x_1, \dots, x_n) = 0 \, . \tag{3.32}$$

3.5.2. Non-vanishing diagrams

As soon as there exists at least one partially local vertex in the flow equation where the δ-function connects an internal and external point, the integrated flow can be non-vanishing. In this scenario, it is important that this δ-distribution connects the external point with the latest time to an internal point. Otherwise, the diagram is again vanishing after the τ-integration. For example, assuming that all vertices in total only have this single locality with $\delta_C(x_1 - z_1)$, the integrated flow from equation (3.26) takes the form

$$\Gamma^{(n)}(x_1, \dots, x_n) \propto \lim_{\varepsilon \to 0_+} \int_{x_1^0 - \varepsilon}^{x_1^0 + \varepsilon} \mathrm{d}\tau \int_{C(\tilde{\mathbf{z}})} \tilde{I}(\mathbf{x}; \tilde{\mathbf{z}}) \left(\prod_{i=1}^{n} \theta(\tau - x_i^0) \right)$$
$$\times \partial_\tau \left(\theta(\tau - x_1^0) \prod_{i=2}^{2m} \theta(\tau - z_i^0) \right), \quad (3.33)$$

where $\tilde{\mathbf{z}} = (z_2, \dots, z_{2m})$, x_1^0 is still the largest time, and the integration over z_1 is already performed. Now, the τ-derivative can either hit the δ-distribution with the external point or an internal point. The latter have to vanish due to the

causal structure of the flow. This can be shown similarly to the previous section. Performing the τ-integration by parts, directly leads to

$$\Gamma^{(n)}(x_1, \dots, x_n) \propto \int_{C(\tilde{\mathbf{z}}) < x_1^0} \tilde{I}(\mathbf{x}; \tilde{\mathbf{z}}), \tag{3.34}$$

which is exactly the term where the τ-derivative hits $\theta(\tau - x_1)$. This examination of non-vanishing diagrams is very useful in the application of truncations to flow equations. It allows to identify the non-vanishing parts of diagrams by using causal arguments without explicitly calculating each diagram in full.

3.5.3. Integrated flow for the propagator

Section 3.5.1 showed which kind of diagrams are vanishing in the integration of flow equations which is helpful in analysing the general structure of integrated flows. Here, the integrated flow of the propagator is discussed for general theories, resulting in a one-loop exact functional relation. The starting point for such a discussion is the full, i.e. not truncated, flow of the 1PI two-point function

$$\partial_\tau \Gamma^{(2)}_{\tau, x_1 x_2} = \frac{1}{2} \int_{C(z_1, z_2)} \partial_\tau G_{\tau, z_1 z_2} \, \Gamma^{(4)}_{\tau, z_1 z_2 x_1 x_2} + \frac{i}{2} \int_{C(z_1, \dots, z_4)} \partial_\tau \big[G_{\tau, z_1 z_2} G_{\tau, z_3 z_4} \big] \Gamma^{(3)}_{\tau, x_1 z_2 z_4} \Gamma^{(3)}_{\tau, x_2 z_1 z_3}. \tag{3.35}$$

Here, a condensed notation with space-time arguments as indices, was introduced. This makes the structural aspects of the following arguments more apparent. See figure 3.2 for a diagrammatic representation of the flow equation. Without loss of generality, in the following, this flow is considered for $x_1^0 > x_2^0 > t_0$. The full $\Gamma^{(2)}$ is then obtained from

$$\Gamma^{(2)}(x_1, x_2) = \Gamma^{(2)}_{t_0}(x_1, x_2) + \lim_{\epsilon \to 0_+} \int_{x_1^0 - \epsilon}^{x_1^0 + \epsilon} \partial_\tau \Gamma^{(2)}_\tau(x, y). \tag{3.36}$$

The infinitesimal shift with ϵ has been introduced as the flow is proportional to $\delta(\tau - x_1^0)$. Indeed, due to causality and locality, the flow is only non-vanishing for $\tau = x_1^0$. For $x_2^0 > x_1^0$ the flow is only non-vanishing for $\tau = x_2^0$.

With the knowledge that diagrams containing only non-local vertices are absent in integrated flows, it is worthwhile to split $\Delta\Gamma^{(n)}$ with $n > 2$ from equation (3.16) into a non-local and local part

$$\Delta\Gamma^{(n)}(x_1, \dots, x_n) = \Delta\Gamma^{(n)}_{\text{nl}}(x_1, \dots, x_n) + \Delta\Gamma^{(n)}_{\text{local}}(x_1, \dots, x_n). \tag{3.37}$$

Figure 3.2. Full flow equation for the 1PI two-point function. It only contains correlation functions of the fully interacting theory, that is the propagator (blue circle with solid outline), the three-point function (green circle with dashed outline) and four-point function (pink circle with dotted outline). The τ-derivative of the regulator is represented by the orange square.

Here, all terms containing $\delta_C(x_i - x_j)$ for $i \neq j$ are collected in the local part. However, this notation still hides the fact that both parts can contain additional θ-distributions of the form $\theta(\tau - x_i)$. This intricacy does not play a role in the flow equation itself, but leads to different prefactors when performing the τ-integration. Terms that cause these non-trivial prefactors, have the form

$$\lim_{r \to 0} \theta_r(\tau - x^0)\, \delta_r(\tau - x^0) = \frac{1}{2}\delta(\tau - x^0), \tag{3.38}$$

where the subscript r indicates a general regularisation of the θ- and δ-distributions. Higher powers of θ-distributions can also be included systematically, using

$$\lim_{r \to 0} f\big[\theta_r(\tau - x^0)\big]\, \delta_r(\tau - x^0) = \delta(\tau - x^0) \int_0^1 dx\, f[x]. \tag{3.39}$$

This subtlety can be concealed within the definition of a $*$-product. It is implicitly defined via the example

$$\int_{C(z_1,z_2)<x_1^0} G_{z_1 z_2} * \Gamma^{(4)}_{z_1 z_2 x_2 x_2} = \int_{x_1^0 - \epsilon}^{x_1^0 + \epsilon} d\tau \int_{C(z_1,z_2)} \partial_\tau G_{\tau, z_1 z_2}\, \Gamma^{(4)}_{\tau, z_1 z_2 x_1 x_2}. \tag{3.40}$$

This definition is directly motivated by section 3.5.1. In that section, only the special case with no additional θ-distribution was studied, and therefore, a normal product was sufficient. However, it was shown where the restriction of the time contour to times smaller than x_1^0 on the left hand side stems from.

With the notation settled, the flow from equation (3.35) can be analysed. The first term on the right hand side, the tadpole, only consists of a single vertex.

From previous results, it is evident that only a local vertex contributes to the integrated flow. In general, this is the initial vertex and some partially local contributions that can be generated. The portion of the integrated flow that contains the tadpole is

$$\frac{1}{2} \int\limits_{C(z_1,z_2)<x_1^0} G_{z_1 z_2} \, \Gamma^{(4)}_{t_0,z_1 z_2 x_1 x_2} + \frac{1}{2} \int\limits_{C(z_1,z_2)<x_1^0} G_{z_1 z_2} * \Delta\Gamma^{(4)}_{\text{local},z_1 z_2 x_1 x_2} \,. \tag{3.41}$$

The term involving the initial vertex is a normal product since there is no additional τ-dependence. The remaining term in equation (3.35) contains two three-point vertices. One of those vertices has to be local in order to be non-zero after the τ-integration. Still considering the case $x_1^0 > x_2^0$, the local vertex has to have the argument x_1. Removing the vanishing non-local part leads to the full integrated flow of the two-point function

$$\Gamma^{(2)}_{x_1 x_2} - \Gamma^{(2)}_{t_0,x_1 x_2} = \frac{1}{2} \int\limits_{C(z_1,z_2)<x_1^0} G_{z_1 z_2} \, \Gamma^{(4)}_{t_0,z_1 z_2 x_1 x_2} + \frac{1}{2} \int\limits_{C(z_1,z_2)<x_1^0} G_{z_1 z_2} * \Delta\Gamma^{(4)}_{\text{local},z_1 z_2 x_1 x_2}$$

$$+ \frac{i}{2} \int\limits_{C(z_1,\dots,z_4)<x_1^0} G_{z_1 z_2} G_{z_3 z_4} * \left(\Gamma^{(3)}_{t_0,x_1 z_2 z_4} + \Delta\Gamma^{(3)}_{\text{local},x_1 z_2 z_4} \right) \Gamma^{(3)}_{x_2 z_1 z_3} \,. \tag{3.42}$$

This functional relation is valid for any theory. No assumption about the kind of interactions has been made. Depending on the theory of interest, further simplifications may be possible. The cases of a theory with either pure cubic or quartic interaction are subject of the next two sections.

Cubic interaction

Deriving the one-loop exact equation for a pure ϕ^3-theory is quite easy since there are no local vertices apart from the initial three-point vertex. This can be seen by considering the flow of any n-point function. Initially there is only the three-point function which needs to include the classical vertex and, therefore, has a local part. But since all diagrams in flow equations are one-loop, two points of the three-vertex are always internal and no generated vertex can be local. Hence, it is true that

$$\Delta\Gamma^{(n)}_{\text{local}} \equiv 0 \,, \quad \forall n > 2 \,. \tag{3.43}$$

Figure 3.3. Diagrammatic representation of the gap equation for the inverse propagator in the ϕ^3-theory. The black dots denote classical quantities. The blue (solid outline) and green (dashed outline) circles represent the dressed propagator and three-point function, respectively.

This is a general property of the theory and not the t-fRG. It is also evident by considering perturbative vertex corrections. In particular, the four-point function is non-local, and the tadpole terms in equation (3.42) are zero. For the three-point function, this implies that the local part is completely contained in the initial vertex. The general result for the integrated flow of the 1PI two-point function reduces to

$$\Gamma^{(2)}_{x_1 x_2} - \Gamma^{(2)}_{t_0, x_1 x_2} = \frac{i}{2} \int\limits_{C(z_1,...,z_4) < x_1^0} G_{z_1 z_2} G_{z_3 z_4} \Gamma^{(3)}_{t_0, x_1 z_2 z_4} \Gamma^{(3)}_{x_2 z_1 z_3}, \tag{3.44}$$

where the $*$-product is equivalent to the normal product because $\Gamma^{(3)}_{t_0}$ does not contain any θ-distribution. When using the classical action as initial condition, i.e. $\Gamma^{(n)}_{t_0} = S^{(n)}$, the initial three-point function is

$$S^{(3)}(x_1, x_2, x_3) = -\lambda\, \delta_C(x_1 - x_2)\, \delta_C(x_2 - x_3), \tag{3.45}$$

and the integrated flow reduces to the familiar gap equation

$$\Gamma^{(2)}_{x_1 x_2} - S^{(2)}_{x_1 x_2} = -\frac{i\lambda}{2} \int\limits_{C(z_1,z_2) < x_1^0} G_{z_1 x_1} G_{z_2 x_1} \Gamma^{(3)}_{x_2 z_1 z_2}. \tag{3.46}$$

Figure 3.3 shows a diagrammatic representation of this equation. The derivation is given in appendix A as example for Dyson-Schwinger equations.

Quartic interaction

For a ϕ^4-theory in the symmetric phase, i.e. with $\phi = 0$, there is no three-point vertex. This reduces the integrated flow of the two-point function to only the

tadpole diagram

$$\Gamma^{(2)}_{x_1 x_2} - \Gamma^{(2)}_{t_0, x_1 x_2} = \frac{1}{2} \int_{C(z_1, z_2)} G_{z_1 z_2} \Gamma^{(4)}_{t_0, z_1 z_2 x_1 x_2} + \frac{1}{2} \int_{C(z_1, z_2) < x_1^0} G_{z_1 z_2} * \Delta\Gamma^{(4)}_{\text{local}, z_1 z_2 x_1 x_2}. \quad (3.47)$$

This relation consists of a tadpole diagram with the initial four-point vertex, as well as one with a local four-point vertex. The latter actually contains most of the complexity of this seemingly simple equation. Due to the $*$-product, different parts of the local four-point function can contribute with different prefactors. A general discussion as for the ϕ^3-theory is not possible here, and it is necessary to explicitly consider vertex corrections. Hence, this topic is deferred to section 5.3 where different truncations are examined.

3.6. Time evolution equations

To this point, the only statement about time evolution has been that it is governed by moving the cutoff time from some initial time to the maximal time of interest. Since this is fully described by the flow equations of correlation functions, formally the time evolution is already described. However, it is important to discuss possible implementations. In this section, problems of a naive approach are discussed, as well as two approaches that have been used successfully.

3.6.1. Equilibrium-inspired approach

The naive approach is directly inspired by fRG computations in equilibrium. There, the regulator can be implemented numerically, and the propagator is easily obtained as the reciprocal of the sum of the 1PI two-point function and regulator. In the t-fRG, however, a key aspect is the causality preserving regulator. In section 3.2, two properties of the regulator shape have been discussed. It needs to be sharp, and take on values that are either zero of infinite. Clearly, both of those requirements are not possible to implement numerically. Nevertheless, it is a valid approach to initially relax both requirements and use a regulator shape function of the form

$$r_{\tau, \varepsilon_1, \varepsilon_2}(x^0) = \frac{1}{\varepsilon_2} \theta_{\varepsilon_1}(x^0 - \tau), \quad (3.48)$$

where ε_1 indicates the regularisation of the θ-distribution, and ε_2 accounts for the prefactor, which is infinite in the causal regulator. In a numerical study, the

dependence on the parameters ε_1 and ε_2 could be investigated and, ultimately, the case

$$r_\tau(x^0) = \lim_{\substack{\varepsilon_1 \to 0_+ \\ \varepsilon_2 \to 0_+}} r_{\tau,\varepsilon_1,\varepsilon_2}(x^0) \tag{3.49}$$

may be recovered. Certainly, this approach, poses the problem that causality is broken in any case, potentially leading to secularities. Consequently, numerical computations are not stable. Additionally, since there is no flow equation for the propagator, an inversion of the 1PI two-point functions is required. The inverse problem is an integral equation and brings multiple challenges. Naively, the integral equation

$$\int_{C(z)} \left[\Gamma_\tau^{(2)} + R_\tau \right](x,z) \, G_\tau(z,y) = i \, \delta_C(x-y) \tag{3.50}$$

from equation (2.32) can be discretised. Let the discretised components of the propagator with time arguments fixed on the closed time path be G_τ^{++}, G_τ^{+-}, G_τ^{-+} and G_τ^{--}, and analogously for the inverse propagator and the regulator. To write the integral equation in a compact form, it is convenient to introduce the matrix-valued quantities

$$G_\tau = \begin{pmatrix} G_\tau^{++} & G_\tau^{+-} \\ G_\tau^{-+} & G_\tau^{--} \end{pmatrix}, \quad \Gamma_\tau^{(2)} = \begin{pmatrix} \Gamma_\tau^{(2)++} & \Gamma_\tau^{(2)+-} \\ \Gamma_\tau^{(2)-+} & \Gamma_\tau^{(2)--} \end{pmatrix}, \quad R_\tau = \begin{pmatrix} R_\tau^{++} & R_\tau^{+-} \\ R_\tau^{-+} & R_\tau^{--} \end{pmatrix}. \tag{3.51}$$

Since those quantities are defined on the real time axis, the integral has to be written analogously to equation (2.12). The correct signs are given by inserting the metric

$$\gamma = \gamma^{-1} = \begin{pmatrix} \mathbb{1} & 0 \\ 0 & -\mathbb{1} \end{pmatrix}. \tag{3.52}$$

The δ-distribution on the time contour is also proportional to that metric. Neglecting integration weights, the discretised integral equation can be rearranged to

$$G_\tau \propto i\gamma \left(\Gamma_\tau^{(2)} + R_\tau \right)^{-1} \gamma. \tag{3.53}$$

The problem is therefore broken down to inverting a matrix. However, as for the propagator, the inverse propagator contains redundant information leading to an ill-conditioned matrix. Secondly, it is actually a differential operator and, therefore, initial conditions have to be provided. Ultimately, such an approach introduces unnecessary numerical complexity, and its study is not motivated by physics due to the causality-breaking regulator.

3.6.2. The t-fRG way

Better approaches circumvent both problems. Firstly, the numerical regulator can be completely avoided. Due to the causal properties discussed in section 3.4, and, in particular, the identity (3.17), the regulator drops out of the flow equations. In this scenario, the regulator and its properties are used exactly, and no breaking of causality is introduced numerically. Secondly, the inversion of the 1PI two-point function can be performed using either a differential equation or an integral equation. In the following, both methods are described. At the core of both methods lies the result that flow equations can be integrated analytically. In this context, the integrated inverse propagator is essential. From the decomposition in equation (3.15), it follows that the integrated flow of the 1PI two-point function is

$$-\mathrm{i}\Sigma(x_1, x_2) = \Delta\Gamma^{(2)}(x_1, x_2) = \int_{t_0}^{\infty} \mathrm{d}\tau\, \partial_\tau \Gamma_\tau^{(2)}(x_1, x_2)\,, \qquad (3.54)$$

which has now been defined as the self-energy Σ. Let the initial inverse propagator always be the classical one, i.e. $\Gamma_{t_0}^{(2)} = S^{(0)}$, then the self-energy is consistent to the ones in the context of Dyson-Schwinger equations and Φ-derivable approximations. Integrating the right hand side of equation (3.54) leads to the gap equation

$$\Gamma^{(2)}(x_1, x_2) = S^{(2)}(x_1, x_2) - \mathrm{i}\,\Sigma(x_1, x_2)\,. \qquad (3.55)$$

Note that the restriction of the initial inverse propagator does not rule out a non-classical propagator as initial condition. For the differential equation, the initial propagator is just the initial condition of the equation. In case of the integral equation, it can be included on the level of the gap equation, see section 3.7. On the other hand, the choice leads to a self-energy that is compatible with the definitions in DSEs and Φ-derivable approximations. Consequently, the t-fRG can viewed as a way to systematically derive approximations without actually solving time evolution equations. The self-energy can then be compared to other functional methods and, in particular, 2PI and DSE approximations can be recovered. As a matter of fact, for the ϕ^3-theory the Dyson-Schwinger equation for the inverse propagator was already obtained in the general discussion in section 3.5.3. Likewise, it is shown in chapter 4 that the applied truncation is equivalent to a Φ-derivable approximation. A more involved example for the ϕ^4-theory is presented in section 5.3. While it is interesting and reassuring to recover established approximations, it is more important that those can be

extended by choosing different truncations. Lastly, it is possible to utilise known methods to solve the time evolution equations. In fact, the integral equation is closely related to the non-equilibrium Dyson equation, whereas the differential equation finds applications in the 2PI effective action formalism, see e.g. [9].

Differential equation

Formerly, the fact that the inverse propagator is actually a differential operator was mentioned as a problem of the inverse problem. Then again, by using an explicit form of the classical inverse propagator, a differential equation for the time evolution is given. For that purpose, the classical inverse propagator

$$S^{(2)}(x, y) = -\delta_C(x - y)\left(\partial_{x^0}^2 - \nabla_{\mathbf{x}}^2 + m_0^2\right) \tag{3.56}$$

is inserted into the gap equation (3.55) and, subsequently, the full propagator is multiplied from the right. This leads to a δ-distribution on the left hand side, and after rearranging, the time evolution equation is

$$\left(\partial_{x^0}^2 - \nabla_{\mathbf{x}}^2 + m_0^2\right)G(x, y) = -\mathrm{i}\delta_C(x - y) - \mathrm{i}\int_{C(a)} \Sigma(x, a)\,G(a, y)\,. \tag{3.57}$$

This equation has no constraint on the initial vertices, and the initial propagator is encoded in the initial conditions for the differential equations. In view of numerical implementations, it is useful to work with the spectral function and statistical propagator introduced in section 2.1.4. Additionally, it is reasonable to Fourier transform in the spatial coordinates. For that purpose, spatial translation and rotational invariance is assumed. The time evolution equation for the propagator is then given as a system of coupled differential equations. See appendices B and C for details and, particularly, equation (C.4) for the final result.

Integral equation

The integral equation is obtained similarly to the differential equation. The full propagator is multiplied from the right to equation (3.55). But instead of using the explicit form of the initial inverse propagator, the free propagator G_0 is multiplied from the left. This directly gives the integral equation on the time contour:

$$G(x, y) = G_0(x, y) + \int_{C(a,b)} G_0(x, a)\,\Sigma(a, b)\,G(b, y)\,. \tag{3.58}$$

Since the definition of the self-energy in this context is analogously to the definition in the Dyson-Schwinger equation for the inverse propagator, the time evolution equation for the propagator resembles the Dyson series on the closed time path. Analogously to the differential equation, using the spectral and statistical parts of the propagator in spatial Fourier space results in a set of coupled integral equations. See appendices B and C for details. The final result is given in equation (C.5).

3.7. Initial conditions and renormalisation

An advantage of the t-fRG is the possibility to include non-classical initial correlation functions. As a special case, this includes equilibrium initial conditions, which are discussed in section 3.7.1. In addition, renormalisation can also be understood as an initial value problem when considering necessary counterterms as vertices, which are clearly not present in the classical theory. In the following, time evolution equations in their integrated form are used.

Providing initial vertices, i.e. 1PI n-point functions for $n > 2$, is straightforward and already fully encoded in equation (3.15). For the propagator, initial conditions can be included on the level of the gap equation. For that purpose, let the initial propagator $\overline{G}$ be the solution to the gap equation

$$i\overline{G}^{-1}(x_1, x_2) = S^{(2)}(x_1, x_2) - i\Sigma_{\text{init}}(x_1, x_2). \tag{3.59}$$

This occurring initial self-energy should generally be understood as input rather than a functional that depends on any correlation function. Solving for the initial propagator, leads again to the Dyson equation

$$\overline{G}(x_1, x_2) = G_0(x_1, x_2) + \int_{C(z_1, z_2)} G_0(x_1, z_1)\, \Sigma_{\text{init}}(z_1, z_2)\overline{G}(z_2, x_2), \tag{3.60}$$

where G_0 denotes the free propagator. To use this propagator as initial condition, the gap equation (3.55) can be rewritten by adding and subtracting the initial self-energy, essentially doing nothing. In the form

$$\Gamma^{(2)}(x_1, x_2) = S^{(2)}(x_1, x_2) - i\,\Sigma_{\text{init}}(x_1, x_2) - i\,[\Sigma - \Sigma_{\text{init}}](x_1, x_2), \tag{3.61}$$

it is clear that the first two terms on the right hand side are just the inverse initial propagator according to equation (3.59). Then the time evolution equation for the full propagator reads

$$G(x, y) = \overline{G}(x, y) + \int_{C(a,b)} \overline{G}(x, a)\, [\Sigma - \Sigma_{\text{init}}](a, b)\, G(b, y). \tag{3.62}$$

In summary, initial conditions are provided as $\Gamma_{t_0}^{(n)}$ for $n > 2$, and the pair of consistent $\overline{G}$ and Σ_{init}.

3.7.1. Equilibrium initial conditions

In the context of the t-fRG, and approximations in general, the term equilibrium is always referring to a given approximation. Writing down an initial action in equilibrium therefore involves including all vertices with their respective structure that are allowed in the truncation. For simplicity, let the truncation be chosen such that only the dynamics of the propagator is considered and the flow of vertices is neglected. Furthermore, the initial vertices are the classical ones. This yields a self-energy which is a functional of the full propagator and classical vertices. Since the latter are of no interest here, they are suppressed in the notation. Let the self-energy without arguments denote

$$\Sigma \equiv \Sigma[G], \tag{3.63}$$

which was already implicitly used before. If the system is prepared in equilibrium, the initial self-energy has to obey the truncation and, therefore,

$$\Sigma_{\text{init}} \equiv \Sigma[\overline{G}]. \tag{3.64}$$

As is evident from equation (3.60), the initial propagator depends on the initial self-energy and vice versa. Finding a solution is therefore non-trivial, which is clear since it actually means solving the quantum field theory. Regardless of this inconvenience, let $\overline{G}$ be the equilibrium solution. According to equation (3.62), the time evolution equation is

$$G(x,y) = \overline{G}(x,y) + \int_{C(a,b)} \overline{G}(x,a) \left[\Sigma[G] - \Sigma[\overline{G}]\right](a,b)\, G(b,y). \tag{3.65}$$

The solution to this equation is obviously the initial propagator, i.e. $G = \overline{G}$. Thus, the time evolution equation is compatible with equilibrium initial conditions. Even though this result is may not be all too relevant in view of applications, it verifies that non-classical initial correlation functions are consistently included in the framework. For an example, see the resummed tadpole in quantum mechanics in section 5.2.2.

3.7.2. Renormalisation

The possibility of using arbitrary initial conditions can also be used for renormalisation. In the t-fRG, the idea is particularly simple because all diagrams are

one-loop and the appropriate counterterms for any vertex can be included in the initial action, or in case of the 1PI two-point function in the gap equation. While an in-depth discussion is beyond the scope of this work, a general outline of the procedure is given here for a divergent vertex. For the inverse propagator, see the example of the tadpole in ϕ^4-theory in section 5.2.1.

For the sake of convenience, let the initial action Γ_{t_0} already be renormalised except for one vertex $\Gamma^{(k)}$, where the initial (finite) vertex is denoted by $\Gamma_{t_0}^{(k)}$. In order to renormalise this vertex, it is necessary to include a counterterm into the initial action. The initial action is therefore modified to be

$$\Gamma_{t_0,\text{ren}}[\phi] = \Gamma_{t_0}[\phi] + \int_{C(x_1,\dots,x_k)} \frac{1}{k!} \Delta^{(c)} \Gamma^{(k)} \phi(x_1) \cdots \phi(x_k). \tag{3.66}$$

With this change, equation (3.16) takes the form

$$\Gamma^{(k)} = \Gamma_{t_0}^{(k)} + \Delta^{(c)} \Gamma^{(k)} + \Delta\Gamma^{(k)}, \tag{3.67}$$

where $\Delta\Gamma^{(k)}$ contains both finite and divergent diagrams from the flow equation. It is therefore clear that a counterterm that contains exactly the divergent part leads to a renormalised vertex. At this point, causality is again crucial to the approach. The k-point function also appears in its own flow equation, which essentially leads to vertex corrections that are not one-loop. Consequently, counterterms would be necessary at any loop-order. However, since all correlation functions in the flow of $\Gamma^{(k)}$ are earlier than the external arguments, they are already renormalised. As a consequence, no diagram contains divergent subdiagrams, and renormalisation is indeed performed at one-loop level.

Chapter 4

Dynamics of the ϕ^3-theory

4

In this chapter, the t-fRG approach is implemented for a scalar field theory with cubic interactions in $1 + 1$ dimensions. This theory is an ideal test case for the present approach because it has no divergent diagrams and a simple truncation already gives rise to non-trivial dynamics of the propagator. Moreover, it is also of interest for extending the far-from-equilibrium universality known from ϕ^4-interactions (relativistic and non-relativistic, e.g. [19]) and gauge theories to the ϕ^3-theory. It is also a necessity regarding applications of the t-fRG to non-Abelian gauge theories. Such theories contain cubic interactions already at the classical level. Even though, there, three-point vertices are momentum dependent, they allow for the same scattering processes. Since those scattering processes are absent in the ϕ^4-theory, the insights from cubic interactions are essential in view of non-Abelian gauge theories.

On a more practical note, this chapter serves as a proving ground for the t-fRG. Up until now, the t-fRG was formally developed, and integrated flows were examined in a very general context. Here, an explicit truncation for the ϕ^3-theory is chosen, which gives a more descriptive access to the method.

4.1. Theory and truncation

The setup for any computation within the framework of the (temporal) fRG consists of an initial action and different kinds of approximations. In momentum space, the initial action is mostly chosen as the classical action, whereas in the t-fRG it depends on how the system is prepared at the initial time. The first required approximation is the truncation of the flow equations. In a vertex expansion of the effective action, this accounts for systematically selecting a finite number of vertices, and diagrams of their respective flows. While already reducing the infinite number of coupled differential equations to a finite number,

it might be necessary to approximate the vertex functions itself. For example, in chapter 5 the four-point function is approximated by only the s-channel contribution. In the context of non-Abelian gauge theories it might also be necessary to approximate vertices in terms of allowed tensor structures, see chapter 6. All these approximations have to be done carefully because they fundamentally limit the processes that are considered in the computation. A reasonable truncation keeps all dominant processes and only ignores subleading ones. Finding such a truncation is far from trivial and, in general, various truncations have to be considered when looking for apparent convergence, see section 6.3.1.

4.1.1. Truncation

A sensible starting point for a truncation is to include all vertices that already appear in the initial action. In this numerical study, the initial action is the classical action of the ϕ^3-theory. Therefore, initial vertices correspond to tree-level vertices. The regarded action reads

$$ S[\varphi] = \int_{C(x)} \left\{ \frac{1}{2} \partial^\mu \varphi(x) \partial_\mu \varphi(x) - \frac{m^2}{2} \varphi(x)^2 - \frac{\lambda}{3!} \varphi(x)^3 \right\}. \tag{4.1} $$

At the classical level, this theory contains only cubic interactions. Following the idea of only keeping exactly those kinds of interactions, all flow equations for higher-order correlation functions are neglected. This condition, which is summarised as

$$ \partial_\tau \Gamma_\tau^{(n)}(x_1, \ldots, x_n) = 0, \quad \text{for } n > 3, \tag{4.2} $$

prevents the generation of corrections to those vertices. Since they do not exist at the initial time, this constraint is equivalent to setting those n-point functions to zero. This truncation already reduces the flow of the three-point function to a single diagram, see figure 4.1. An even more restrictive approach is to neglect this diagram, which is equivalent to setting the flow to zero. Similarly to the n-point functions with $n > 3$, this choice prevents corrections to the vertex. However, the three-point function does not vanish, but is fixed to the initial (classical) vertex

$$ \Gamma_\tau^{(3)}(x_1, x_2, x_3) = S^{(3)}(x_1, x_2, x_3) = -\lambda \, \delta_C(x_1 - x_2) \, \delta_C(x_2 - x_3). \tag{4.3} $$

Although, in this setup, the initial action is chosen to be the classical one, the same procedure can be applied for any initial action. The only change

Figure 4.1. Flow equation of the three-point function in the ϕ^3-theory with the truncation from equation (4.2). The green circles with dashed outline denote the three-point function, and the blue circles with solid outline represent the propagator. The τ-derivative of the regulator is depicted by the orange square. 'perm.' refers to permutations of the external leg as well as the insertion of the regulator.

appears in equation (4.3) where the classical three-point function is replaced by an initial three-point function that is given as input. In any case, only the dynamics of the propagator is considered because the flow of the three-point function is still neglected. It is noteworthy that this truncation gives rise to a non-trivial dynamical evolution in the ϕ^3-theory regardless of the initial three-point function. In contradistinction, in the ϕ^4-theory, a non-local, i.e. non-classical, initial four-point function is necessary. Otherwise, the only diagram in the flow of the two-point function is the tadpole diagram with local vertex. This further motivates using the ϕ^3-theory as a test case.

4.1.2. Truncated flow for the propagator

After having established the truncation, it is now possible to turn to the only remaining flow, that is for the 1PI two-point function. For that purpose, the discussed truncation is applied to the full flow equation from section 3.5.3, which was given as

$$\partial_\tau \Gamma^{(2)}_{\tau,x_1 x_2} = \frac{1}{2} \int_{C(z_1,z_2)} \partial_\tau G_{\tau,z_1 z_2} \, \Gamma^{(4)}_{\tau,z_1 z_2 x_1 x_2} + \frac{i}{2} \int_{C(z_1,\dots,z_4)} \partial_\tau \big[G_{\tau,z_1 z_2} G_{\tau,z_3 z_4} \big] \Gamma^{(3)}_{\tau,x_1 z_2 z_4} \, \Gamma^{(3)}_{\tau,x_2 z_1 z_3} \, .$$

$$(4.4)$$

In this equation, the regulator was already replaced using the identity from equation (3.17). The first term on the right hand side completely drops out in this setup, whereas in the second one, the classical vertices are inserted and, subsequently, the integration over internal points is performed. In the last step,

it is important to note that the integration is possible since the δ-distributions in the local vertices do not share the same regularisation as the θ-distributions in the τ-dependent propagator. The latter all originate from the θ-distribution in the regulator, while those in the local vertices are directly given in the initial action. In fact, this statement is true for any local vertex, even those generated via flow equations, because they inherit the locality from the initial vertices. The truncated flow of the two-point function then reads

$$\partial_\tau \Gamma_\tau^{(2)}(x_1 x_2) = \frac{i\lambda^2}{2} \partial_\tau G_\tau^2(x_1 x_2). \tag{4.5}$$

Figure 4.2 shows a graphical representation of this flow. Note that the permutations indicated in said figure are encoded in the τ-derivative in the second term on the right hand side of equation (4.4), as well as in equation (4.5). In the truncated flow with the classical three-point function, this fact is obscured by the symmetry of the vertex. Finally, the integrated flow is easily obtained since the flow is a total τ-derivative. In section 3.6.2, the integrated flow of the 1PI two-point function was defined as the self-energy Σ in equation (3.54). Using this convention, the self-energy reads

$$\Sigma(x_1, x_2) = -\frac{\lambda^2}{2} G^2(x_1, x_2). \tag{4.6}$$

In the present truncation, the self-energy is one-loop, and only depends on the fully dressed propagator. The latter is actually not a feature of the truncation, but the t-fRG itself. As a matter of fact, it is possible to write the self-energy as functional of the propagator in any truncation. For that purpose, the integrated flows of higher-order correlation functions is inserted into the self-energy. As a consequence, the obtained functional is generally of any loop-order but only depends on the propagator. This is a property that is also present in the 2PI effective action formalism. Interestingly, the truncation in this study directly leads to the self-energy that is obtained in the two-loop perturbative 2PI approach. From the definition in equation (2.47), it is clear that the functional

$$\Phi[G] = \frac{i\lambda^2}{12} \int_{C(z_1, z_2)} G^3(z_1, z_2) = \frac{i}{12} \, \ominus\!\!\!-\!\!\!\ominus \tag{4.7}$$

indeed results in the same self-energy. As a consequence, the present truncation is manifestly energy conserving. Since the approximation was not constructed in this respect, this result could hint at truncations in the t-fRG generally being energy conserving. A more ambitious example that results in the same observation is presented in chapter 5 for the ϕ^4-theory.

Figure 4.2. Truncated flow equation of the two-point function. The black dot with three legs denotes the classical vertex $S^{(3)}$, the blue circles with solid outline represent the propagator, and the orange square is the τ-derivative of the regulator. 'perm.' refers to permutations of the external legs.

4.2. Numerical setup

With the theory and truncation fixed, the numerical setup needs to be discussed. In this section, the choice of a suitable representation of the propagator is justified, and subsequently, initial conditions for multiple solvers are provided.

4.2.1. Representation of the propagator

In a numerical study, it is essential to choose the optimal representation for the objects of interest. For the computations in this chapter, the propagator is parameterised as

$$G(x, y) = F(x, y) - \frac{i}{2} \rho(x, y) \, \text{sgn}_C(x^0 - y^0), \tag{4.8}$$

which was introduced in section 2.1.4. The spectral function ρ and the statistical propagator F are defined as the expectation value of the commutator and anti-commutator of two field operators, respectively. This choice is particularly useful because both of those functions are real, and each exhibits a symmetry under the permutation of time arguments. Contrary, the naive approach using the matrix representation with G^{++}, G^{+-}, G^{-+} and G^{--}, involves four complex functions. A direct implementation of the latter representation requires eight times as much memory as the implementation using the spectral function and statistical propagator. Another, even more important, reason are cancellations on the closed time path that occur in time integrals. In the matrix representation, those cancellations have to occur numerically and, therefore, errors accumulate with each time step. On the other hand, those cancellations are explicit in the formulation with the spectral function and statistical propagator, eliminating

one source of numerical errors. For details, see appendix B. Lastly, spatial coordinates are Fourier transformed, see appendix C.

4.2.2. Initial conditions

In case of using the integral equation (3.58), the initial conditions are encoded in the solution of the Dyson equation for the initial propagator $\bar{G}$. For a free theory at initial time, which is regarded here, it is just the solution to the free equation of motion. In terms of the spectral function and the statistical propagator, this solution can be written as

$$\bar{F}(t, t'; \mathbf{p}) = \frac{1}{\omega_{\mathbf{p}}} \left(\frac{1}{2} + f_0(\mathbf{p}) \right) \cos \left[\omega_{\mathbf{p}}(t - t') \right],$$

$$\bar{\rho}(t, t'; \mathbf{p}) = \frac{1}{\omega_{\mathbf{p}}} \sin \left[\omega_{\mathbf{p}}(t - t') \right], \tag{4.9}$$

where $f_0(\mathbf{p})$ denotes the initial occupation number. The initial occupation number can be considered as a free parameter that needs to be additionally fixed for a particular preparation of the system. On the other hand, the dispersion relation at initial time $\omega_{\mathbf{p}}^2 = \mathbf{p}^2 + m_0^2$ is fixed by the initial (bare) mass. For the differential equation approach from equation (3.57), initial values have to be provided for F and ρ, as well as their first derivatives at the initial time. Those values can be readily obtained from the free propagator (4.9).

For the results presented in this chapter, the initial occupation number is chosen such that momentum modes below the initial mass are evenly occupied, otherwise the occupation number vanishes. It is parameterised as

$$f_0(\mathbf{p}) = \frac{\widetilde{N}}{\widetilde{\lambda}} \, \theta(m_0 - |\mathbf{p}|), \tag{4.10}$$

where the prefactor determines the total particle number and hence the total energy. In this study $\widetilde{N} = 100$ is chosen, and the dimensionless coupling of the three-point function is given by $\widetilde{\lambda} = \lambda/m_0^2 = 0.01$.

4.3. Total energy

Since the truncation in this numerical study is equivalent to a Φ-derivable approximation, the total energy is evidently conserved. In order to verify this statement numerically, it is necessary to work out the appropriate expression

for the energy in the given truncation. In this particular case, it is possible to utilise the Dyson-Schwinger equation of the inverse propagator to express the energy solely in terms of the propagator.

The total energy is given by $\langle T_{00} \rangle$, that is the 00-component of the expectation value of the energy-momentum tensor. In general, the expectation value of the energy-momentum tensor is obtained from the effective action as

$$\langle T_{\mu\nu}(x) \rangle = \frac{2}{\sqrt{-g(x)}} \frac{\delta \Gamma[\phi, g]}{\delta g^{\mu\nu}(x)} \bigg|_{g^{\mu\nu} = \eta^{\mu\nu}} . \qquad (4.11)$$

In equation (4.11), the metric $g^{\mu\nu}$ is identified with the Minkowski metric $\eta^{\mu\nu}$. The flow of $\langle T_{\mu\nu} \rangle$ can be derived from the metric variation of $\partial_\tau \Gamma_\tau$ and will be discussed in future work. Here, the derivation follows closely the ones also found in the 2PI framework, e.g. [20], which allows to discuss the diagrammatic consistency of the truncation at hand. Concentrating on the energy-component, T_{00} is derived from equation (4.11) by substituting Γ by the classical action. This leads to

$$T_{00}(x) = \partial_0 \varphi \, \partial_0 \varphi - g_{00} \left(\frac{1}{2} \partial_\mu \varphi \, \partial^\mu \varphi - \frac{1}{2} m_0^2 \varphi^2 - \frac{\lambda}{3!} \varphi^3 \right). \qquad (4.12)$$

Its expectation value can be obtained from a general form that follows closely the derivation in section 2.2.5, see also e.g. [10]. For powers of the field operator, it can be written as

$$\left\langle \prod_{i=1}^{n} \varphi(x_i) \right\rangle = \prod_{i=1}^{n} \left[\int_{C(z_i)} G(x_i, z_i) \frac{\delta}{\delta \phi(z_i)} + \phi(x_i) \right]_{\phi_{\text{EoM}}}, \qquad (4.13)$$

with the full mean-field-dependent propagator $G[\phi](x, y)$ and the mean field $\phi = \langle \varphi \rangle$ being evaluated on the equations of motion (EoM). In the present case, it is $\phi_{\text{EoM}} = 0$, thus the energy reduces to

$$\langle T_{00}(x) \rangle = \frac{1}{2} \lim_{y \to x} \left[\partial_{x^0} \partial_{y^0} G(x, y) + \left(-\partial_x^2 + m_0^2 \right) G(x, y) \right]$$

$$+ \frac{i\lambda}{3!} \int_{C(z_1, z_2, z_3)} \Gamma^{(3)}(z_1, z_2, z_3) \prod_{i=1}^{3} G(x, z_i), \qquad (4.14)$$

where the variation of the field-dependent propagator with respect to the field was used as given in equation (3.11). The last term in equation (4.14) is the
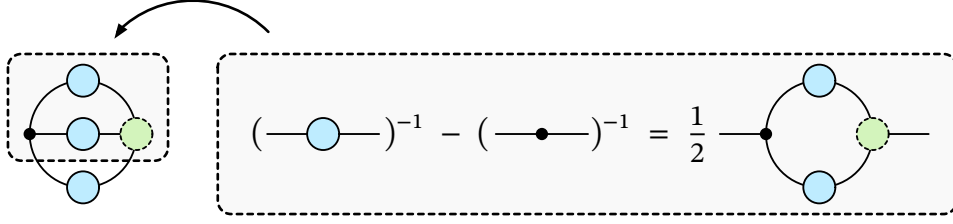
Figure 4.3. The sunset diagram on the left, which contributes to the energy in equation (4.14), contains a one-loop subgraph (left box) which is related to the gap equation (DSE) in the right box. The black dots represent the classical propagator and three-point function, respectively. The dressed propagator is depicted by blue circles with solid outline. The green circle with dashed outline denotes the dressed three-point function.

vacuum sunset diagram. Its one-loop subgraph is related to the Dyson-Schwinger equation of the inverse propagator for $\phi = 0$. The derivation of this equation is presented in appendix A.1. The diagrammatic representations of the DSE as well as the subgraph are shown in figure 4.3. Inserting the gap equation (A.7) into the sunset diagram leads to

$$\frac{i\lambda}{3!} \int\limits_{C(z_1,z_2,z_3)} \Gamma^{(3)}(z_1, z_2, z_3) \prod_{i=1}^{3} G(x, z_i) = \frac{1}{3} \int\limits_{C(z)} \left[S^{(2)}(x, z) - \Gamma^{(2)}(x, z) \right] G(z, x). \quad (4.15)$$

The second term is proportional to an irrelevant constant, $(\Gamma^{(2)} \cdot G)(x, y) = i\,\delta_C(x - y)$, while the first one simply changes the prefactors of the first and second term on the right hand side of equation (4.14). Fourier transforming the spatial coordinates, the final expression for the total energy is

$$\langle T_{00}(t) \rangle = \frac{5}{6} \lim_{t \to t'} \partial_t \partial_{t'} \int_{\mathbf{p}} G(t, t'; \mathbf{p}) + \frac{1}{6} \int_{\mathbf{p}} \left(\mathbf{p}^2 + m_0^2 \right) G(t, t; \mathbf{p}). \quad (4.16)$$

Note that the explicit occurrence of $\Gamma^{(3)}$ has dropped out. This trivially ensures the self-consistency of equation (4.16) with the approximation of $\Gamma^{(3)}$ used in the computation of the propagator. Equation (4.16) also readily extends to all components of the expectation value of the energy momentum tensor $\langle T_{\mu\nu} \rangle$.

4.4. Results

The propagator already allows for the discussion of relevant observables such as the occupation number and the dispersion relation. Although, in non-equilibrium situations, there are no unique definitions, versions analogue to the ones in equilibrium can be defined. To that end, a decomposition of the equal-time statistical propagator, see e.g. [21], is used that has the form

$$F(t, t, \mathbf{p}) = \frac{f(t, \mathbf{p}) + \frac{1}{2}}{\omega(t, \mathbf{p})} .$$
(4.17)

The non-equilibrium generalisations of the occupation number $f(t, \mathbf{p})$ and dispersion relation $\omega(t, \mathbf{p})$ are chosen such that they coincide with their time-independent counterparts in equilibrium. The occupation number can be computed as

$$f(t, \mathbf{p}) = \left[\partial_t \partial_{t'} F(t, t'; \mathbf{p})|_{t'=t} F(t, t; \mathbf{p}) \right]^{1/2} - \frac{1}{2},$$
(4.18)

and for the dispersion relation, the generalisation reads

$$\omega(t, \mathbf{p}) = \left(\frac{\partial_t \partial_{t'} F(t, t'; \mathbf{p})|_{t'=t}}{F(t, t; \mathbf{p})} \right)^{1/2} .$$
(4.19)

The free propagator (4.9), which is evidently in equilibrium, exemplifies the above definitions. There, it can be directly verified that the definitions indeed coincide with the expected values in equilibrium.

For the results shown in this section, the initial conditions describe a system far from equilibrium: it is prepared with highly over-occupied momentum modes at small momenta and none for high momenta. Explicitly, the initial occupancies are characterised by a (sharp) box of height $\tilde{N}/\tilde{\lambda}$ such that momentum modes are evenly occupied for momenta $|\mathbf{p}| < m_0$, see equation (4.10). In particular, $\tilde{N} = 100$ is chosen and the dimensionless coupling of the three-point function is given by $\tilde{\lambda} = \lambda/m_0^2 = 0.01$. The results in this chapter were obtained solving the integro-differential version of the time evolution equation.

4.4.1. Dispersion relation

A first interesting result is the time evolution of the dispersion relation shown in figure 4.4. At small momenta the dispersion decreases with time. This region is dominated by the mass. The mass m of the interacting particles can therefore be
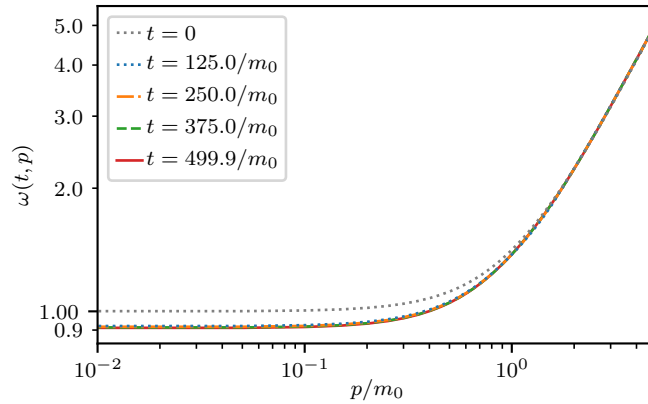
Figure 4.4. Time evolution of the dispersion relation as defined in equation (4.19). It is depicted by showing the result for various times. The grey dashed line corresponds to the dispersion at the initial time. At zero momentum, the mass of the interacting theory is obtained as $m \approx 0.9 m_0$ relative to the bare mass.

read off at zero momentum. For late times, the mass is obtained from figure 4.4 as $m \approx 0.9 \, m_0$ relative to the bare mass m_0. For higher momenta, where the mass is negligible, the dispersion agrees for all times.

4.4.2. Occupation number

The time evolution of the occupation number is shown in figure 4.5 for the same times as used for the dispersion relation. Naturally, the initial sharp box is softened during the time evolution, and particles are redistributed over the range of momenta. The momentum regime around $p/m_0 \approx 2$ is particularly interesting. In this regime, self-similar scaling may be identified where the occupation number exhibits a power law decay

$$f(t, \mathbf{p}) \propto |\mathbf{p}|^{-\kappa}. \tag{4.20}$$

In order to estimate the exponent κ, the power law could be directly fitted to the available data in the appropriate momentum range. However, it is not clear over which momenta the power law behaviour is given. Alternatively, the momentum-dependent exponent can be computed by

$$\kappa(t, p) = -p \, \partial_p \ln f(t, p). \tag{4.21}$$
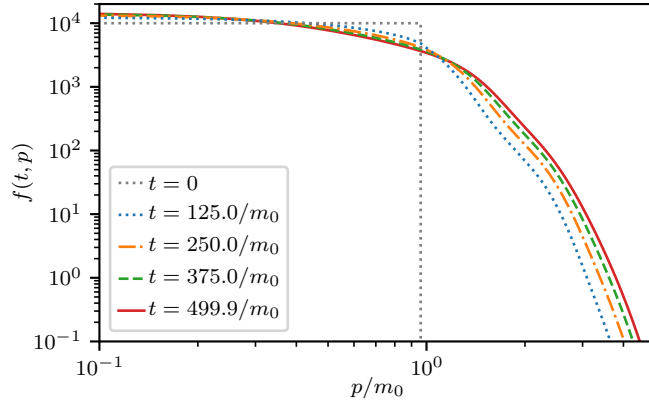
Figure 4.5. Time evolution of the occupation number as defined in equation (4.18) represented by the result for various times. The grey dashed line shows the initial occupations. For later times the initial box is smoothed out, and the result indicates a self-similar scaling regime around $p/m_0 \approx 2$ exhibiting a power law decay.

This exponent is shown for different times in figure 4.6. In the momentum range $p/m_0 \in [1.8, 2.1]$ this exponent is approximately constant. At later times this constant scaling regime is more pronounced, and the exponent for the momentum range above is evaluated at $t = 499.9/m_0$ as

$$\kappa \in [5.57,\ 5.69], \qquad \frac{p}{m_0} \in [1.8,\ 2.1]. \tag{4.22}$$

The analysis above suggests a power law behaviour. Moreover, the exponent is similar for all times considered. This indicates a self-similar scaling, although the regime is rather small.

In regimes with self-similar scaling, the time evolution is characterised by a self-similar scaling of the occupancies, see e.g. [19, 22]. This scaling reads

$$f(t_{\text{ref}}, |\mathbf{p}|) = \left(\frac{t}{t_{\text{ref}}}\right)^{-\alpha} f\left[t, \left(\frac{t}{t_{\text{ref}}}\right)^{-\beta} |\mathbf{p}|\right]. \tag{4.23}$$

In the regime $p/m_0 \in [1.8, 2.1]$, a least squares fit for the times $tm_0 = 312.5, 375.0, 437.6$ with respect to the occupancies at the reference time $t_{\text{ref}} = 499.9/m_0$ leads to the exponents $\alpha = 0.82, 1.03, 1.39$ and $\beta = -0.02, 0.02, 0.09$. The left panel of figure 4.7 shows the original occupation numbers for the above times and the right panel those that are rescaled each by their corresponding exponents. The rescaled occupation numbers match in the momentum range found from the power law exponent in accordance with a self-similar time evolution.
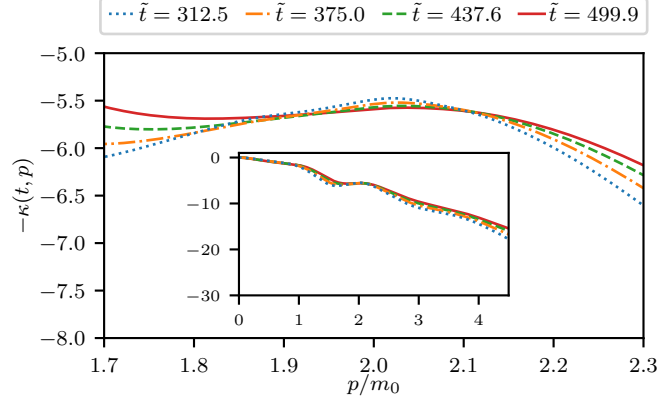
Figure 4.6. Momentum-dependent exponents of the occupation number for various times $\tilde{t} = tm_0$ as defined in equation (4.21). In the momentum range $p/m_0 \in [1.8, 2.1]$, the exponents are approximately constant. At later times this constant regime is more pronounced, and the exponent is evaluated at $t = 499.9/m_0$ as $\kappa \in [5.57, 5.69]$. The inset shows the momentum-dependent exponents for the full available momentum range.
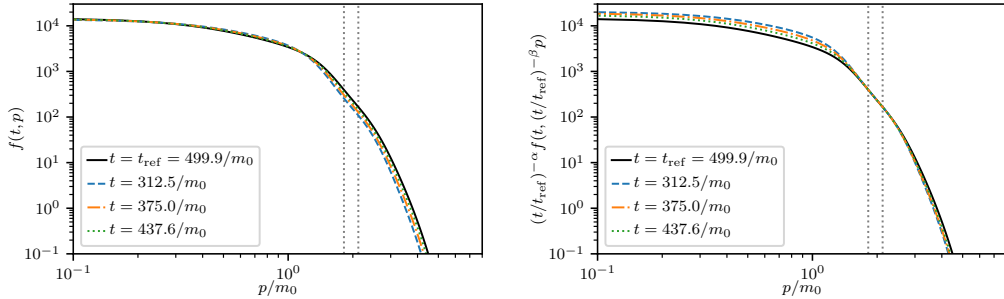
Figure 4.7. Self-similar time evolution in the momentum range $p/m_0 \in [1.8, 2.1]$, which is marked by vertical dashed lines. • *Left*: Occupation numbers without rescaling as obtained directly from the computation. • *Right*: Occupation numbers rescaled according to equation (4.23) for an assumed self-similar time evolution in the given momentum range. The exponents computed for times $tm_0 =$ 312.5, 375.0, 437.6 are given by $\alpha =$ 0.82, 1.03, 1.39 and $\beta =$ −0.02, 0.02, 0.09.
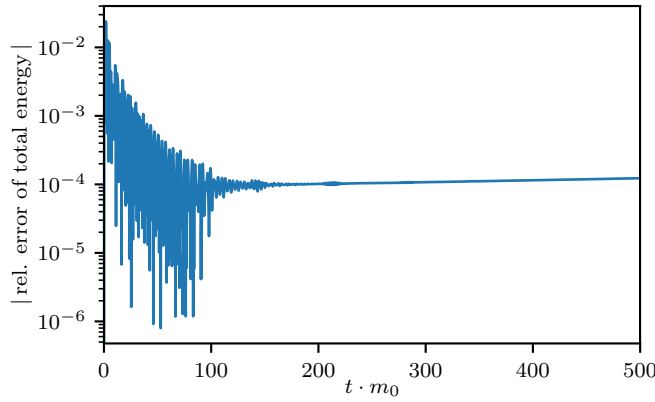
Figure 4.8. Relative error of the total energy $E(t)$, see equation (4.24), with respect to the initial total energy $E(0)$. The applied convention is $|[E(t) - E(0)]/E(0)|$. After an initial tune in, the relative error stabilises at around 10^{-4}.

4.4.3. Energy and particle number

A non-trivial and important consistency check for the present computation is the conservation of energy and particle number. The total energy is obtained by computing the expectation value of the time-time component of the energy-momentum tensor $T_{\mu\nu}$. The details of this computation were discussed in section 4.3, where a representation of the energy solely in terms of the propagator was derived. Using $\rho(t, t, \mathbf{p}) = 0$ in equation (4.16), the total energy is

$$E(t) = \langle T_{00}(t) \rangle = \lim_{t \to t'} \frac{5}{6} \partial_t \partial_{t'} \int_{\mathbf{p}} F(t, t'; \mathbf{p}) + \frac{1}{6} \int_{\mathbf{p}} (\mathbf{p}^2 + m_0^2) F(t, t; \mathbf{p}). \qquad (4.24)$$

Figure 4.8 shows the relative error of the total energy over time. After a short tune in period, the error stabilises at around 10^{-4} and the total energy is conserved.

Finally, conservation of the total particle is considered. For that purpose, a definition based on the flow of particle numbers is useful. The definition used in this context is

$$\Delta f(t) = \frac{\int_p \{f(t, p) - f(0, p)\}}{\int_p |f(t, p) - f(0, p)|}, \qquad (4.25)$$

which measures the sum of positive and negative flow of particle numbers normalised to the difference of positive and negative flow of particle numbers (total flow). Figure 4.9 shows this quantity. Similarly to the total energy, the total particle number is conserved after the initial oscillations.
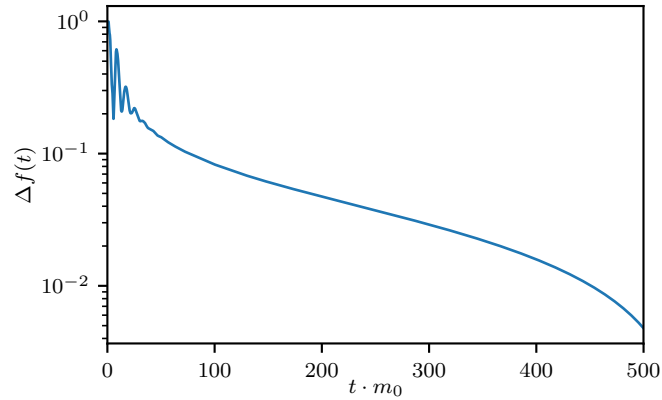
Figure 4.9. Sum of positive and negative flows in particle number, which is normalised to the difference of positive and negative flow (total flow) of particle number, see the definition in equation (4.25). After initial oscillations the total particle number is conserved.

4.5. Conclusion

In this chapter, the t-fRG approach in its integrated form has been applied to the ϕ^3-theory in $1 + 1$ dimensions. This theory serves as a test case for the approach and simulates the cubic interactions in a non-Abelian gauge theory. Here, the simplest approximation of the dynamics of the propagator has been studied by using classical vertices in the integrated flow. This approximation leads to a dynamical resummation of the propagator. The results indicate a scaling regime out of equilibrium with a momentum scaling $|\mathbf{p}|^{-\kappa}$ with $\kappa \in [5.57, 5.69]$ at $t = 499.9/m_0$, see equation (4.22). An investigation of the self-similarity of the three times available led to the coefficients $\alpha \in [0.82, 1.39]$ and $\beta \in [-0.02, 0.09]$, see equation (4.23).

In the previous chapter, only cubic interactions have been considered. Now the t-fRG approach is extended to quartic interactions. Not only are four-point functions necessary to describe a ϕ^3-theory with non-vanishing macroscopic field, but four-vertices are also essential on the way to gauge theories. Yang-Mills theory, for example, includes both three- and four-point functions in the gauge-fixed action. The former are the ghost-gluon- and three-gluon-vertices, and the latter is the four-gluon-vertex. Although those vertices are momentum dependent and additionally include tensor structures, the causal structure is still the same. A scalar field theory is therefore appropriate for the discussion of the t-fRG.

Together with the ϕ^4-theory inevitably comes the problem of renormalisation. Even in $1 + 1$ dimensions, the tadpole diagram with the classical local four-point function is logarithmically divergent. However, the upside is that the most simple truncation only includes exactly that diagram. Hence, the problem of renormalisation can be regarded isolated for the tadpole, see section 5.2.1. Similarly, the general discussion of equilibrium initial conditions is exemplified in section 5.2.2 for the same truncation in $1 + 0$ dimensions.

In addition to those important topics, the dynamical vertex is discussed in two truncations. The considered truncations comprise a one-loop correction to the vertex in section 5.3.1, and the resummed s-channel in section 5.3.2. Finally, the t-fRG approach is extended to an N-component scalar field theory in section 5.3.3. In this case, the resummed vertex leads to a $1/N$ expansion.

Figure 5.1. Diagrammatic flow equation of the inverse propagator in the ϕ^4-theory. The blue circles with solid outline denote the propagator while the pink circle with dotted outline denotes the four-point function. The τ-derivative of the regulator is depicted as orange square.

5.1. Flow equations

In this chapter, the ϕ^4-theory is considered for vanishing background fields only. As a consequence no vertex with an odd number of legs can be generated. The remaining set of flow equations is truncated such that the four-point function is the highest-order correlation function. In this truncation, the only non-vanishing flows are those of the two- and four-point function. The former is given in its entirety in equation (3.35). Due to the absence of the three-point function, the only remaining diagram is the tadpole. Therefore, in a pure ϕ^4-theory with vanishing background field, the flow equation is

$$\partial_\tau \Gamma^{(2)}_{\tau, x_1 x_2} = \frac{1}{2} \int_{C(z_1, z_2)} \partial_\tau G_{\tau, z_1 z_2} \, \Gamma^{(4)}_{\tau, z_1 z_2 x_1 x_2} \,. \tag{5.1}$$

Figure 5.1 shows a diagrammatic representation of this flow equation. The flow of the four-point function also only consists of one distinct diagram, see figure 5.2. The corresponding equation that contains all permutation of external legs is

$$\partial_\tau \Gamma^{(4)}_{\tau, x_1 x_2 x_3 x_4} = \quad \frac{i}{2} \int_{C(y_1, y_2, y_3, y_4)} \partial_\tau \Big[G_{\tau, y_1 y_2} G_{\tau, y_3 y_4} \Big] \Gamma^{(4)}_{\tau, y_2 x_2 x_3 y_3} \, \Gamma^{(4)}_{\tau, y_4 x_1 x_4 y_1}$$

$$+ \frac{i}{2} \int_{C(y_1, y_2, y_3, y_4)} \partial_\tau \Big[G_{\tau, y_1 y_2} G_{\tau, y_3 y_4} \Big] \Gamma^{(4)}_{\tau, y_4 x_1 x_3 y_1} \, \Gamma^{(4)}_{\tau, y_2 x_2 x_4 y_3}$$

$$+ \frac{i}{2} \int_{C(y_1, y_2, y_3, y_4)} \partial_\tau \Big[G_{\tau, y_1 y_2} G_{\tau, y_3 y_4} \Big] \Gamma^{(4)}_{\tau, y_4 x_1 x_2 y_1} \, \Gamma^{(4)}_{\tau, y_2 x_3 x_4 y_3} \,. \tag{5.2}$$

Figure 5.2. Diagrammatic flow equation of the four-point function in the ϕ^4-theory. The blue circles with solid outline denote the propagator while the pink circles with dotted outline denote the four-point function. The τ-derivative of the regulator is depicted as orange square. 'perm.' refers to permutations of the external legs.

5.2. The tadpole diagram

The simplest truncation is obtained by approximating the four-point function with the classical one, i.e. neglecting its flow equation. As a consequence, the tadpole diagram in the flow of the 1PI two-point function is solely computed using the local vertex, which is given by

$$S^{(4)}(x_1, \dots, x_4) = -\lambda \, \delta_C(x_1 - x_2) \, \delta_C(x_2 - x_3) \, \delta_C(x_3 - x_4). \qquad (5.3)$$

This resulting diagram is logarithmically divergent already in 1+1 dimensions, so that renormalisation is necessary. Since the considered truncation leads to this single diagram, the investigation of renormalisation is particularly accessible. Additionally, equilibrium initial conditions as a special case can be studied. Integrating the flow of the 1PI two-point function results in the self-energy where the local part is

$$\Sigma^{(0)}(t) = \frac{\lambda}{2} \int_{\mathbf{p}} F(t, t; \mathbf{p}), \qquad (5.4)$$

with the momentum integral $\int_{\mathbf{p}} = \int_{\mathbb{R}^d} \frac{d^d\mathbf{p}}{(2\pi)^d}$ in $1 + d$ dimensions.

5.2.1. Tadpole renormalisation

In this section, mass renormalisation within the t-fRG is investigated. The general idea was presented in section 3.7.2. Since this problem can be considered as an initial value problem, the notation is closely related to the one introduced for the time evolution equations in section 3.6.2. Let the local self-energy from

equation (5.4) define the naive self-energy with both finite and divergent part

$$\Sigma^{(0)}_{\text{non-ren.}}(t) = \frac{\lambda}{2} \int_{\mathbf{p}} F(t,t;\mathbf{p})\,. \tag{5.5}$$

The divergence originates from the zero-temperature part of the statistical propagator. The finite-temperature part contains a particle number distribution that vanishes in the ultraviolet limit. The necessary counterterm is time-independent and only contributes to the mass, which makes it sensible to define it as the mass shift

$$\Sigma^{(0)}_{\text{counter}}(t) = \Delta m^2 = \frac{\lambda}{2} \int_{\mathbf{p}} \bar{F}_{T=0}(t,t;\mathbf{p}) = \frac{\lambda}{4} \int_{\mathbf{p}} \left(m_R^2 + \mathbf{p}^2\right)^{-1/2}, \tag{5.6}$$

where m_R denotes the renormalised mass. The counterterm Σ_{counter} is inserted into the gap equation like Σ_{init} in equation (3.61), which leads to the gap equation for the initial propagator

$$\mathrm{i}\bar{G}^{-1}(x_1, x_2) = S^{(2)}(x_1, x_2) - \Delta m^2 \, \delta_C(x_1 - x_2)\,. \tag{5.7}$$

The solution to this equation is evidently the free propagator with renormalised mass

$$m_R^2 = m_0^2 + \Delta m^2\,. \tag{5.8}$$

Finally, the time evolution equation (3.62), where Σ_{init} is replaced by Σ_{counter} reads

$$G(x,y) = \bar{G}(x,y) + \int_{C(a,b)} \bar{G}(x,a)\,\Sigma(a,b)\,G(b,y)\,, \tag{5.9}$$

with the finite self-energy

$$\Sigma^{(0)}(t) = -\Delta m^2 + \frac{\lambda}{2} \int_{\mathbf{p}} F(t,t;\mathbf{p})\,. \tag{5.10}$$

For numerical computations it is useful to split the propagator into the zero-temperature part of the free propagator with renormalised mass and the rest. That way, the cancellation in equation (5.10) is performed on the level of the equation.

5.2.2. Equilibrium initial conditions in quantum mechanics

In a quantum mechanical system, that is in $1+0$ dimensions, the tadpole diagram is not divergent. With renormalisation out of the way, it is easier to focus on equilibrium initial conditions. Following the more general discussion from section 3.7.1, the equation to obtain the equilibrium propagator is

$$i\overline{G}^{-1}(x_1, x_2) = S^{(2)}(x_1, x_2) - i\Sigma_{\text{init}}(x_1, x_2). \tag{5.11}$$

where the local self-energy is given by equation (5.4) with the full propagator replaced by the initial one. Since the initial propagator is in equilibrium, the self-energy is time independent and defines the mass shift

$$\Delta m^2 = \Sigma_{\text{init}}^{(0)}(t) = \frac{\lambda}{2}\,\overline{F}(t, t). \tag{5.12}$$

As a consequence, the solution of equation (5.11) is

$$\overline{F}(t, t') = \frac{1}{2m}\cos\left[m\,(t - t')\right],$$

$$\overline{\rho}(t, t') = \frac{1}{m}\sin\left[m\,(t - t')\right], \tag{5.13}$$

with the resummed mass $m^2 = m_0^2 + \Delta m^2$. Plugging the statistical propagator from equation (5.13) into the self-energy from equation (5.12) leads to a fixed point equation for the mass shift,

$$\Delta m^2 = \frac{\lambda}{4}\left(m_0^2 + \Delta m^2\right)^{-1/2}. \tag{5.14}$$

To close this discussion, the time-dependent local self-energy is computed for equilibrium and out-of-equilibrium initial conditions. The corresponding initial self-energies are $\Sigma_{\text{init}} = \Sigma[\overline{G}]$ and $\Sigma_{\text{init}} = 0$ (free propagator with bare mass), respectively. Due to the construction of the initial propagator in equilibrium, see also section 3.7.1, the self-energy has to be constant in time. Therefore, a numerical computation merely serves as a tool to verify the formal result, but also checks that the employed solver is accurate enough. Figure 5.3 shows the result for both initial conditions. The equilibrium case behaves as intended. In the out-of-equilibrium scenario, the time-dependent mass shift oscillates around the resummed mass with the maxima taking on the value of the one-loop mass correction. Clearly, the used truncation does not allow for equilibration. As a matter of fact, it was already stated in section 4.1.1 that such a truncation does not give rise to meaningful dynamics of the propagator.
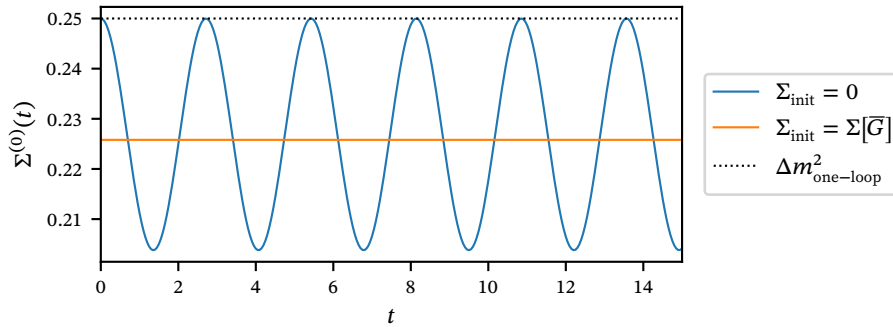
Figure 5.3. Time-dependent self-energy for different initial conditions. The blue line depicts a system initially prepared at equilibrium. The orange line corresponds to a free propagator at initial time. The latter oscillates around the resummed mass with the maxima taking on the value of the one-loop mass correction (dashed black line) to the bare mass.

5.3. Dynamics of the vertex

The previously used truncation, where the four-point function was fixed to the classical one, clearly does not involve the dynamics of the vertex. Additionally, the self-energy in such a truncation is purely local. Hence, the self-energy contributes only to the mass, and there is actually no meaningful dynamics of the propagator. In the ϕ^3-theory such a simple truncation already leads to a dynamical propagator, see chapter 4. In the ϕ^4-theory it is therefore indispensable to include a dynamical vertex. From the full flow equation of the four-point function, see figure 5.2, it is clear that in general the fully dressed vertex feeds back into its own flow equation. In this section, two truncations are examined. In the first one, the four-point function inside the flow is replaced by its classical counterpart. In the second truncation, the vertex couples back into its flow, but is approximated only by its s-channel.

5.3.1. One-loop vertex

If the flow of the four-point vertex is truncated such that it does not include the fully dressed four-point vertex itself, the vertex corrections are all one-loop, see figure 5.4. Of course, this refers to loops containing the full propagator and, thus, higher-order loops are still implicitly included. Paying attention to all permutations of the external legs and the regulator insertion, the flow equation

Figure 5.4. Truncated flow equation of the four-point function. The black dots denote classical four-point functions while the pink circle (dotted outline) represents the fully dressed one. The blue circles (solid outline) are the full propagators. The τ-derivative of the regulator is represented by the orange square.

is given by

$$\partial_\tau \Gamma_\tau^{(4)}(x_1, x_2, x_3, x_4) = \frac{i\lambda^2}{2} \partial_\tau \Big[G_\tau(x_1, x_3)^2 \Big] \delta_C(x_1 - x_2)\, \delta_C(x_3 - x_4)$$

$$+ \frac{i\lambda^2}{2} \partial_\tau \Big[G_\tau(x_1, x_2)^2 \Big] \delta_C(x_1 - x_3)\, \delta_C(x_2 - x_4)$$

$$+ \frac{i\lambda^2}{2} \partial_\tau \Big[G_\tau(x_1, x_2)^2 \Big] \delta_C(x_2 - x_3)\, \delta_C(x_1 - x_4). \qquad (5.15)$$

The different combinations of δ-distributions show that all channels are included in the flow equation. This is important, because in this truncation no specific channel is singled out. However, as soon as the integrated flow is inserted into the flow of the inverse propagator which is subsequently integrated over τ, the t-channel drops out. This a direct consequence of the δ-distribution not connecting internal and external point, see section 3.5.1 for the general discussion. The s- and u-channels contribute equally to the self-energy. The full expression for the self-energy is

$$\Sigma(x_1, x_2) = -\frac{i\lambda}{2} G(x_1, x_2)\, \delta_C(x_1 - x_2) - \frac{\lambda^2}{6} G(x_1, x_2)^3\,, \qquad (5.16)$$

where the first term on the right hand side is again the tadpole. This self-energy is evidently a perturbative approximation up to two loops. Moreover, it is equivalent to 2PI perturbation theory. In that framework, the self-energy is obtained by opening one propagator line of the vacuum diagrams that are contained in the Φ-functional. Keeping combinatorial factors in mind, from the definition in

equation (2.47), it follows that the appropriate functional is given by

$$\Phi[G] = \frac{1}{8} \; \bigcirc\!\!\bullet\!\!\bigcirc \; + \; \frac{i}{48} \; \ominus \; .$$

(5.17)
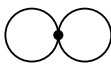
Without further considerations, it is therefore evident that the chosen truncation leads to an energy-conserving approximation. Since the truncation has not been chosen in view of energy conservation, this finding is a welcome side effect.

5.3.2. S-channel resummation

Going beyond the one-loop vertex requires the four-point function to feed back into its own flow equation. Yet it is still allowed to approximate the vertex. In this respect, it is useful to split the vertex into δ-distributions and vertex functions. Since the initial vertex always includes the classical one, which is completely local, the flow equation directly shows that the generated vertex can have one or two δ-distributions. This holds true in the present truncation with a vanishing background field. It can also contain a non-local part. Choosing an approximation where only the case with two δ-distributions is considered, the vertex can be split as

$$\Gamma_\tau^{(4)}(x_1, x_2, x_3, x_4) = S^{(4)}(x_1, x_2, x_3, x_4)$$

$$+ i \, \Gamma_\tau^{(4s)}(x_1, x_3) \, \delta_C(x_1 - x_2) \, \delta_C(x_3 - x_4)$$

$$+ i \, \Gamma_\tau^{(4t)}(x_1, x_2) \, \delta_C(x_1 - x_3) \, \delta_C(x_2 - x_4)$$

$$+ i \, \Gamma_\tau^{(4u)}(x_1, x_2) \, \delta_C(x_1 - x_4) \, \delta_C(x_2 - x_3) \,,$$

(5.18)

where the introduced functions on the right hand side represent the different channels. This decomposition allows for the derivation of a flow equation for every channel. In this section, however, only the dominant s-channel is considered. Its flow equation is obtained from the flow of the full vertex in equation (5.2). Dropping all permutations of the external legs that do not contribute

to the s-channel, the flow reads

$$i \partial_\tau \Gamma_\tau^{(4s)}(x_1, x_3) \, \delta_C(x_1 - x_2) \, \delta_C(x_3 - x_4)$$

$$= \frac{i}{2} \int_{C(y_1, y_2, y_3, y_4)} \partial_\tau \Big[G_\tau(y_1, y_2) G_\tau(y_3, y_4) \Big] \Gamma_\tau^{(4)}(x_1, x_2, y_1, y_4) \, \Gamma_\tau^{(4)}(y_2, y_3, x_3, x_4). \quad (5.19)$$

This equation can be further simplified by identifying vanishing diagrams. Since the vertices are either classical or s-channel, there are in total four diagrams. Without loss of generality, let $x_1^0 > x_3^0$. With the result from section 3.5.1, it follows that the first vertex in equation (5.19) has to be the classical one. Otherwise, the internal and external points are not connected by a δ-distribution. Inserting the decomposition of the vertex as well as the explicit form of the classical vertex, the flow equation ultimately is

$$\partial_\tau \Gamma_\tau^{(4s)}(x_1, x_3) = \frac{\lambda^2}{2} \partial_\tau \Big[G_\tau(x_1, x_3)^2 \Big] - \frac{i\lambda}{2} \int_{C(z_1)} \partial_\tau \Big[G_\tau(x_1, z_1)^2 \Big] \Gamma_\tau^{(4s)}(z_1, x_3). \quad (5.20)$$

Integrating the flow requires the causal property of 1PI correlation functions. In case of the s-channel vertex, this property is expressed as

$$\Gamma_\tau^{(4s)}(x_1, x_2) = \Gamma^{(4s)}(x_1, x_2) \, \theta(\tau - x_1^0)^2 \, \theta(\tau - x_2^0)^2, \quad (5.21)$$

where the θ-distributions are to the power of two because the arguments are pairwise identical. Using equation (3.39) to deal with the product of distributions, the integrated flow is obtained as

$$\Gamma^{(4s)}(x_1, x_2) = \frac{\lambda^2}{2} G(x_1, x_3)^2 - \frac{i\lambda}{2} \int_{C(z_1) < x_1^0} G(x_1, z_1)^2 \, \Gamma^{(4s)}(z_1, x_3). \quad (5.22)$$

The property in equation (5.21) has to be considered also in the integration of the flow of the inverse propagator. The result is the self-energy

$$\Sigma(x_1, x_2) = -\frac{i\lambda}{2} G(x_1, x_1) \, \delta_C(x_1 - x_2) - \frac{1}{6} G(x_1, x_2) \, \Gamma^{(4s)}(x_1, x_2), \quad (5.23)$$

where the first term constitutes the tadpole diagram with the classical four-point function. The second term contains the s-channel vertex which itself is resummed using equation (5.22). When the resummation is not performed, the

s-channel remains at one-loop order, and the two-loop self-energy takes the closed form

$$\Sigma_{\text{two-loop}}(x_1, x_2) = -\frac{i\lambda}{2} \, G(x_1, x_1) \, \delta_C(x_1 - x_2) - \frac{\lambda^2}{12} \, G(x_1, x_2)^3 \,. \tag{5.24}$$

Comparing this approximation to the result from section 5.3.1 it stands out that the *sunset diagram* in the self energy (5.16) has a factor of two, which is absent here. This factor arises because, previously, both the s- and u-channel are included, which lead to the same term. In this section, the vertex is restricted to the s-channel only, and consequently there is no contribution from the u-channel.

5.3.3. $1/N$ expansion

The extension of the t-fRG to an N-component scalar field theory is straightforward. Due to the introduced tensor structure, every integral also contains a summation over the field indices. Naturally, the regulator needs to be a tensor as well. For the local regulator, the tensor structure is completely given by the Kronecker delta. Therefore, the regulator is

$$R_\tau^{ab}(x, y) = \delta^{ab} \, R_\tau(x, y) \,. \tag{5.25}$$

As a matter of fact, for a vanishing background field, the Kronecker delta is the only tensor. Consequently, the tensor structure of correlation functions is determined by combinations of the Kronecker delta. Similar to the regulator, the propagator is decomposed into

$$G_\tau^{ab}(x, y) = \delta^{ab} \, G_\tau(x, y) \,. \tag{5.26}$$

The self-energy and higher-order correlation functions can be split similarly. In this form, it is easy to trace over field indices. For example, a propagator loop can be traced as

$$\left[G_\tau^{ab}(z_1, z_2) \right]^2 = \delta^{ab} \, \delta^{ab} \, G_\tau(z_1, z_2)^2 = N \cdot G_\tau(z_1, z_2)^2 \,. \tag{5.27}$$

In fact, this is the only ingredient to generalise the s-channel resummation to an N-component scalar field, which directly gives the $1/N$ expansion. Let the interaction part of the action be

$$S_{\text{int}}[\varphi] = -\frac{\lambda}{4! \, N} \int_{C(x)} \varphi^a(x) \, \varphi^a(x) \, \varphi^b(x) \, \varphi^b(x) \,. \tag{5.28}$$

The classical four-point function is then given by

$$S^{(4),abcd}(x_1, x_2, x_3, x_4) = -\frac{\lambda}{3N}\left(\delta^{ab}\,\delta^{cd} + \delta^{ac}\,\delta^{bd} + \delta^{ad}\,\delta^{bc}\right)$$

$$\times\,\delta_C(x_1 - x_2)\,\delta_C(x_2 - x_3)\,\delta_C(x_3 - x_4). \quad (5.29)$$

The 1PI four-point function is again approximated by the s-channel, such that

$$\Gamma_\tau^{(4),abcd}(x_1, x_2, x_3, x_4) = S^{(4),abcd}(x_1, x_2, x_3, x_4)$$

$$+\,\mathrm{i}\,\Gamma_\tau^{(4s)}(x_1, x_3)\,\delta^{ab}\,\delta^{cd}\,\delta_C(x_1 - x_2)\,\delta_C(x_3 - x_4). \quad (5.30)$$

Equation (5.19) can be readily extended to include field indices. After performing the trace and integrating over τ, the vertex is given by

$$\Gamma^{(4s)}(x_1, x_2) = \frac{\lambda^2}{18N}\,G(x_1, x_3)^2 - \frac{\mathrm{i}\lambda}{6}\int_{C(z_1)<x_1^0} G(x_1, z_1)^2\,\Gamma^{(4s)}(z_1, x_3), \quad (5.31)$$

which is evidently of order $\mathcal{O}(N^{-1})$. The self-energy (5.23) only changes in the tadpole diagram with the classical vertex. In that case, the full tensor structure from equation (5.29) has to be regarded. The result is the self-energy

$$\Sigma(x_1, x_2) = -\frac{\mathrm{i}\lambda}{2}\frac{N+2}{3N}\,G(x_1, x_1)\,\delta_C(x_1 - x_2) - \frac{1}{6}\,G(x_1, x_2)\,\Gamma^{(4s)}(x_1, x_2). \quad (5.32)$$

Note that the tadpole diagram contributes to $\mathcal{O}(N^{-1})$ as well as $\mathcal{O}(N^0)$. As a consistency check, let $N = 1$. In that case, the self-energy seems identical to equation (5.23). However, also the resummed vertex from equation (5.31) has to be considered. In comparison to equation (5.23), the first and second term have an extra factor of 1/9 and 1/3, respectively. The reason is that for a single component the classical four-point function does not distinguish between different channels. However, for $N > 2$ the classical vertex consists of the three channels, see equation (5.29). In the flow of the s-channel vertex, only the s-channel of the classical vertex contributes. In the first term, there are two classical vertices leading to nine distinct tensor structures, whereas in the second term, the single classical vertex leads to three distinct diagrams. In both cases, only a single diagram survives the projection to the s-channel.

Chapter 6

6

Three-dimensional Yang-Mills theory in equilibrium

This final chapter is separate from the rest of the work in the sense that it focuses on the functional renormalisation group in equilibrium. For that purpose, all computations are performed in momentum space. The reduced computational cost compared to the t-fRG allows for the investigation of (three-dimensional) Yang-Mills theory, which is of course more involved than the previously considered scalar field theories. In this chapter, the non-perturbative ghost and gluon propagators as well as the momentum-dependent ghost-gluon, three-gluon, and four-gluon vertices are computed in a comprehensive truncation scheme. Compared to the physical case of four space-time dimensions, more sophisticated truncations are necessary due to significant contributions from non-classical tensor structures. In particular, a special technique is applied to compute the tadpole diagrams of the propagator equations, which also captures all perturbative two-loop effects. The correlators obtained within the fRG are compared to lattice and Dyson-Schwinger results. The necessity of the used elaborate truncation scheme indicates that achieving apparent convergence is not trivial. Therefore, performing this examination in a computationally less intensive setting, i.e. in equilibrium, is crucial. Even though there might be additional subtleties out of equilibrium, the insights from this chapter are important. A truncation not accurately describing equilibrium, will also present issues for initially out-of-equilibrium systems in view of equilibration.

6.1. Introduction

Functional methods such as the functional renormalisation group (fRG) or Dyson-Schwinger equations (DSEs) are non-perturbative first-principles approaches to quantum chromodynamics (QCD), and they are complementary to lattice simulations. At finite density the latter approach is hampered by a sign problem, while the former approaches face convergence and accuracy problems. The aim of the fQCD collaboration [23] is to establish the fRG as a quantitative continuum approach to QCD, with the phase diagram and the hadron spectrum as primary applications, see [24–29] for recent works.

Building on the advances made in a previous work in four-dimensional spacetime [27], we consider Landau-gauge Yang-Mills (YM) theory in three dimensions, in this work. Similar to its four-dimensional analogue, it is asymptotically free and confining. Upon adding an adjoint scalar, it corresponds to the dimensionally reduced asymptotic high-temperature limit of four-dimensional YM theory. Furthermore, the reduced dimensionality allows lattice simulations at a considerably reduced numerical expense, making the three-dimensional theory an interesting testing case that allows truncation checks in functional approaches. Therefore, the propagators of three-dimensional YM theory have been studied intensively on the lattice [30–46], with DSEs [47–53], and in semi-perturbative settings [54–56]. Its vertices have been investigated on the lattice [33, 35] as well as with continuum methods [51, 53, 56].

So far, the most advanced results for YM theory in three dimensions within functional approaches have been obtained in a recent DSE investigation [53]. There, the coupled system of equations for the classical tensor structures has been solved self-consistently. In terms of the complexity of the truncation, the investigation [53] is comparable to the calculation performed in [27] for the four-dimensional case, which is more complicated due to non-trivial renormalisation. The present work builds on these advances, with a focus on the effects of including non-classical vertices and tensor structures in the tadpole diagrams of the gluon and ghost propagator equations.

This chapter is organized as follows: in section 6.2 we review the treatment of YM theory with the fRG using a vertex expansion for the effective action. We focus on new developments for the inclusion of the propagator tadpole diagrams. In section 6.3 we discuss our results, which includes a thorough investigation of apparent convergence and a comparison to DSE and lattice results. The conclusion is given in section 6.4. We check the independence of the regulator and describe the computational setup in the appendices.

6.2. Yang-Mills theory from the fRG

In this section we review the fRG approach to YM theory using a vertex expansion for the effective action. Although the overall set-up follows [27, 57], we repeat the most important steps for the convenience of the reader.

The fRG is a non-perturbative continuum method that implements Wilson's idea of including quantum fluctuations in momentum shells for the effective action, see [10, 58–61] for QCD-related reviews. The key object in this approach, pioneered by Wetterich [13], is the scale-dependent analogue of the effective action Γ_k. The RG or infrared cutoff scale k is introduced via a momentum-dependent regulator function R_k that acts like a fluctuation-suppressing mass term on momentum scales $p^2 \lesssim k^2$. The scale dependence of Γ_k is governed by an exact equation with a simple one-loop structure,

$$\partial_t \Gamma_k[\phi] = \frac{1}{2} \int_p G^{ab}_{\mu\nu}[\phi] \, \partial_t R^{ba}_{\nu\mu} - \int_p G^{ab}[\phi] \, \partial_t R^{ba} \,, \tag{6.1}$$

where $\int_p = \int \mathrm{d}^3 p / (2\pi)^3$ and the full field-, momentum-, and scale-dependent gluon and ghost propagator

$$G_k[\phi] = \frac{1}{\Gamma^{(2)}[\phi] + R_k} \,, \qquad \text{with} \quad \Gamma^{(n)}_k[\phi] = \frac{\delta^n \Gamma[\phi]}{\delta \phi^n} \,. \tag{6.2}$$

The superfield $\phi = (A_\mu, c, \bar{c})$ consists of gauge, ghost, and anti-ghost fields. In equation (6.1) the propagators $G^{\mu\nu}_{ab}[\phi]$ and $G^{ab}[\phi]$ are the diagonal gluon and off-diagonal ghost–anti-ghost components of the propagator (6.2). A pictorial representation of equation (6.1) is given in figure 6.1. The regulator functions are given in appendix D.1, where we also demonstrate the independence of the results from the choice of the regulator function. Flow equations for the 1PI n-point functions are straightforwardly derived from equation (6.1) by taking functional derivatives with respect to the fields, see figure 6.2 for the diagrammatic equations.

6.2.1. Vertex expansion

Due to the structure of the flow equation (6.1), the flow equation for an n-point correlator depends on up to $(n + 2)$-point functions. This leads to an infinite tower of coupled equations, which have to be truncated within appropriate non-perturbative expansion schemes in order to be numerically solvable. As in [27],

Figure 6.1. Flow equation. Wiggly and dotted lines represent the dressed gluon and ghost propagators, respectively. The crossed circles denote regulator insertions $\partial_t R$, see equation (6.1).

we work in a systematic vertex expansion scheme, corresponding to an expansion of the effective action in terms of 1PI correlation functions. Relying on the structural similarities of the three-dimensional theory to its four-dimensional analogue, we take all classical vertices into account, i.e. the ghost-gluon, three- and four-gluon vertex. In addition, we compute so-called tadpole vertices as discussed in section 6.2.2. For later reference we quickly recapitulate the parametrisations for the propagators and classical vertex functions considered in this work. The gluon and ghost two-point functions are parametrised in terms of scalar dressing functions $1/Z_A(p)$ and $1/Z_c(p)$,

$$\left[\Gamma_{AA}^{(2)}\right]_{\mu\nu}^{ab}(p) = Z_A(p)\, p^2\, \delta^{ab}\, \Pi_{\mu\nu}^{\perp}(p)\,,$$

$$\left[\Gamma_{\bar{c}c}^{(2)}\right]^{ab}(p) = Z_c(p)\, p^2\, \delta^{ab}\,, \tag{6.3}$$

where $\Pi_{\mu\nu}^{\perp}(p) = \delta_{\mu\nu} - p_\mu p_\nu/p^2$ denotes the transverse projection operator. We parametrise the three-point vertices by

$$\left[\Gamma_{\bar{c}cA}^{(3)}\right]_{\mu}^{abc}(p,q) = \sqrt{4\pi\,\alpha(\mu)}\,\lambda_{\bar{c}cA}(p,q)\left[\mathcal{T}_{\bar{c}cA}^{\mathrm{cl}}\right]_{\mu}^{abc}(p,q)\,,$$

$$\left[\Gamma_{A^3}^{(3)}\right]_{\mu\nu\rho}^{abc}(p,q) = \sqrt{4\pi\,\alpha(\mu)}\,\lambda_{A^3}(p,q)\left[\mathcal{T}_{A^3}^{\mathrm{cl}}\right]_{\mu\nu\rho}^{abc}(p,q)\,. \tag{6.4}$$

Their classical tensor structures are given by

$$\left[\mathcal{T}_{\bar{c}cA}^{\mathrm{cl}}\right]_{\mu}^{abc}(p,q) = \mathrm{i}f^{abc}\,q_\mu\,,$$

$$\left[\mathcal{T}_{A^3}^{\mathrm{cl}}\right]_{\mu\nu\rho}^{abc}(p,q) = \mathrm{i}f^{abc}\left\{(p-q)_\rho\delta_{\mu\nu} + \text{ perm.}\right\}. \tag{6.5}$$

The transversely projected basis for the ghost-gluon vertex consists of only one single element, whereas the corresponding basis for the three-gluon vertex counts four elements. The impact of non-classical tensor structures in the three-gluon vertex have been found to be subleading [62] in four space-time dimensions. Here we assume that they are also subleading in three dimensions and neglect them. The parametrisation of the four-gluon vertex is given by

$$\left[\Gamma_{A^4}^{(4)}\right]_{\mu\nu\rho\sigma}^{abcd}(p,q,r) = 4\pi\,\alpha(\mu)\,\lambda_{A^4}(\bar{p})\left[\mathcal{T}_{A^4}^{\text{cl}}\right]_{\mu\nu\rho\sigma}^{abcd}, \tag{6.6}$$

where the classical tensor structure is given by

$$\left[\mathcal{T}_{A^4}^{\text{cl}}\right]_{\mu\nu\rho\sigma}^{abcd} = f^{abn}f^{cdn}\delta_{\mu\rho}\delta_{\nu\sigma} + \text{perm.}. \tag{6.7}$$

The inclusion of non-classical tensor structures in the four-gluon vertex is discussed in section 6.2.2. The four-gluon dressing function(s) are approximated as a function of the average momentum $\bar{p}^2 = \frac{1}{4}(p_1^2+p_2^2+p_3^2+p_4^2)$ which was shown to be a good approximation for the full momentum dependence in four space-time dimensions [63] and we assume that the same holds in three dimensions.

From the momentum-dependent dressing functions of the different correlators, we can define corresponding running couplings via

$$\alpha_{\bar{c}cA}(p) = \alpha(\mu)\frac{\lambda_{\bar{c}cA}^2(p)}{Z_A(p)\,Z_c^2(p)},$$

$$\alpha_{A^3}(p) = \alpha(\mu)\frac{\lambda_{A^3}^2(p)}{Z_A^3(p)},$$

$$\alpha_{A^4}(p) = \alpha(\mu)\frac{\lambda_{A^4}(p)}{Z_A^2(p)}. \tag{6.8}$$

Due to gauge invariance, encoded in the Slavnov-Taylor identities, all couplings (6.8) have to agree in the perturbative regime of the theory. Furthermore, the dimensional suppression of the running coupling ensures that the dressing functions take their bare values at large momentum scales,

$$\lim_{p\to\infty}\lambda_{\bar{c}cA}(p) = \lim_{p\to\infty}\lambda_{A^3}(p) = \lim_{p\to\infty}\lambda_{A^4}(p) = 1, \tag{6.9}$$

for UV-trivial wave function renormalisations

$$\lim_{p\to\infty}Z_A(p) \to 1, \qquad \lim_{p\to\infty}Z_c(p) \to 1. \tag{6.10}$$
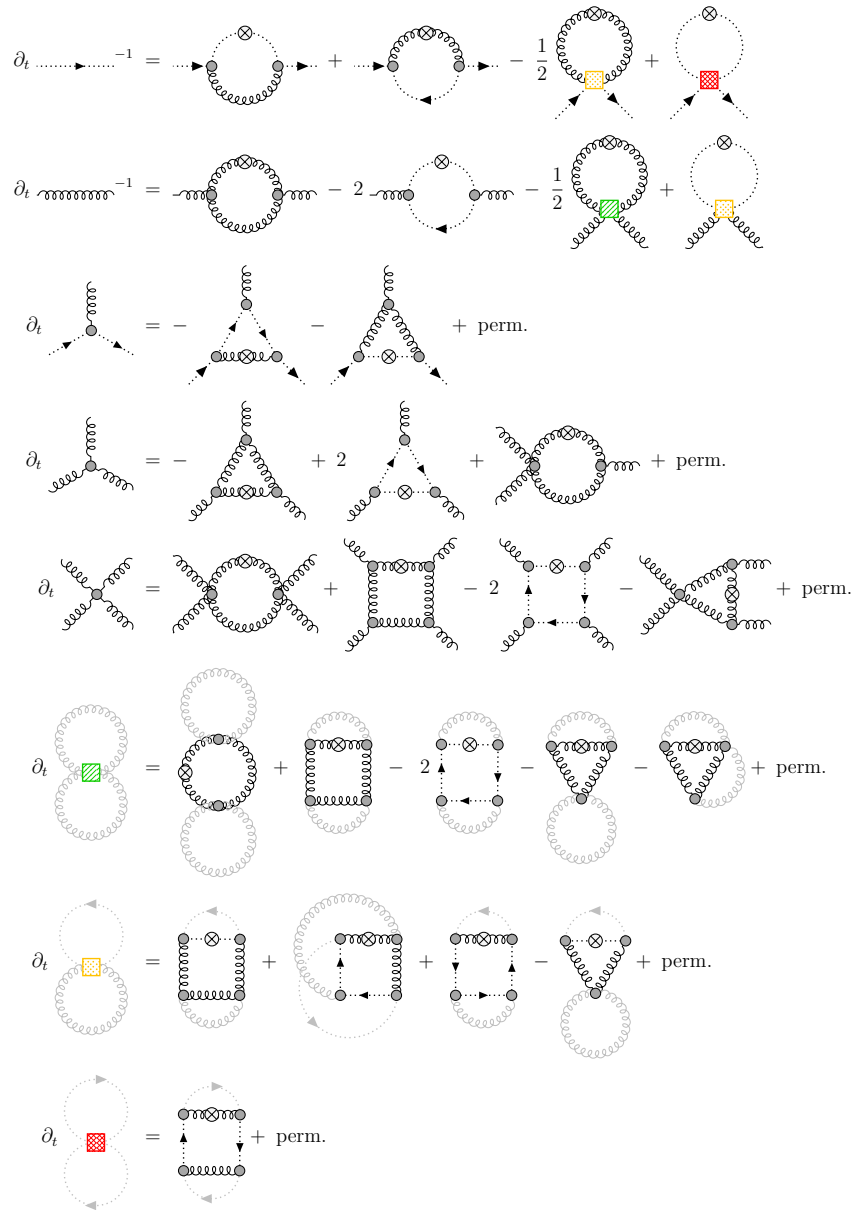
Figure 6.2. Diagrams that contribute to the truncated flows of propagators and vertices. While filled circles denote dressed (1PI) vertices, the squares denote the tadpole vertices explained in section 6.2.2. Shaded lines indicate the projection procedure of the tadpoles vertices. Permutations include not only (anti-)symmetric permutations of external legs but also permutations of the regulator insertions.

The truncation described above depends only trivially on the gauge group. In particular, only the quadratic casimir of the adjoint representation appears in the truncated set of equations. Therefore, it can be absorbed into a redefinition of the coupling, which in turn can be turned into a redefinition of the physical scale, see [29, 57] for a more detailed discussion. The same holds for the extended truncation described in the next subsection. Thus, our results are effectively independent of the gauge group. However, this does not indicate a bad truncation since also in perturbation theory, Yang-Mills theory is independent of the gauge group up to three loops, see e.g. [64] for a recent discussion. Also the DSE results from [53] do not possess a genuine gauge group dependence and lattice results for the propagators show only a mild dependence on the gauge group [65, 66]. Consequently, we compare our results to $SU(2)$ lattice results.

6.2.2. Tadpole vertices

The structure of the flow equation (6.1) implies that fully dressed four-point functions appear on the right hand side of the propagator equations, see figure 6.2. In general, this requires the full knowledge of all momentum-dependent non-classical four-point tensor dressings. Although some exploratory studies exist [63, 67–70], their dynamical back-coupling into the propagator equations has still not been achieved. In the following, we propose a method that captures most of the dynamics on the level of the propagator equations, while it keeps the numerical effort at a manageable level. As an example, we consider the gluon tadpole contribution to the gluon propagator equation. All other tadpole diagrams are obtained analogously. The gluon tadpole contribution to the flow of the gluon two-point function is given by

$$\partial_t \left[\Gamma^{(2)}_{A^2}\right]^{ab}_{\mu\nu}(p) = \frac{1}{2} \int_p \left[\Gamma^{(4)}_{A^4}\right]^{abcd}_{\mu\nu\rho\sigma}(p,-p,q) \cdot \left[G\,\partial_t R\,G\right]^{dc}_{\sigma\rho}(q). \tag{6.11}$$

Exploiting that the gluon propagator is diagonal in colour space and transverse with respect to its momentum in Landau gauge, we can project equation (6.11) with $\delta^{ab}\,\Pi^{\perp}_{\mu\nu}(p)$. From this we see that the gluon propagator equation depends only on the projected four-point function

$$T_{A^4}(p,q) = \Pi^{\perp}_{\mu\nu}(p)\left[\Gamma^{(4)}_{A^4}\right]^{abcd}_{\mu\nu\rho\sigma}(p,-p,q)\,\Pi^{\perp}_{\rho\sigma}(q). \tag{6.12}$$

Therefore, the full contribution of the four-gluon vertex to the tadpole is already contained in this single scalar function, whose flow we can compute directly

from projecting the corresponding equation accordingly, cf. figure 6.2. In particular, this procedure includes the back-coupling effect of all non-classical tensor structures that are generated at the perturbative one-loop level, including therefore also all two-loop effects of the tadpole diagrams in the propagator equations. The non-classical tensor structures couple back into the vertices indirectly via the propagators. We neglect their direct back-coupling into the vertex equations. However, we expect this approximate treatment to yield a considerable improvement of the truncation at comparably moderate numerical costs.

6.3. Results

In this section we present the main findings of our investigation. Our solutions are of the scaling type, and are obtained as described in appendix D.2. After discussing the truncation dependence of our results we provide an extensive comparison to results from lattice gauge theory and Dyson-Schwinger equations. We close with a determination of the infrared scaling coefficients and their comparison to those of finite temperature Yang-Mills theory in four dimensions.

6.3.1. Truncation and apparent convergence

In order to assess the influence of the truncation on our results, we compare three different extensions of our simplest symmetric point approximation:

1. *symmetric point*: only classical vertices with dressing functions that depend only on the symmetric momentum configuration,

2. *full momentum*: same as 1. symmetric point, but including the full momentum dependence of the ghost-gluon and three-gluon vertex dressings,

3. *sym. point + 4gl tadp.*: same as 1., but with the effects of the non-classical tensors of the four-gluon-vertex included in the tadpole diagram of the gluon propagator equation as described in section 6.2.2,

4. *sym. point + all tadp.*: same as 3., but additionally including the effects of the two-ghost-two-gluon and four-ghost vertices in both propagator equations, see section 6.2.2 and figure 6.2 for a visualisation.

The corresponding results for the propagators are shown in figure 6.3. The first immediate observation is that the additional momentum dependence (2.) in
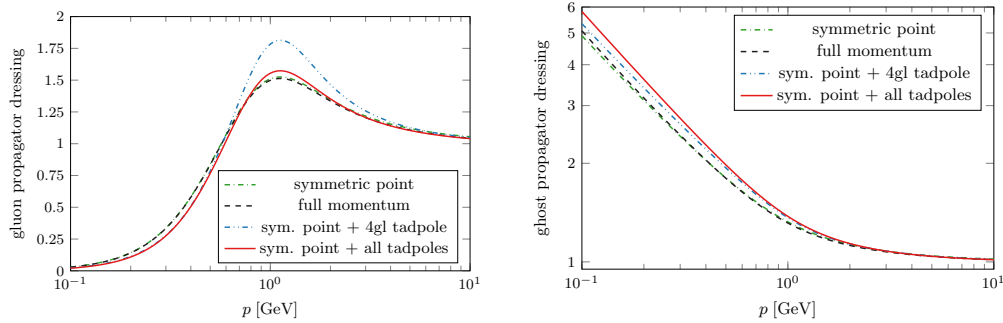
Figure 6.3. Truncation dependence of the gluon propagator dressing $1/Z_A(p)$ (left) and ghost propagator dressing $1/Z_c(p)$ (right). *Symmetric point* and *full momentum* denotes using the average momentum and full momentum dependence, respectively, in the three-gluon vertex. Results with + *4gl tadpole* and + *all tadpoles* include the respective tadpole diagrams.

the three-gluon and ghost-gluon vertices does not visibly affect the propagators. On the contrary, the full momentum dependence and tensor structures of the four-point functions in the tadpole diagrams significantly affect the propagators. Concerning the goal of apparent convergence, we observe that including the tadpole contribution of the four-gluon vertex alone has a comparably pronounced effect, most of which is counteracted by the remaining tadpoles. This indicates that a fast convergence may be achieved if the underlying consistent resummation pattern is preserved within the truncation scheme. A similar observation has already been made in the matter sector of QCD in four space-time dimensions [24, 28]. There, it is found that the effect of non-classical tensor structures in the quark-gluon vertex is counter-acted by corresponding structures in higher quark-gluon interactions that stem from the same BRST-invariant operator. We conclude that it is of chief importance to fully reveal these resummation patterns.

6.3.2. Comparison to DSE and lattice

In this section we compare the results from our most extensive truncation, 4. *sym. point + all tadp.* (see section 6.3.1), to results obtained from $SU(2)$ lattice gauge theory [33, 35, 45, 71] and with Dyson-Schwinger equations [53]. To that end, we normalise both, lattice and DSE results respective to our results in the UV regime, for more details see appendix D.3. We emphasise again that the
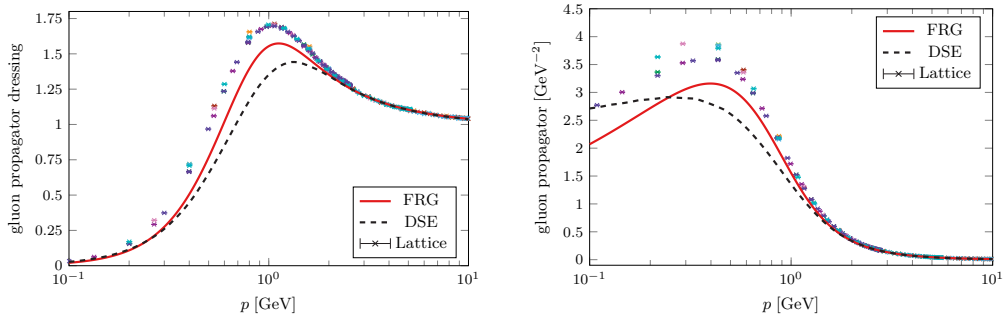
Figure 6.4. Gluon propagator dressing $1/Z_A(p)$ (left) and the dimensionful propagator $1/(p^2 Z_A(p))$ (right) in comparison with DSE [53] and lattice [33, 35, 45, 71] results.

presented fRG result is of the scaling type [72–80], whereas the lattice and DSE results are decoupling solutions [34, 36, 39, 81, 82], characterised by a finite, non-vanishing value of the gluon propagator at $p = 0$.

Propagators

From figure 6.4 and the left panel of figure 6.5, it is clearly seen that our results agree well with the rescaled lattice results in the UV regime with a discrepancy arising below 3 GeV. This difference is most likely due to truncation artefacts in our results which has to be clarified in future work. The most obvious culprits are missing effects in the equations for the classical vertex tensor structures due to the leading non-classical tensor structures of the three- and four-point functions.

The DSE gluon propagator from [53] has a smaller bump than both the fRG and lattice propagators. In section 6.3.1 we have shown that non-classical tensor structures have the net effect of increasing the bump in the gluon propagator. In comparison to the DSE truncation in [53], the present approximation includes more non-classical tensor structures. Although this may serve as an explanation, the system of equations is highly non-linear, and such an incomplete comparison is potentially misleading. Another factor may be that the DSE results are of the decoupling type whereas our results are of the scaling type, which generically show a larger bump [27]. In order to perform a more informative comparison between the DSE and fRG results, a DSE scaling solution would be preferable because of its uniqueness [78, 80].
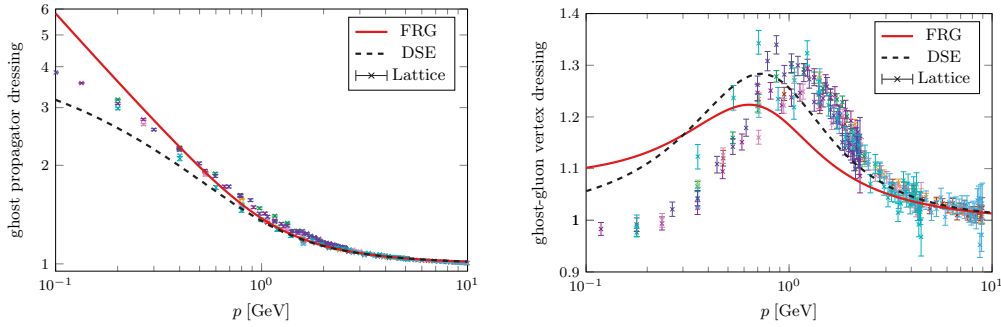
Figure 6.5. Ghost propagator dressing $1/Z_c(p)$ (left) and ghost-gluon vertex dressing $\lambda_{\bar{c}cA}(\bar{p})$ (right) compared to DSE [53] and lattice [33, 35, 45, 71] results.
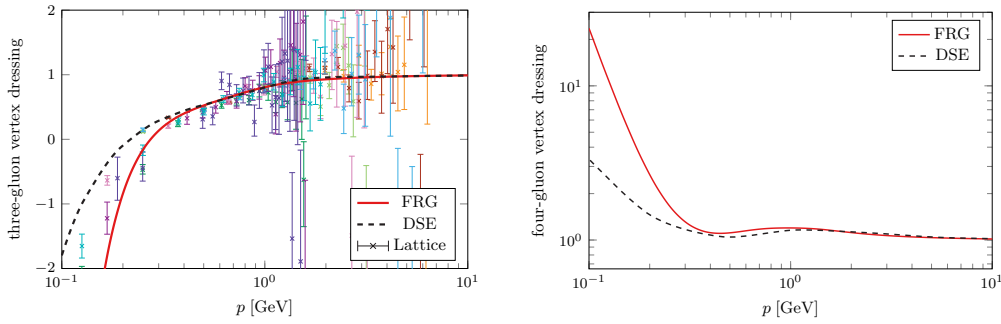
Figure 6.6. Three-gluon (left) and four-gluon (right) vertex dressings, $\lambda_{A^3}(\bar{p})$ and $\lambda_{A^4}(\bar{p})$, compared to DSE [53] and lattice [33, 35, 45, 71] results.

Vertices

The ghost-gluon and gluonic vertex dressings are shown in comparison with DSE [53] and lattice [33, 35, 45, 71] results in figure 6.5 and figure 6.6, where the momentum scale was set using the fit parameters from the gluon propagator in the previous section. Similar to the propagators, all dressings converge to unity in the ultraviolet.

Concerning the ghost-gluon vertex dressing, we find that the lattice result has its peak at a higher scale than the dressings computed with functional methods. A similar but, at least in the fRG result less obvious, deviation can be observed already in the ghost propagator dressing, indicating a general scale mismatch between ghost- and glue sector. This is particularly interesting, since also recent

QCD investigations with very sophisticated truncation schemes [24, 28] show such a scale mismatch between the matter sector and the glue part of the theory, whereas the glue sector in itself runs consistently. We think that in both cases, missing higher-order effects are the most likely source of these deviations.

The fRG three-gluon vertex dressing shows very good agreement with the lattice results over all momenta. In particular, the agreement in the infrared is surprising, since the lattice features a decoupling solution, which has a linearly divergent three-gluon vertex dressing function [51, 53, 56], whereas our solution is the scaling solution, which has a stronger divergence in the infrared, $\lambda_{A^3}(p) \propto \left(p^2\right)^{-3\kappa-1/2}$, cf. section 6.3.3. The fRG and DSE four-gluon vertices agree well, whereas lattice measurements of the four-gluon vertex are not available as of now.

6.3.3. Infrared scaling exponents

In the scaling solution, all correlators scale with a specific power law in the infrared. It can be shown that self-consistency demands that the anomalous scaling behaviour of any $(2n + m)$-point function with $2n$ ghost and m gluon legs in d dimensions is determined by one single scaling exponent and can be written as [47, 78, 80]

$$\lim_{p\to 0} \lambda^{(2n,m)}(p) \propto \left(p^2\right)^{(n-m)\kappa+(1-n)\left(\frac{d}{2}-2\right)} .$$ (6.13)

In particular, for the two-point functions, the scaling power laws are then given by [73, 74]

$$\Gamma_{\bar{c}c}(p) \propto p^2 \cdot \left(p^2\right)^{\kappa} ,$$

$$\Gamma_{AA}(p) \propto p^2 \cdot \left(p^2\right)^{-2\kappa+\frac{d}{2}-2} ,$$ (6.14)

where we took their canonical scaling into account. The right panel of figure 6.4 and the left panel of figure 6.5 clearly reveal the power law behaviour. Fitting the propagators with equation (6.14), we obtain the three-dimensional scaling exponents,

$$\kappa_{\text{sym. p.}} = 0.321 \pm 0.001 ,$$

$$\kappa_{\text{full mom.}} = 0.348 \pm 0.013 ,$$

$$\kappa_{\text{sym. p. + tad.}} = 0.349 \pm 0.003 ,$$ (6.15)

for the different truncations. The uncertainty stems from the difference of the ghost and gluon propagator fits. In contrast to the large- and mid-momentum behaviour of the correlators, the scaling coefficient is also susceptible to the full momentum dependence of the vertices.

We also compare these scaling coefficients with those of four-dimensional Yang-Mills theory at finite temperature [29]. There an approximation similar to the symmetric point approximation, (1) in section 6.3.1, was used. Fitting the magnetic part of gluon propagators to the scaling formula equation (6.14) yields $\kappa_T = 0.323(3)$. Hence, the magnetic scaling exponent agrees very well with the scaling exponent of the three-dimensional theory in the approximation (1). This is expected from dimensional reduction, and yields a very consistent picture.

6.4. Conclusion

We have presented non-perturbative correlators of three-dimensional Landau-gauge Yang-Mills theory obtained from first principles with the functional renormalisation group. We have checked the reliability of the results by comparing to lattice results and achieved better agreement by including non-classical tensors structures in the truncation scheme. However, at lower momenta the functional and the lattice results still show a discrepancy of $10\,\%$. This hints at sizeable truncation artefacts in three-dimensional Yang-Mills theory with functional methods at the current truncation level.

These findings are particularly interesting, because an analogous investigation with the fRG in four dimensions shows considerably better agreement with the corresponding lattice results already at a simpler truncation level, based on classical tensor structures only. This indicates that apparent convergence is achieved with less effort in the four-dimensional theory. A possible explanation are the stronger infrared effects that are generically present in lower dimensions. Phrased differently, the three-dimensional theory features a weakened RG irrelevance of the operators corresponding to the non-classical vertex components.

Interestingly, the effects of non-classical tensors seem to cancel largely. Although individual contributions result in large corrections, their overall effect is relatively small but notable. In this work this is explicitly shown in the propagator tadpole contributions, whose overall effect is small, when compared to the individual contributions. A similar observation has also been made in the matter sector of four-dimensional QCD for the effect of non-classical quark-gluon interactions [24, 28]. This finding is particularly important for devising quickly converging truncation schemes by preserving the underlying resummation patterns.

Chapter 7
Conclusion and outlook
7

In this thesis, the method of the t-fRG was further developed to the point where applications are viable. The crucial aspect of causality was discussed throughout the work, which led to properties and identities that simplify computations to a great extent. The framework permits using any reasonable initial action and, subsequently, deriving the necessary flow equations. As a unique feature of the t-fRG, the resulting flows can always be integrated analytically. Thereby, the locality of vertices and flows readily allow for the identification of vanishing and non-vanishing diagrams. Consequently, the derivation of diagrammatic expressions is significantly simplified. For non-vanishing diagrams, the intricacy of occurring θ- and δ-distribution has been dealt with in a systematic way in order to obtain the non-trivial prefactors.

Beyond the diagrammatics, multiple ways on how to solve the time evolution equations have been discussed. A naive approach that is based on ideas from momentum-space fRG has been discarded as handling the regulator numerically turned out to not be feasible. The alternative of using the integrated flow has been successfully used with an integro-differential and integral equation. In particular, numerical computations have been performed for the ϕ^3-theory where a dynamical propagator was considered. In that context, self-similar time evolution was investigated and scaling exponents were determined.

To further establish the formalism of the t-fRG, the ϕ^4-theory was used to discuss renormalisation and equilibrium initial conditions. Furthermore, the integrated flow of the four-point function was investigated in multiple truncations. In that context, the t-fRG was also extended to an N-component scalar field theory. As a result of approximating the four-vertex solely by the s-channel, a $1/N$ expansion was derived.

Lastly, sophisticated truncations in the framework of equilibrium fRG have been investigated for Yang-Mills theory. Such truncations are yet out of reach in the t-fRG. But the insights regarding the convergence of different truncations should proof to be useful on the way to out-of-equilibrium computations.

The development of the t-fRG is mostly complete in view of the concept and technical difficulties. However, some details are rather formal so far. Among these is the inclusion of non-zero background fields. While this should not pose a problem (at least for constant background fields), no numerical study has been performed. The same is true for renormalisation. The obvious candidate for verifying renormalisation in a numerical setup, is the ϕ^4-theory. With those two topics verified, the t-fRG would be applicable to any theory with cubic and quartic interactions. The long term goal is an application to non-Abelian gauge theories.

In this thesis, the focus was on a very general framework, which essentially allows for a system to be prepared with any set of initial correlation functions. The time evolution of the initial system is determined by the truncation. This approach comes at the cost that numerical implementations are computational intensive. Additionally, accurately resolving full correlation functions requires a lot of memory. While a long runtime may be considered as an inconvenience, the memory consumption quickly exceeds available resources on a single computational node (server), so that a distributed memory system is necessary. In order to limit the required resources, the t-fRG may be applied in a more problem-specific way in future work. For example, an application in equilibrium should be possible by demanding equilibrium initial conditions in the time evolution equations. Of course this prevents the use of the explicit solvers from this work, and constitutes a variational problem. Similarly, a scaling ansatz for correlators may be used. However, that approach is vastly different and has to be thoroughly studied. The advantage for a scaling ansatz is that no time evolution is necessary to reach a non-thermal fixed point. The system would be already prepared at a time with self-similar dynamics, and scaling exponents could be determined.

Dyson-Schwinger equations for the ϕ^3-theory

In section 2.2.5, the Dyson-Schwinger equation for the 1PI effective action is derived. The result is the master equation

$$\frac{\delta\Gamma[\phi]}{\delta\phi(x)} = \frac{\delta S[\varphi]}{\delta\varphi(x)}\bigg|_{\varphi=\phi+G\cdot\frac{\delta}{\delta\phi}} . \tag{A.1}$$

Functional derivatives of this equation with respect to the macroscopic field result in the Dyson-Schwinger equations for 1PI n-point functions. As an example, in this chapter, the gap equation for the inverse propagator, i.e. 1PI two-point function, is computed for the ϕ^3-theory.

A.1. Inverse propagator

A theory with only three-point functions at tree-level can be described by a classical action of the form

$$S[\varphi] = \frac{1}{2}\int_{C(z_1,z_2)} S^{(2)}(z_1,z_2)\,\varphi(z_1)\,\varphi(z_2) + \frac{1}{3!}\int_{C(z_1,z_2,z_3)} S^{(3)}(z_1,z_2,z_3)\,\varphi(z_1)\,\varphi(z_2)\,\varphi(z_3) \tag{A.2}$$

where the vertex is assumed to be symmetric under permutations of the arguments. The Dyson-Schwinger equation is obtained in two steps. At first, the variation of the classical action with respect to the field is computed. Using the symmetry of the vertex, this variation reads

$$\frac{\delta S[\varphi]}{\delta\varphi(x_1)} = \int_{C(z_1)} S^{(2)}(x_1,z_1)\,\varphi(z_1) + \frac{1}{2}\int_{C(z_1,z_2)} S^{(3)}(x_1,z_1,z_2)\,\varphi(z_1)\,\varphi(z_2) . \tag{A.3}$$

Figure A.1. Dyson-Schwinger equation for the inverse propagator in the ϕ^3-theory. The solid line with a black dot denotes the free propagator whereas the blue circle (solid outline) denotes the dressed propagator. The vertex with a black dots represent the classical three-point vertex and the green circle (dashed outline) the 1PI three-point function.

This functional has to be evaluated at $\varphi = \phi + G \cdot \frac{\delta}{\delta\phi}$. In a more verbose notation, this means replacing every occurrence of the field with

$$\varphi(x) = \phi(x) + \int_{C(y)} G(x, y)\, \frac{\delta}{\delta\phi(y)} \,. \tag{A.4}$$

It is clear that the rightmost field is simply the macroscopic field. The functional derivative vanishes here. For the other derivatives the identity

$$\frac{\delta}{\delta\phi(y)} G(x_1, x_2) = i \int_{C(z_1, z_2)} G(x_1, z_1)\, \Gamma^{(3)}(z_1, y, z_2)\, G(z_2, x_2) \tag{A.5}$$

is employed. Ultimately, this leads to

$$\frac{\delta\Gamma[\phi]}{\delta\phi(x_1)} = \int_{C(z_1)} S^{(2)}(x_1, z_1)\, \phi(z_1) + \frac{1}{2} \int_{C(z_1, z_2)} S^{(3)}(x_1, z_1, z_2) \Big[\phi(z_1)\, \phi(z_2) + G(z_1, z_2) \Big] . \tag{A.6}$$

The variation of this master equation with respect to the macroscopic field is the gap equation for the inverse propagator. Using again equation (A.5), it is given as

$$\Gamma^{(2)}(x_1, x_2) = S^{(2)}(x_1, x_2) + \int_{C(z_1)} S^{(3)}(x_1, x_2, z_1)\, \phi(z_1)$$

$$+ \frac{i}{2} \int_{C(z_1, z_2, y_1, y_2)} S^{(3)}(x_1, z_1, z_2)\, G(z_1, y_1)\, \Gamma^{(3)}(y_1, x_2, y_2)\, G(y_2, z_2) . \tag{A.7}$$

Figure A.2. Dyson-Schwinger equation for the three-point function in the ϕ^3-theory. The blue circles with solid outline denote the dressed propagator. Black dots represent the classical three-point vertex and the green (dashed outline) and pink (dotted outline) circles the 1PI three- and four-point functions, respectively. 'perm.' refers to the permutation of the external legs at the dressed three-point functions.

This equation is in fact the full Dyson-Schwinger equation for the theory, i.e. no truncation has been employed. See figure A.1 for a graphical representation.

A.2. Three-point function

The gap equation for the inverse propagator depends on the dressed three-point function. It is possible to employ the simplest truncation where $\Gamma^{(3)} = S^{(3)}$. However, in an improved approximation, also the dressed three-point function is considered. In order to obtain the DSE for the three-point function, the functional derivative of equation (A.7) with respect to the macroscopic field is computed. The derivative can either hit a propagator or the 1PI three-point function resulting in

$$\Gamma^{(3)}_{x_1 x_2 x_3} = S^{(3)}_{x_1 x_2 x_3} + \frac{\mathrm{i}}{2} \int\limits_{C(z_1, z_2, y_1, y_2)} S^{(3)}_{x_1 z_1 z_2} \, G_{z_1 y_1} \, \Gamma^{(4)}_{y_1 x_2 x_3 y_2} \, G_{y_2 z_2}$$

$$- \frac{1}{2} \int\limits_{C(z_1, z_2, z_3, z_4, z_5, z_6)} \left\{ S^{(3)}_{x_1 z_1 z_2} \, G_{z_1 z_5} \, \Gamma^{(3)}_{z_5 x_3 z_6} \, G_{z_6 z_3} \, \Gamma^{(3)}_{z_3 x_2 z_4} \, G_{z_4 z_2} + x_2 \leftrightarrow x_3 \right\}, \quad \text{(A.8)}$$

where a condensed notation with arguments as indices is used. The diagrammatic expression for this equation is shown in figure A.2. Here, the four-point function is in general non-vanishing even in ϕ^3-theory since it can be generated using only three-point functions.

Appendix B

Bookkeeping in Keldysh space

B

In section 2.1.4, the propagator on the closed time path is expressed in terms of two real functions on the real time axis: the spectral function and statistical propagator. Only the occurring contour-sign function is actually defined on the time contour. In this form, equations can be simplified to a great extent. Moreover, cancellations on the contour are more evident. In this chapter, identities of integrals on the closed time path are derived, so that they can be expressed as integrals on the real time axis. Furthermore, frequently used expressions like pointwise products and contractions are explicitly given. The latter is then employed to derive time evolution equations for the spectral function and statistical propagator.

B.1. Explicitly contour-time-ordered functions

Analogously to the decomposition of the propagator into statistical two-point function F and spectral function ρ, other two-point functions can be written in this explicitly contour-time-ordered form. For example, the different channels of a four-point vertex can be understood in such a way. The propagator has the form

$$G(x, y) = F(x, y) - \frac{\mathrm{i}}{2} \rho(x, y) \, \mathrm{sgn}_C(x^0 - y^0), \tag{B.1}$$

where F is symmetric and ρ is antisymmetric. Those properties are directly evident due to their definition as the anti-commutator and commutator of two field operators. For other two-point functions, this decomposition is extended to include a local part. Such a generic function then reads

$$A(x, y) = -\mathrm{i} A^{(0)}(x) \, \delta_C(x - y) + A^{(F)}(x, y) - \frac{\mathrm{i}}{2} A^{(\rho)}(x, y) \, \mathrm{sgn}_C(x^0 - y^0). \tag{B.2}$$

The inclusion of a local part is necessary when applying this decomposition to the self-energy. In the style of the propagator, $A^{(F)}$ is meant to be symmetric and $A^{(\rho)}$ anti-symmetric. Any function in the above form with these symmetry properties is called *Keldysh function* within this work.

B.2. Integrals on the closed time path

In the contraction of two Keldysh functions appear integrals over the closed time path, where the integrand depends on the branches of the time contour only in the contour-sign functions. Therefore, identities between the integration on the contour and an integration on the real time axis can be derived. Since spatial integration is not relevant here, all identities are derived in $1 + 0$ dimensions. Spatial integration can be added afterwards. Additionally, each integrand should be understood as also including arbitrary functions that are defined on the real time axis. Those functions do not depend on the branches of the contour and only clutter up the notation.

The first identity is for integrands that do not include any contour-sign function at all. In this case, the forward and backward integrations cancel, and the integral vanishes:

$$\int_{C(a)} = 0. \tag{B.3}$$

Another integral that appears has only one sgn_C-function. When splitting the integral into the forward (C^+) and backward (C^-) branches the contour-sign function can be evaluated. For this purpose, also the cases where the external point is located on the close time path have to be distinguished. For the external point on the forward branch, that is $x^0 \in C^+$, this leads to

$$\int_{C(a)} \mathrm{sgn}_C(x^0 - a^0) = \int_{t_0}^{\infty} \mathrm{d}a^0 \left[\mathrm{sgn}(x^0 - a^0) + 1 \right] = 2 \cdot \int_{t_0}^{\infty} \mathrm{d}a^0 \, \theta(x^0 - a^0). \tag{B.4}$$

The θ-distribution just restricts the integration to times smaller than x^0. Analogously, for $x^0 \in C^-$ the same result is obtained. Hence, no matter where the external point is located, the identity for the integral is

$$\int_{C(a)} \mathrm{sgn}_C(x^0 - a^0) = 2 \cdot \int_{t_0}^{x^0} \mathrm{d}a^0. \tag{B.5}$$

Integrals with two sgn_C-functions in the integrand can be evaluated in a similar way. In this case, there are four distinct combinations where the external points are located on the contour. Examining each case results in

$$\int_{C(a)} \mathrm{sgn}_C(x^0 - a^0) \, \mathrm{sgn}_C(y^0 - a^0)$$

$$= \int_{t_0}^{\infty} \mathrm{d}a^0 \begin{cases} \mathrm{sgn}(x^0 - a^0) \, \mathrm{sgn}(y^0 - a^0) - 1 & \text{if } x, y \in C^+ \\ 1 - \mathrm{sgn}(x^0 - a^0) \, \mathrm{sgn}(y^0 - a^0) & \text{if } x, y \in C^- \\ \mathrm{sgn}(x^0 - a^0) - \mathrm{sgn}(y^0 - a^0) & \text{if } x \in C^+, \ y \in C^- \\ \mathrm{sgn}(y^0 - a^0) - \mathrm{sgn}(x^0 - a^0) & \text{if } x \in C^-, \ y \in C^+ \end{cases}$$

$$= 2 \cdot \int_{x^0}^{y^0} \mathrm{d}a^0 \begin{cases} \mathrm{sgn}(x^0 - y^0) & \text{if } x, y \in C^+ \\ -\mathrm{sgn}(x^0 - y^0) & \text{if } x, y \in C^- \\ -1 & \text{if } x \in C^+, \ y \in C^- \\ 1 & \text{if } x \in C^-, \ y \in C^+ \end{cases}$$

$$= 2 \cdot \mathrm{sgn}_C(x^0 - y^0) \int_{x^0}^{y^0} \mathrm{d}a^0 \,, \tag{B.6}$$

and the same result is obtained for each case. This leads to an identity that expresses the integral over the closed time path in terms of an integration over the real time axis and a contour-sign function outside the integral

$$\int_{C(a)} \mathrm{sgn}_C(x^0 - a^0) \, \mathrm{sgn}_C(y^0 - a^0) = 2 \cdot \mathrm{sgn}_C(x^0 - y^0) \int_{x^0}^{y^0} \mathrm{d}a^0 \,. \tag{B.7}$$

B.3. Pointwise product

Pointwise products of Keldysh functions appear for example in diagrams of the self-energy. Those functions are always the propagator and, therefore, do not have a local part. In this respect, it is sufficient to examine the pointwise product of two Keldysh functions without a local term. Let A and B be two such functions and (AB) the pointwise product. Using the decomposition from equation (B.2)

and expanding the equation, the product reads

$$(A\,B)(x,y) = A^{(F)}(x,y)\,B^{(F)}(x,y) - \frac{1}{4}A^{(\rho)}(x,y)\,B^{(\rho)}(x,y)$$

$$- \frac{\mathrm{i}}{2}\Big(A^{(\rho)}(x,y)\,B^{(F)}(x,y) + A^{(F)}(x,y)\,B^{(\rho)}(x,y)\Big)\,\mathrm{sgn}_C(x^0 - y^0)\,, \quad \text{(B.8)}$$

where the identity $\mathrm{sgn}_C\big(x^0 - y^0\big)^2 = 1$ was used in the first line. The (F)- and (ρ)-parts can be read off, and the pointwise product is summarised as

$$(A\,B)^{(F)}(x,y) = A^{(F)}(x,y)\,B^{(F)}(x,y) - \frac{1}{4}A^{(\rho)}(x,y)\,B^{(\rho)}(x,y)\,,$$

$$(A\,B)^{(\rho)}(x,y) = A^{(\rho)}(x,y)\,B^{(F)}(x,y) + A^{(F)}(x,y)\,B^{(\rho)}(x,y)\,. \quad \text{(B.9)}$$

The (F)- and (ρ)-parts are evidently symmetric and antisymmetric, respectively. Accordingly, the pointwise product of two Keldysh functions (without a local term) is again a Keldysh function. As an example, this identity can be applied to the computation of self-energy diagrams. In the ϕ^3-theory, the one-loop contribution contains

$$(G^2)^{(F)}(x,y) = F(x,y)^2 - \frac{1}{4}\,\rho(x,y)^2\,,$$

$$(G^2)^{(\rho)}(x,y) = 2\,F(x,y)\,\rho(x,y)\,, \quad \text{(B.10)}$$

and in the ϕ^4 theory the two-loop contribution is proportional to

$$(G^3)^{(F)}(x,y) = F(x,y)^3 - \frac{3}{4}F(x,y)\rho(x,y)^2\,,$$

$$(G^3)^{(\rho)}(x,y) = 3\,F(x,y)^2\,\rho(x,y) - \frac{1}{4}\rho(x,y)^3\,. \quad \text{(B.11)}$$

B.4. Contraction

The contraction of two Keldysh functions is especially useful in the derivation of the time evolution equations. Let A and B be two Keldysh functions and $A \cdot B$ a shorthand notation for the contraction

$$(A \cdot B)(x,y) = \int_{C(a)} A(x,a)\,B(a,y)\,. \quad \text{(B.12)}$$

In the following an extra factor of the imaginary unit is used. This choice becomes clear in the result of the contraction when reading off the real and imaginary parts. Inserting the decomposition from equation (B.2) into the definition of the contraction leads to

$$
\mathrm{i}\,(A \cdot B)(x, y) = \mathrm{i} \int_{C(a)} \left\{ \left[-\mathrm{i}\, A^{(0)}(x)\, \delta_C(x-a) + A^{(F)}(x, a) - \frac{\mathrm{i}}{2}\, A^{(\rho)}(x, a)\, \mathrm{sgn}_C(x^0 - a^0) \right] \right.
$$

$$
\left. \times \left[-\mathrm{i}\, B^{(0)}(a)\, \delta_C(a-y) + B^{(F)}(a, y) - \frac{\mathrm{i}}{2}\, B^{(\rho)}(a, y)\, \mathrm{sgn}_C(a^0 - y^0) \right] \right\}. \quad \text{(B.13)}
$$

In total, this expression consists of nine terms. The term containing only the (F)-parts have no dependence on the time contour and vanish due to equation (B.3). Five terms contain a δ-distribution and are easily obtained. For the two terms with one sgn_C-function, the identity (B.5) is utilised to obtain

$$
\frac{1}{2} \int_{C(a)} \left\{ A^{(\rho)}(x, a)\, B^{(F)}(a, y)\, \mathrm{sgn}_C(x^0 - a^0) - A^{(F)}(x, a)\, B^{(\rho)}(a, y)\, \mathrm{sgn}_C(y^0 - a^0) \right\}
$$

$$
= \int_{t_0}^{x^0} \mathrm{d}a^0\, A^{(\rho)}(x, a)\, B^{(F)}(a, y) - \int_{t_0}^{y^0} \mathrm{d}a^0\, A^{(F)}(x, a)\, B^{(\rho)}(a, y). \quad \text{(B.14)}
$$

For the remaining term with two contour-sign functions, the identity (B.7) is used to find

$$
\frac{\mathrm{i}}{4} \int_{C(a)} \left\{ A^{(\rho)}(x, a)\, B^{(\rho)}(a, y)\, \mathrm{sgn}_C(x^0 - a^0)\, \mathrm{sgn}_C(y^0 - a^0) \right\}
$$

$$
= \frac{\mathrm{i}}{2}\, \mathrm{sgn}_C(x^0 - y^0) \int_{x^0}^{y^0} \mathrm{d}a^0\, A^{(\rho)}(x, a)\, B^{(\rho)}(a, y). \quad \text{(B.15)}
$$

Separating the real and imaginary parts leads to the decomposition of the contraction

$$i\,(A \cdot B)^{(0)}(x) = A^{(0)}(x)\,B^{(0)}(x),$$

$$i\,(A \cdot B)^{(F)}(x,y) = A^{(0)}(x)\,B^{(F)}(x,y) + A^{(F)}(x,y)\,B^{(0)}(y)$$

$$+ \int_{t_0}^{x^0} da^0\, A^{(\rho)}(x,a)\,B^{(F)}(a,y)$$

$$- \int_{t_0}^{y^0} da^0\, A^{(F)}(x,a)\,B^{(\rho)}(a,y),$$

$$i\,(A \cdot B)^{(\rho)}(x,y) = A^{(0)}(x)\,B^{(\rho)}(x,y) + A^{(\rho)}(x,y)\,B^{(0)}(y)$$

$$- \int_{x^0}^{y^0} da^0\, A^{(\rho)}(x,a)\,B^{(\rho)}(a,y). \tag{B.16}$$

Evidently, the contraction of two Keldysh functions is, in general, not a Keldysh function itself. It can be brought into the same form, but the demanded symmetry properties are not fulfilled. The contraction of a function with itself, on the other hand, is again a Keldysh function.

B.5. Time evolution equations for the propagator

In this section, the two versions of the time evolution equations from section 3.6.2, namely the differential and integral equations, are given in terms of the spectral function and statistical propagator. For the 1PI n-point functions with $n > 2$, the time evolution is directly given by the integrated flow of the respective correlation function. Contrary, there is no flow equation for the propagator but rather its inverse. The integrated flow of the inverse propagator has been defined as the self-energy in section 3.6.2. This leads to the relation between the *classical* and *full* inverse propagator

$$\Gamma^{(2)}(x,y) = S^{(2)} - i\Sigma(x,y), \tag{B.17}$$

which was the starting point to get both a differential and integral equation for the time evolution of the propagator.

B.5.1. Differential equation

The differential equation has been obtained by explicitly using the classical inverse propagator, leading to the time evolution equation on the closed time path

$$\left(\partial_{x^0}^2 - \nabla_{\mathbf{x}}^2 + m_0^2\right) G(x, y) = -\mathrm{i}\delta_C(x - y) - \mathrm{i} \int_{C(a)} \Sigma(x, a)\, G(a, y). \tag{B.18}$$

On the left hand side, care has to be taken in view of the time derivative since there is a contour-sign function within the propagator. A careful analysis of this term can be circumvented by considering the equation where x and y are on opposite branches of the closed time path. Then the contour-sign function is just a constant. Additionally, the δ_C-distribution on the right hand side drops out. Without loss of generality, let $x^0 \in C^+$ and $y^0 \in C^-$. After writing the integral on the real time axis using equation (B.16) and separating the real and imaginary parts, the time evolution equations for the spectral function and statistical propagator are obtained as

$$\left(\partial_{x^0}^2 - \nabla_{\mathbf{x}}^2 + m_0^2\right) F(x, y) = -\Sigma^{(0)}(x)\, F(x, y) - \int_{t_0}^{x^0} \mathrm{d}a^0\, \Sigma^{(\rho)}(x, a)\, F(a, y)$$

$$+ \int_{t_0}^{y^0} \mathrm{d}a^0\, \Sigma^{(F)}(x, a)\, \rho(a, y),$$

$$\left(\partial_{x^0}^2 - \nabla_{\mathbf{x}}^2 + m_0^2\right) \rho(x, y) = -\Sigma^{(0)}(x)\, \rho(x, y) + \int_{x^0}^{y^0} \mathrm{d}a^0\, \Sigma^{(\rho)}(x, a)\, \rho(a, y). \tag{B.19}$$

B.5.2. Integral equation

For the derivation of the integral equation, no explicit form of the classical inverse propagator was used, but rather its inverse. For non-classical initial conditions the gap equation was also generalised in 3.7. For this general case the time evolution equation on the closed time path is

$$G(x, y) = \bar{G}(x, y) + \int_{C(a, b)} \bar{G}(x, a) \left[\Sigma - \Sigma_{\mathrm{init}}\right](a, b)\, G(b, y). \tag{B.20}$$

Depending on the use case, the initial propagator $\bar{G}$ could be the free propagator G_0, then the initial self-energy is absent. In the following, only the structure

of the equation is of interest. Therefore, the initial self-energy is dropped to simplify the notation, which actually corresponds to the redefinition $\Sigma \to \Sigma + \Sigma_{\text{init}}$. As this time evolution equation only contains two contractions, rewriting it on the real time axis just requires applying the identity (B.16) twice. With $\overline{G}$ and Σ decomposed as in equation (B.2), the time evolution equations are

$$
F(x,y) - \overline{F}(x,y) = -\int_{t_0}^{x^0} \mathrm{d}a^0 \, \bar{\rho}(x,a) \, \Sigma^{(0)}(a) \, F(a,y)
$$

$$
+ \int_{t_0}^{y^0} \mathrm{d}a^0 \, \overline{F}(x,a) \, \Sigma^{(0)}(a) \, \rho(a,y)
$$

$$
+ \int_{t_0}^{x^0} \mathrm{d}a^0 \int_{x^0}^{a^0} \mathrm{d}b^0 \, \bar{\rho}(x,b) \, \Sigma^{(\rho)}(b,a) \, F(a,y)
$$

$$
+ \int_{t_0}^{y^0} \mathrm{d}a^0 \int_{t_0}^{x^0} \mathrm{d}b^0 \, \bar{\rho}(x,b) \, \Sigma^{(F)}(b,a) \, \rho(a,y)
$$

$$
- \int_{t_0}^{y^0} \mathrm{d}a^0 \int_{t_0}^{a^0} \mathrm{d}b^0 \, \overline{F}(x,b) \, \Sigma^{(\rho)}(b,a) \, \rho(a,y) \,,
$$

$$
\rho(x,y) - \bar{\rho}(x,y) = \int_{x^0}^{y^0} \mathrm{d}a^0 \, \bar{\rho}(x,a) \, \Sigma^{(0)}(a) \, \rho(a,y)
$$

$$
- \int_{x^0}^{y^0} \mathrm{d}a^0 \int_{x^0}^{a^0} \mathrm{d}b^0 \, \bar{\rho}(x,b) \, \Sigma^{(\rho)}(b,a) \, \rho(a,y) \,. \tag{B.21}
$$

This appendix provides additional details for numerical computations. In appendix C.1, the time evolution equations are Fourier transformed in the spatial coordinates. Subsequently, those equations are discretised in appendix C.2, leading to explicit solvers for the differential as well as the integral equation. Both solvers are compared in appendix C.3.

C.1. Spatial momentum space

For a numerical implementation, the time evolution equations in position space from appendix B.5 are not particularly well suited. In the differential equation, there are temporal and spatial derivatives, and in the integral form there are two convolutions. A more appropriate choice is to Fourier transform the spatial coordinated, while leaving the temporal coordinates untouched. Assuming spatial translation invariance, this work uses the convention

$$f(x, y) \equiv f(x^0, y^0; \mathbf{x} - \mathbf{y}) = \int_{\mathbf{p}} e^{i(\mathbf{x}-\mathbf{y}) \cdot \mathbf{p}} \, \hat{f}(x^0, y^0; \mathbf{p}) \,, \tag{C.1}$$

where $\int_{\mathbf{p}} = \int_{\mathbb{R}^d} \frac{\mathrm{d}^d \mathbf{p}}{(2\pi)^d}$ in $1 + d$ dimensions. Since there is no transformation in the temporal coordinates, the identities for the time contour that were derived in appendix B are still valid. Due to the spatial translation invariance, rewriting the pointwise product and contraction in position space boils down to using the *convolution theorem*. The pointwise product in position space becomes a convolution in momentum space. Let f and g, be two functions in position space, then

$$\widehat{(fg)}(x^0, y^0; \mathbf{p}) = \int_{\mathbf{q}} f(x^0, y^0; \mathbf{p} - \mathbf{q}) \, g(x^0, y^0; \mathbf{q}) \,, \tag{C.2}$$

where (fg) denotes the pointwise product in position space. A contraction of two translation invariant functions in position space $(f \cdot g)$, on the other hand, is actually a convolution, and becomes a pointwise product in spatial momentum space

$$\widehat{(f \cdot g)}(x^0, y^0; \mathbf{p}) = \int_{C(z^0)} f(x^0, z^0; \mathbf{p}) \, g(x^0, z^0; \mathbf{p}) \,. \tag{C.3}$$

Note that due to the spatial translation invariance, all local parts of Keldysh functions only depend on a single time and not on space. In other words, those functions are momentum independent. In the following, the hat is dropped for functions in spatial Fourier space.

C.1.1. Differential equation

Getting the differential time evolution equations of the propagator in spatial momentum space is straightforward. Starting from equation (B.19), the spatial derivative becomes the momentum and the spatial integration in the contraction is just a product in spatial momentum space. The time integrals stay the same, and the equations are

$$\partial_{x^0}^2 F(x^0, y^0; p) = - \left(p^2 + m_0^2 + \Sigma^{(0)}(x^0) \right) F(x^0, y^0; p)$$

$$- \int_{t_0}^{x^0} \mathrm{d}a^0 \, \Sigma^{(\rho)}(x^0, a^0; p) \, F(a^0, y^0; p)$$

$$+ \int_{t_0}^{y^0} \mathrm{d}a^0 \, \Sigma^{(F)}(x^0, a^0; p) \, \rho(a^0, y^0; p) \,,$$

$$\partial_{x^0}^2 \rho(x^0, y^0; p) = - \left(p^2 + m_0^2 + \Sigma^{(0)}(x^0) \right) \rho(x^0, y^0; p)$$

$$+ \int_{x^0}^{y^0} \mathrm{d}a^0 \, \Sigma^{(\rho)}(x^0, a^0; p) \, \rho(a^0, y^0; p) \,. \tag{C.4}$$

C.1.2. Integral equation

For the integral equation (B.21), the procedure is similar. Again, the contraction in position space becomes a pointwise product in the spatial momenta. The resulting equations are

$$F(x^0, y^0; p) = \bar{F}(x^0, y^0; p)$$

$$- \int_{t_0}^{x^0} \mathrm{d}a^0 \, \bar{\rho}(x^0, a^0; p) \, \Sigma^{(0)}(a^0) \, F(a^0, y^0; p)$$

$$+ \int_{t_0}^{y^0} \mathrm{d}a^0 \, \bar{F}(x^0, a^0; p) \, \Sigma^{(0)}(a^0) \, \rho(a^0, y^0; p)$$

$$+ \int_{t_0}^{x^0} \mathrm{d}a^0 \int_{x^0}^{a^0} \mathrm{d}b^0 \, \bar{\rho}(x^0, b^0; p) \, \Sigma^{(\rho)}(b^0, a^0; p) \, F(a^0, y^0; p)$$

$$+ \int_{t_0}^{y^0} \mathrm{d}a^0 \int_{t_0}^{x^0} \mathrm{d}b^0 \, \bar{\rho}(x^0, b^0; p) \, \Sigma^{(F)}(b^0, a^0; p) \, \rho(a^0, y^0; p)$$

$$- \int_{t_0}^{y^0} \mathrm{d}a^0 \int_{t_0}^{a^0} \mathrm{d}b^0 \, \bar{F}(x^0, b^0; p) \, \Sigma^{(\rho)}(b^0, a^0; p) \, \rho(a^0, y^0; p),$$

$$\rho(x, y) = \bar{\rho}(x^0, y^0; p)$$

$$+ \int_{x^0}^{y^0} \mathrm{d}a^0 \, \bar{\rho}(x, a) \, \Sigma^{(0)}(a) \, \rho(a, y)$$

$$- \int_{x^0}^{y^0} \mathrm{d}a^0 \int_{x^0}^{a^0} \mathrm{d}b^0 \, \bar{\rho}(x, b) \, \Sigma^{(\rho)}(b, a) \, \rho(a, y). \tag{C.5}$$

C.2. Explicit solvers

Both types of time evolution equations can be solved explicitly, which means computing the propagator at a time slice with maximal time $t_{\max}$ only requires knowledge of the propagator and self-energy for times $t < t_{\max}$. This property is

obvious for the differential equation, because any explicit solver for differential equations can be used. For the integral equation, the equations have to be carefully analysed to observe the same property. No matter what equation is used for the time evolution, one time step can be computed for each momentum separately. Therefore, momentum arguments are dropped for a clearer notation. The time is discretised using a linear grid with times

$$t_k = t_0 + k \, \Delta t \,, \quad \text{for } k \geq 0 \,. \tag{C.6}$$

For the statistical propagator on that grid, the time arguments are denoted by indices such that

$$F_{ij} = F(t_i, t_j) \,, \tag{C.7}$$

and analogously for the spectral function and the self-energy. Time integrals on the discretised function can be written as weighted sums. Assuming f is discretised as introduced above, this sum is

$$\int_{t_i}^{t_j} \mathrm{d}a^0 f(a^0) = \sum_{k=i}^{j} w_k(i, j) \, f_k \,, \tag{C.8}$$

where the weights $w_k(i, j)$ depend on the integral limits. For example, the weights for the composite trapezoidal rule are

$$w_k(i, j) = \Delta t \cdot \begin{cases} \frac{1}{2} & \text{for } k = i \text{ or } k = j \\ 1 & \text{else} \,. \end{cases} \tag{C.9}$$

C.2.1. Differential equation

Discretising the differential equation requires to introduce the time derivative on the grid. Here symmetric finite differences are used, such that

$$\partial_t^2 F(t, t') = \frac{1}{(\Delta t)^2} \left[F(t, t') - 2F(t - \Delta t, t') + F(t - 2\Delta t, t') \right] + \mathcal{O}(\Delta t) \,. \tag{C.10}$$

Using this discrete derivative in equation (C.4) and also applying the trapezoidal rule for the time integrals directly leads to an explicit solver for the differential

equation. For a fixed momentum p, and $i, j \geq 2$ it reads

$$F_{ij} = 2F_{i-1,j} - F_{i-2,j} - (\Delta t)^2 \big(p^2 + m_0^2 + \Sigma_{i-1}^{(0)} \big) F_{i-1,j}$$

$$- (\Delta t)^2 \sum_{k=0}^{i-2} w_k(0, i-1) \Sigma_{i-1,k}^{(\rho)} F_{kj}$$

$$+ (\Delta t)^2 \sum_{k=0}^{j-1} w_k(0, j) \Sigma_{i-1,k}^{(F)} \rho_{kj} \, ,$$

$$\rho_{ij} = 2\rho_{i-1,j} - \rho_{i-2,j} - (\Delta t)^2 \big(p^2 + m_0^2 + \Sigma_{i-1}^{(0)} \big) \rho_{i-1,j}$$

$$- \big[j < i - 2 \big] (\Delta t)^3 \sum_{k=j+1}^{i-2} \Sigma_{i-1,k}^{(\rho)} \rho_{kj} \, , \tag{C.11}$$

where $\bar{\rho}_{ii} = \rho_{ii} = \Sigma_{ii}^{(\rho)} = 0$ was used. Additionally, the notation for a conditional term was introduced. It is defined as

$$[a] = \begin{cases} 1 & \text{if } a = \text{true} \\ 0 & \text{if } a = \text{false}. \end{cases} \tag{C.12}$$

While explicitly denoting the conditional term is not necessary, it points out which terms are vanishing and is useful for the implementation of the solver. Let the next time slice to be computed have the index N, then the spectral function only contains correlation functions and the self-energy for indices smaller than N. Hence, the time step is explicit. Subsequently, the entries of the statistical propagator can be explicitly computed for $i = N$ and $j < N$. Finally, the entry F_{NN} can be computed. Note that the symmetry and antisymmetry of the statistical propagator and spectral function, respectively, are used in intermediate steps.

C.2.2. Integral equation

The integral equation is discretised analogously. Without loss of generality, considering the case $x^0 \geq y^0 \geq t_0$, that is $i \geq j \geq 0$, the time evolution equations

are obtained as

$$F_{ij} - \bar{F}_{ij} = -\,[i > 0] \sum_{k=0}^{i-1} w_k(0,i)\,\bar{\rho}_{ik}\,\Sigma_k^{(0)}\,F_{kj}$$

$$+\,[j > 0] \sum_{k=0}^{j-1} w_k(0,j)\,\bar{F}_{ik}\,\Sigma_k^{(0)}\,\rho_{kj}$$

$$-\,[i > 1] \sum_{k=0}^{i-2} \sum_{l=k+1}^{i-1} w_k(0,i)\,w_l(k,i)\,\bar{\rho}_{il}\,\Sigma_{lk}^{(\rho)}\,F_{kj}$$

$$-\,[j > 1] \sum_{k=1}^{j-1} \sum_{l=0}^{k-1} w_k(0,j)\,w_l(0,k)\,\bar{F}_{il}\,\Sigma_{lk}^{(\rho)}\,\rho_{kj}$$

$$+\,[i > 0 \wedge j > 0] \sum_{k=0}^{j-1} \sum_{l=0}^{i-1} w_k(0,j)\,w_l(0,i)\,\bar{\rho}_{il}\,\Sigma_{lk}^{(F)}\,\rho_{kj}\,,$$

$$\rho_{ij} - \bar{\rho}_{ij} = -\,[i > j+1] \sum_{k=j+1}^{i-1} w_k(j,i)\,\bar{\rho}_{ik}\,\Sigma_k^{(0)}\,\rho_{kj}$$

$$-\,[i > j+2] \sum_{k=j+1}^{i-2} \sum_{l=k+1}^{i-1} w_k(j,i)\,w_l(k,i)\,\bar{\rho}_{il}\,\Sigma_{lk}^{(\rho)}\,\rho_{kj}\,, \qquad\text{(C.13)}$$

where again $\bar{\rho}_{ii} = \rho_{ii} = \Sigma_{ii}^{(\rho)} = 0$ was used.

In order that these equations are explicitly solvable, the time on the left hand side must not appear on the right hand side. Otherwise, the time step is implicit and some iterative method has to be employed. To examine one time step, the new time is denoted by t_N. All correlation functions up to that time, i.e. $t < t_N$, are known. Additionally, the spectral function $\bar{\rho}$ and statistical propagator $\bar{F}$, that are the inverse of the initial 1PI two-point function, are known for any time.

Starting with the spectral function in equation (C.13), one can set the index $i = N$ and $j < N$. The latter is just reflects that the spectral function vanishes for

equal times. This leads to

$$\rho_{Nj} - \bar{\rho}_{Nj} = -\left[i > j+1\right] \sum_{k=j+1}^{N-1} w_k(j,i)\, \bar{\rho}_{ik}\, \Sigma_k^{(0)}\, \rho_{kj}$$

$$-\left[i > j+2\right] \sum_{k=j+1}^{N-2} \sum_{l=k+1}^{N-1} w_k(j,i)\, w_l(k,i)\, \bar{\rho}_{il}\, \Sigma_{lk}^{(\rho)}\, \rho_{kj}. \tag{C.14}$$

It is sufficient to look at the indices of summation. Because all summation indices are smaller than $N-1$, the right hand side does not involve the time of the current time step. Even more, only values on the lower triangular matrix of the spectral function are used, and the sequence in which to compute the elements of the time slice is arbitrary. Therefore, the time step of the spectral function is explicit. It also independent from the statistical propagator, which only couples to the equation via the self-energy.

As a consequence, for the statistical propagator in equation (C.13), the spectral function is known up to the time t_N. Setting $i = N$, and looking again at the indices of summation, all terms that include the spectral function pose no problem in view of an explicit time step. The remaining terms are

$$F_{Nj} - \bar{F}_{Nj} = -\left[N > 0\right] \sum_{k=0}^{N-1} w_k(0,N)\, \bar{\rho}_{Nk}\, \Sigma_k^{(0)}\, F_{kj}$$

$$-\left[N > 1\right] \sum_{k=0}^{N-2} \sum_{l=k+1}^{N-1} w_k(0,N)\, w_l(k,N)\, \bar{\rho}_{Nl}\, \Sigma_{lk}^{(\rho)}\, F_{kj}$$

$$+\dots. \tag{C.15}$$

These terms suggest that the order of computation is important. In the case $j < N$ the examination is similar to the previous one for the spectral function. All elements F_{Nj} for $j < N$ can be computed explicitly and in an arbitrary order. The element F_{NN} has to be computed at last, because it involves the previous values of the statistical propagator.

In summary, each time step is explicit. The order of computation is crucial and involves three steps. Let the time of the step correspond to the index N, then the following steps have to be taken:

- Compute the elements ρ_{Nj} with $j = 0..N-1$ of the spectral function in arbitrary order.
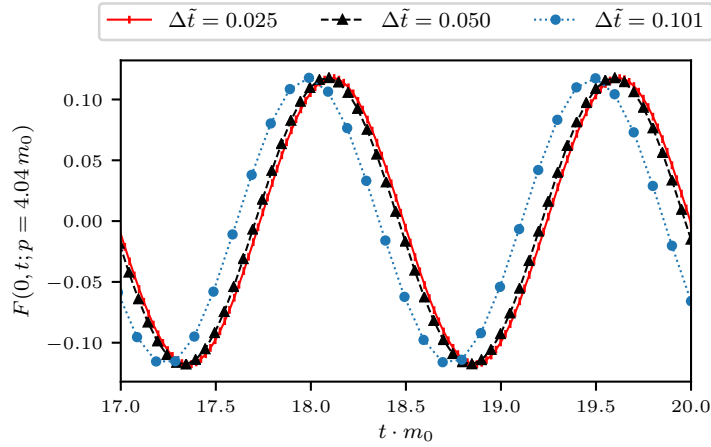
Figure C.1. Time evolution of the statistical propagator obtained using the differential solver for various time resolutions $\Delta \tilde{t} = \Delta t \cdot m_0$. The curves get closer to each other for decreasing time-step size.

- Compute the elements F_{Nj} with $j = 0..N - 1$ of the statistical propagator in arbitrary order.

- Compute the element F_{NN} of the statistical propagator.

The fact that elements can be computed in arbitrary order is emphasised here because it allows for parallel implementations.

C.3. Comparison of solvers

In this section, results obtained from both types of time evolutions are compared. For this purpose, theory, truncation and initial conditions from chapter 4 are used. In figure C.1, the solution for statistical propagator $F(0, t, p = 4.04m_0)$ for three different time-step sizes $\Delta \tilde{t} = \Delta t \cdot m_0$ is shown. For a decreasing step size, the curves get closer to each other and no instabilities are observed for the step sizes used. In figure C.2, the solution of the statistical propagator $F(0, t, p = 4.04m_0)$ that was obtained from the integral equation is shown for the same times as in figure C.1 and the same step sizes. We observe that the curves are perfectly on top of each other for all shown step sizes. Thus, the explicit solver obtained from the discretisation of the integral equation converges faster than the differential one.
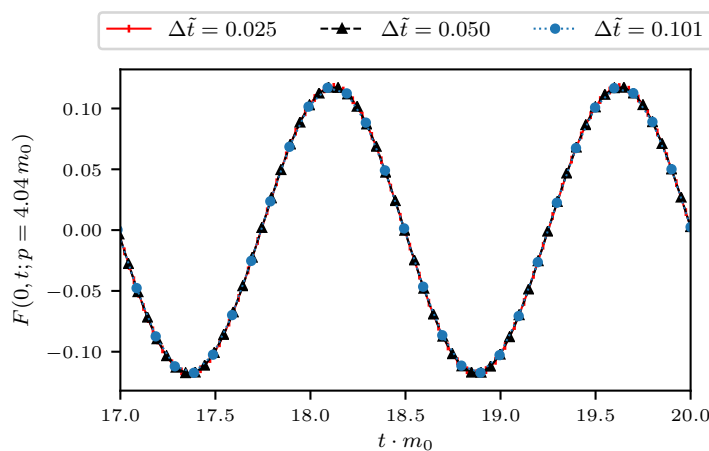
Figure C.2. Time evolution of the statistical propagator obtained using the integral solver for various time resolutions $\Delta \tilde{t} = \Delta t \cdot m_0$. The curves are perfectly on top of each other. This demonstrates the faster convergence of the integral solver as compared to the differential one.

For sufficiently small step sizes, i.e. where the solution apparently already converged, the results from both solvers should agree. For this purpose, the results for the smallest available step size are compared in figure C.3. The solution agree within a small error. The same agreement is obtained comparing the largest step size of the integral solver with the smallest one of the differential solver. Taking a closer look at figure C.3, the black dashed line (differential equation) is still slightly shifted compared to the red one (integral equation). This again demonstrates the faster convergence of the solver using the integral equation.

The faster convergence comes at the price of an additional time integral that has to be computed. However, the differential solver requires a smaller time-step size to produce results of the same accuracy. For the results shown in this section for $\Delta \tilde{t} = 0.025$ for the differential solver and $\Delta \tilde{t} = 0.101$ for the explicit solver, the runtime of both solvers is comparable (same order of magnitude).
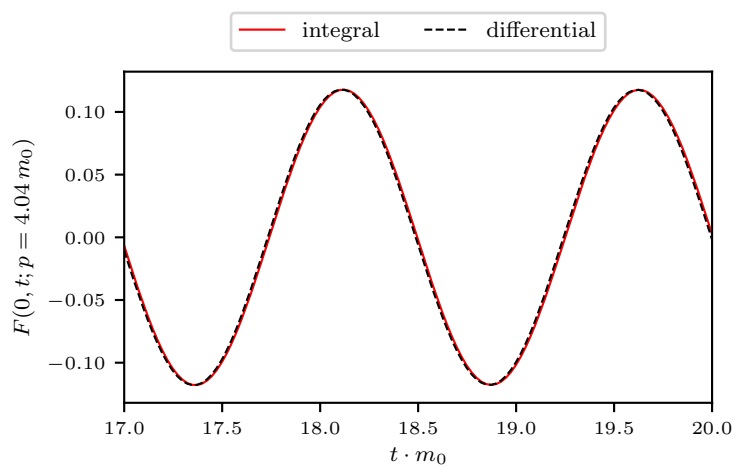
Figure C.3. Time evolution of the statistical propagator obtained using the differential and explicit solver for $\Delta\tilde{t} = \Delta t \cdot m_0 = 0.025$. Both solvers agree for small enough time-step size.

Three-dimensional Yang-Mills theory

In this appendix, numerical results in view of regulator independence in the momentum-space fRG are presented. Additionally, it provides details for the numerical computations in chapter 6, as well as the procedure of scale setting and renormalisation.

D.1. Regulator independence

To check the stability of our results, we repeat the computations above with the flat [83] instead of the exponential regulator shape function. We parametrise the ghost and gluon regulators by

$$R^{ab}(p) = p^2\, \delta^{ab}\, r\left(\frac{p^2}{k^2}\right),$$

$$R^{ab}_{\mu\nu}(p) = p^2\, \delta^{ab}\, \Pi^{\perp}_{\mu\nu}\, r\left(\frac{p^2}{k^2}\right). \tag{D.1}$$

The exponential shape function is given by

$$r_{\exp}(x) = \frac{x^{m-1}}{\exp(x^m) - 1}, \tag{D.2}$$

whereas the flat one is given by

$$r_{\text{flat}}(x) = \left(x^{-1} - 1\right)\cdot \theta\left(x^{-1} - 1\right). \tag{D.3}$$

The dependence of propagator dressings on the regulator shape functions is shown in figure D.1 as relative errors, defined by

$$\Delta^2_{\text{rel}} = 2 \cdot \frac{(\mathcal{O}_{\exp} - \mathcal{O}_{\text{flat}})^2}{\mathcal{O}^2_{\exp} + \mathcal{O}^2_{\text{flat}}}. \tag{D.4}$$
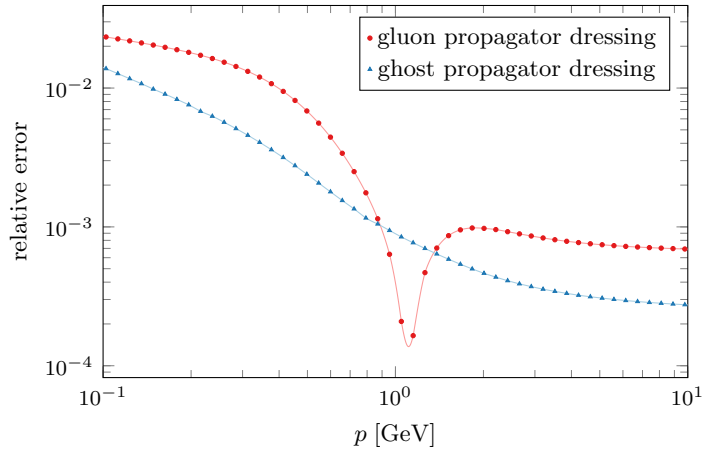
Figure D.1. Relative errors Δ_{rel} of propagator dressings obtained with different regulator shape functions, given in equation (D.2) and equation (D.3), in the symmetric point approximation.

Clearly, the relative errors are well below the percent level in the IR, and even smaller in the mid-momentum and UV regimes that are relevant for hadronic observables. Importantly, the regulator dependence is significantly smaller than the truncation dependence.

Explicitly demonstrating regulator independence is a standard quality and self-consistency check for truncations in the fRG. It is a necessary but not sufficient criterion for the convergence of a given truncation. Indeed, we observe that the dependence of our results on the regulator shape function is negligible although the truncations are not yet converged. Nonetheless, this regulator independence already at low truncation orders is a very welcome property.

D.2. Numerical computation

Landau gauge has the convenient property that the transverse correlation functions close among themselves [27, 84], i.e. correlators with at least one longitudinal leg do not couple back into the transverse subsystem. In the presence of a regulator term, the BRST symmetry is encoded in modified Slavnov-Taylor identities. Their most important consequence is a non-vanishing gluon mass term at finite cutoff scales [85]. Here we present only results for one choice of the gluon mass term, determined uniquely by the scaling solution [73, 74]. The

consequences of other choices for the gluon mass term are qualitatively similar
to YM theory in four space-time dimensions and we refer to the discussion
presented in [27] for details.

This work relies on the workflow established within the fQCD collaboration
[23], see [27] for details. Symbolic flow equations were derived using *DoFun* [86],
traced using *FormTracer* [87], which makes use of *FORM* [88] and its optimization
procedure [89].

D.3. Scale setting and normalisation

For comparison, the DSE and lattice results for the propagators in section 6.3
are normalised in amplitude and momentum scale relative to the fRG results.
To that end we normalise the DSE/lattice gluon dressings with a least squares fit
to the fRG gluon propagator dressing in the range 3 GeV to 6 GeV with

$$\min_{c_A, c_p} \left\{ \sum_{p_{i,\text{lattice}}} \left[c_A Z^{-1}_{A,\text{FRG}}(c_p p_i) - Z^{-1}_{A,\text{lat/DSE}}(p_i) \right]^2 \right\}. \tag{D.5}$$

Here, c_A normalises the amplitude while c_p normalises the momentum scale.
The momentum scale normalisation has to be used for all correlation functions.
Hence it is only left to fix the amplitudes for the other correlation functions. In
particular the amplitude of the ghost propagator dressing is normalised with

$$\min_{c_c} \left\{ \sum_{p_{i,\text{lattice}}} \left[c_c Z^{-1}_{c,\text{FRG}}(c_p p_i) - Z^{-1}_{c,\text{lat/DSE}}(p_i) \right]^2 \right\}. \tag{D.6}$$

The lattice results for the vertices have large statistical lattice errors, and we
refrain from normalising the amplitudes. The dressing of the DSE vertices is
trivial for large momenta.

Danksagung

Bibliography

[1]   L. Corell et al. 'Correlation functions of three-dimensional Yang-Mills theory from the FRG'. *SciPost Phys.* 5.6 (2018), p. 066.
      DOI: 10.21468/SciPostPhys.5.6.066. arXiv: 1803.10092 [hep-ph].

[2]   L. Corell et al. 'Flowing with the Temporal Renormalisation Group' (Oct. 2019). arXiv: 1910.09369 [hep-th].

[3]   J. S. Schwinger. 'Brownian motion of a quantum oscillator'.
      J. Math. Phys. 2 (1961), pp. 407–432. DOI: 10.1063/1.1703727.

[4]   K. T. Mahanthappa.
      'Multiple production of photons in quantum electrodynamics'.
      Phys. Rev. 126 (1962), pp. 329–340. DOI: 10.1103/PhysRev.126.329.

[5]   P. M. Bakshi and K. T. Mahanthappa.
      'Expectation value formalism in quantum field theory. 2.'
      J. Math. Phys. 4 (1963), pp. 12–16. DOI: 10.1063/1.1703879.

[6]   L. V. Keldysh. 'Diagram technique for nonequilibrium processes'.
      Zh. Eksp. Teor. Fiz. 47 (1964), pp. 1515–1527.

[7]   L. Keldysh. 'Diagram technique for nonequilibrium processes'.
      Sov. Phys. JETP 20.4 (1965), p. 1018.

[8]   E. A. Calzetta and B.-L. B. Hu. *Nonequilibrium Quantum Field Theory*.
      Cambridge Monographs on Mathematical Physics.
      Cambridge University Press, 2008. DOI: 10.1017/CBO9780511535123.

[9]   J. Berges.
      'Nonequilibrium Quantum Fields: From Cold Atoms to Cosmology'
      (Mar. 2015). arXiv: 1503.02907 [hep-ph].

[10] J. M. Pawlowski. 'Aspects of the functional renormalisation group'.
      Annals Phys. 322 (2007), pp. 2831–2915.
      DOI: 10.1016/j.aop.2007.01.007.

[11] J.-P. Blaizot, J. M. Pawlowski and U. Reinosa.
      'Exact renormalization group and Φ-derivable approximations'.
      Phys. Lett. B 696 (2011), pp. 523–528.
      DOI: 10.1016/j.physletb.2010.12.058. arXiv: 1009.6048 [hep-ph].

[12]   K. G. Wilson. 'The Renormalization Group: Critical Phenomena and the
        Kondo Problem'. *Rev. Mod. Phys.* 47 (1975), p. 773.
        DOI: 10.1103/RevModPhys.47.773.

[13]   C. Wetterich. 'Exact evolution equation for the effective potential'.
        Phys.Lett. B301 (1993), pp. 90–94. DOI: 10.1016/0370-2693(93)90726-X.

[14]   R. Alkofer and L. von Smekal.
        'The Infrared behavior of QCD Green's functions: Confinement
        dynamical symmetry breaking, and hadrons as relativistic bound states'.
        Phys. Rept. 353 (2001), p. 281. DOI: 10.1016/S0370-1573(01)00010-2.
        arXiv: hep-ph/0007355.

[15]   G. Stefanucci and R. van Leeuwen. *Nonequilibrium Many-Body Theory of
        Quantum Systems: A Modern Introduction.*
        Cambridge University Press, 2013. DOI: 10.1017/CBO9781139023979.

[16]   J. Rammer. *Quantum Field Theory of Non-equilibrium States.*
        Cambridge University Press, 2007. DOI: 10.1017/CBO9780511618956.

[17]   T. Gasenzer and J. M. Pawlowski. 'Towards far-from-equilibrium quantum
        field dynamics: A functional renormalisation-group approach'.
        Phys. Lett. B 670 (2008), pp. 135–140.
        DOI: 10.1016/j.physletb.2008.10.049.
        arXiv: 0710.4627 [cond-mat.other].

[18]   T. Gasenzer, S. Kessler and J. M. Pawlowski.
        'Far-from-equilibrium quantum many-body dynamics'.
        Eur. Phys. J. C 70 (2010), pp. 423–443.
        DOI: 10.1140/epjc/s10052-010-1430-3.
        arXiv: 1003.4163 [cond-mat.quant-gas].

[19]   A. Piñeiro Orioli, K. Boguslavski and J. Berges.
        'Universal self-similar dynamics of relativistic and nonrelativistic field
        theories near nonthermal fixed points'. *Phys. Rev. D* 92.2 (2015), p. 025041.
        DOI: 10.1103/PhysRevD.92.025041. arXiv: 1503.02498 [hep-ph].

[20]   J. Berges and B. Wallisch. 'Nonthermal Fixed Points in Quantum Field
        Theory Beyond the Weak-Coupling Limit'.
        Phys. Rev. D 95.3 (2017), p. 036016. DOI: 10.1103/PhysRevD.95.036016.
        arXiv: 1607.02160 [hep-ph].

[21]   J. Berges. 'Introduction to nonequilibrium quantum field theory'.
        AIP Conf. Proc. 739.1 (2004). Ed. by M. Bracco et al., pp. 3–62.
        DOI: 10.1063/1.1843591. arXiv: hep-ph/0409233.

[22] C.-M. Schmied, A. N. Mikheev and T. Gasenzer.
'Non-thermal fixed points: Universal dynamics far from equilibrium'.
Int. J. Mod. Phys. A 34.29 (2019), p. 1941006.
DOI: 10.1142/S0217751X19410069.
arXiv: 1810.08143 [cond-mat.quant-gas].

[23] fQCD Collaboration. J. Braun, L. Corell, A. K. Cyrol, W.-J. Fu, M. Leonhardt, M. Mitter, J. M. Pawlowski, M. Pospiech, F. Rennecke, C. Schneider, N. Strodthoff, N. Wink.

[24] M. Mitter, J. M. Pawlowski and N. Strodthoff.
'Chiral symmetry breaking in continuum QCD'.
Phys.Rev. D91 (2015), p. 054035. DOI: 10.1103/PhysRevD.91.054035.

[25] J. Braun et al. 'From Quarks and Gluons to Hadrons: Chiral Symmetry Breaking in Dynamical QCD'. *Phys. Rev.* D94.3 (2016), p. 034016.
DOI: 10.1103/PhysRevD.94.034016.

[26] F. Rennecke. 'Vacuum structure of vector mesons in QCD'.
Phys. Rev. D92.7 (2015), p. 076012. DOI: 10.1103/PhysRevD.92.076012.

[27] A. K. Cyrol et al. 'Landau gauge Yang-Mills correlation functions'.
Phys. Rev. D94.5 (2016), p. 054005. DOI: 10.1103/PhysRevD.94.054005.

[28] A. K. Cyrol et al. 'Non-perturbative quark, gluon and meson correlators of unquenched QCD'. *Phys. Rev.* D97.5 (2018), p. 054006.
DOI: 10.1103/PhysRevD.97.054006.

[29] A. K. Cyrol et al. 'Non-perturbative finite-temperature Yang-Mills theory'.
Phys. Rev. D97 (2018), p. 054015. DOI: 10.1103/PhysRevD.97.054015.

[30] A. Cucchieri. 'Infrared behavior of the gluon propagator in lattice Landau gauge: The three-dimensional case'. *Phys. Rev.* D60 (1999), p. 034508.
DOI: 10.1103/PhysRevD.60.034508.

[31] A. Cucchieri, T. Mendes and A. R. Taurines.
'SU(2) Landau gluon propagator on a 140^3 lattice'.
Phys. Rev. D67 (2003), p. 091502. DOI: 10.1103/PhysRevD.67.091502.

[32] A. Cucchieri, T. Mendes and A. R. Taurines.
'Positivity violation for the lattice Landau gluon propagator'.
Phys. Rev. D71 (2005), p. 051902. DOI: 10.1103/PhysRevD.71.051902.

[33] A. Cucchieri, A. Maas and T. Mendes. 'Exploratory study of three-point Green's functions in Landau-gauge Yang-Mills theory'.
Phys. Rev. D74 (2006), p. 014503. DOI: 10.1103/PhysRevD.74.014503.

[34] A. Cucchieri and T. Mendes. 'Constraints on the IR behavior of the gluon propagator in Yang-Mills theories'. *Phys. Rev. Lett.* 100 (2008), p. 241601. DOI: 10.1103/PhysRevLett.100.241601.

[35] A. Cucchieri, A. Maas and T. Mendes. 'Three-point vertices in Landau-gauge Yang-Mills theory'. *Phys. Rev.* D77 (2008), p. 094510. DOI: 10.1103/PhysRevD.77.094510.

[36] A. Cucchieri and T. Mendes. 'Constraints on the IR behavior of the ghost propagator in Yang-Mills theories'. *Phys. Rev.* D78 (2008), p. 094503. DOI: 10.1103/PhysRevD.78.094503.

[37] A. Maas. 'More on Gribov copies and propagators in Landau-gauge Yang-Mills theory'. *Phys.Rev.* D79 (2009), p. 014505. DOI: 10.1103/PhysRevD.79.014505.

[38] A. Cucchieri and T. Mendes. 'Landau-gauge propagators in Yang-Mills theories at beta = 0: massive solution versus conformal scaling'. *Phys. Rev.* D81 (2010), p. 016005. DOI: 10.1103/PhysRevD.81.016005.

[39] A. Maas et al. 'Strong-coupling study of the Gribov ambiguity in lattice Landau gauge'. *Eur.Phys.J.* C68 (2010), pp. 183–195. DOI: 10.1140/epjc/s10052-010-1306-6.

[40] A. Maas. 'On the gauge-algebra dependence of Landau-gauge Yang-Mills propagators'. *JHEP* 1102 (2011), p. 076. DOI: 10.1007/JHEP02(2011)076.

[41] A. Maas. 'Describing gauge bosons at zero and finite temperature'. *Phys.Rept.* 524 (2013), pp. 203–300. DOI: 10.1016/j.physrep.2012.11.002.

[42] A. Cucchieri et al. 'Modeling the Gluon Propagator in Landau Gauge: Lattice Estimates of Pole Masses and Dimension-Two Condensates'. *Phys. Rev.* D85 (2012), p. 094513. DOI: 10.1103/PhysRevD.85.094513.

[43] V. G. Bornyakov, V. K. Mitrjushkin and R. N. Rogalyov. 'Gluon Propagators in 3D SU(2) Theory and Effects of Gribov Copies'. *Phys. Rev.* D86 (2012), p. 114503. DOI: 10.1103/PhysRevD.86.114503.

[44] V. G. Bornyakov, V. K. Mitrjushkin and R. N. Rogalyov. 'Infinite volume and continuum limits for the gluon propagator in 3d SU(2) lattice gauge theory'. *Phys. Rev.* D89.5 (2014), p. 054504. DOI: 10.1103/PhysRevD.89.054504.

[45] A. Maas. 'Some more details of minimal-Landau-gauge SU(2) Yang-Mills propagators'. *Phys. Rev.* D91.3 (2015), p. 034502.
DOI: 10.1103/PhysRevD.91.034502.

[46] A. Cucchieri and T. Mendes. 'Bloch Waves in Minimal Landau Gauge and the Infinite-Volume Limit of Lattice Gauge Theory'.
Phys. Rev. Lett. 118.19 (2017), p. 192002.
DOI: 10.1103/PhysRevLett.118.192002.

[47] M. Q. Huber et al. 'The infrared behavior of Landau gauge Yang-Mills theory in d=2, 3 and 4 dimensions'. *Phys. Lett.* B659 (2008), pp. 434–440.
DOI: 10.1016/j.physletb.2007.10.073.

[48] D. Dudal et al. 'The Landau gauge gluon and ghost propagator in the refined Gribov-Zwanziger framework in 3 dimensions'.
Phys.Rev. D78 (2008), p. 125012. DOI: 10.1103/PhysRevD.78.125012.

[49] R. Alkofer, M. Q. Huber and K. Schwenzer. 'Infrared Behavior of Three-Point Functions in Landau Gauge Yang-Mills Theory'.
Eur. Phys. J. C62 (2009), pp. 761–781.
DOI: 10.1140/epjc/s10052-009-1066-3.

[50] A. C. Aguilar, D. Binosi and J. Papavassiliou.
'Nonperturbative gluon and ghost propagators for d=3 Yang- Mills'.
Phys. Rev. D81 (2010), p. 125025. DOI: 10.1103/PhysRevD.81.125025.

[51] A. Aguilar et al.
'Effects of divergent ghost loops on the Green's functions of QCD'.
Phys.Rev. D89 (2014), p. 085008. DOI: 10.1103/PhysRevD.89.085008.

[52] J. M. Cornwall.
'Exploring dynamical gluon mass generation in three dimensions'.
Phys. Rev. D93.2 (2016), p. 025021. DOI: 10.1103/PhysRevD.93.025021.

[53] M. Q. Huber. 'Correlation functions of three-dimensional Yang-Mills theory from Dyson-Schwinger equations'.
Phys. Rev. D93.8 (2016), p. 085033. DOI: 10.1103/PhysRevD.93.085033.

[54] M. Tissier and N. Wschebor.
'Infrared propagators of Yang-Mills theory from perturbation theory'.
Phys.Rev. D82 (2010), p. 101701. DOI: 10.1103/PhysRevD.82.101701.

[55] M. Tissier and N. Wschebor.
'An Infrared Safe perturbative approach to Yang-Mills correlators'.
Phys. Rev. D84 (2011), p. 045018. DOI: 10.1103/PhysRevD.84.045018.

[56] M. Peláez, M. Tissier and N. Wschebor.
'Three-point correlation functions in Yang-Mills theory'.
Phys.Rev. D88 (2013), p. 125003. DOI: 10.1103/PhysRevD.88.125003.

[57] A. K. Cyrol. 'Non-perturbative QCD correlation functions'.
PhD thesis. Heidelberg U., 2017. DOI: 10.11588/heidok.00023766.
URL: http://doi.org/10.11588/heidok.00023766.

[58] J. Berges, N. Tetradis and C. Wetterich. 'Non-perturbative
renormalization flow in quantum field theory and statistical physics'.
Phys. Rept. 363 (2002), pp. 223–386.
DOI: 10.1016/S0370-1573(01)00098-9.

[59] H. Gies.
'Introduction to the functional RG and applications to gauge theories'.
Lect.Notes Phys. 852 (2012), pp. 287–348.
DOI: 10.1007/978-3-642-27320-9_6.

[60] B.-J. Schaefer and J. Wambach.
'Renormalization group approach towards the QCD phase diagram'.
Phys.Part.Nucl. 39 (2008), pp. 1025–1032.
DOI: 10.1134/S1063779608070083.

[61] J. Braun. 'Fermion Interactions and Universal Behavior in Strongly
Interacting Theories'. *J.Phys.* G39 (2012), p. 033001.
DOI: 10.1088/0954-3899/39/3/033001.

[62] G. Eichmann et al. 'The three-gluon vertex in Landau gauge'.
Phys.Rev. D89 (2014), p. 105014. DOI: 10.1103/PhysRevD.89.105014.

[63] A. K. Cyrol, M. Q. Huber and L. von Smekal.
'A Dyson–Schwinger study of the four-gluon vertex'.
Eur. Phys. J. C75 (2015), p. 102. DOI: 10.1140/epjc/s10052-015-3312-1.

[64] F. Herzog et al.
'The five-loop beta function of Yang-Mills theory with fermions'.
JHEP 02 (2017), p. 090. DOI: 10.1007/JHEP02(2017)090.

[65] A. Cucchieri et al. 'Just how different are SU(2) and SU(3) Landau-gauge
propagators in the IR regime?' *Phys. Rev.* D76 (2007), p. 114507.
DOI: 10.1103/PhysRevD.76.114507.

[66] A. Sternbeck et al.
'Comparing SU(2) to SU(3) gluodynamics on large lattices'.
PoS LAT2007 (2007), p. 340. DOI: 10.22323/1.042.0340.

[67] C. Kellermann and C. S. Fischer. 'The running coupling from the
      four-gluon vertex in Landau gauge Yang-Mills theory'.
      Phys. Rev. D78 (2008), p. 025015. DOI: 10.1103/PhysRevD.78.025015.

[68] D. Binosi, D. Ibáñez and J. Papavassiliou.
      'Nonperturbative study of the four gluon vertex'. *JHEP* 09 (2014), p. 059.
      DOI: 10.1007/JHEP09(2014)059.

[69] J. A. Gracey.
      'Symmetric point quartic gluon vertex and momentum subtraction'.
      Phys. Rev. D90.2 (2014), p. 025011. DOI: 10.1103/PhysRevD.90.025011.

[70] M. Q. Huber. 'On non-primitively divergent vertices of Yang–Mills theory'.
      Eur. Phys. J. C77.11 (2017), p. 733.
      DOI: 10.1140/epjc/s10052-017-5310-y.

[71] A. Maas, in preparation.

[72] L. von Smekal, R. Alkofer and A. Hauck. 'The Infrared behavior of gluon
      and ghost propagators in Landau gauge QCD'.
      Phys. Rev. Lett. 79 (1997), pp. 3591–3594.
      DOI: 10.1103/PhysRevLett.79.3591.

[73] D. Zwanziger.
      'Non-perturbative Landau gauge and infrared critical exponents in QCD'.
      Phys. Rev. D65 (2002), p. 094039. DOI: 10.1103/PhysRevD.65.094039.

[74] C. Lerche and L. von Smekal. 'On the infrared exponent for gluon and
      ghost propagation in Landau gauge QCD'. *Phys. Rev.* D65 (2002), p. 125006.
      DOI: 10.1103/PhysRevD.65.125006.

[75] C. S. Fischer, R. Alkofer and H. Reinhardt. 'The elusiveness of infrared
      critical exponents in Landau gauge Yang-Mills theories'.
      Phys. Rev. D65 (2002), p. 094008. DOI: 10.1103/PhysRevD.65.094008.

[76] J. M. Pawlowski et al.
      'Infrared behavior and fixed points in Landau gauge QCD'.
      Phys.Rev.Lett. 93 (2004), p. 152002.
      DOI: 10.1103/PhysRevLett.93.152002.

[77] R. Alkofer, C. S. Fischer and F. J. Llanes-Estrada. 'Vertex functions and
      infrared fixed point in Landau gauge SU(N) Yang-Mills theory'.
      Phys. Lett. B611 (2005), pp. 279–288.
      DOI: 10.1016/j.physletb.2005.02.043.

[78]   C. S. Fischer and J. M. Pawlowski.
       'Uniqueness of infrared asymptotics in Landau gauge Yang- Mills theory'.
       Phys. Rev. D75 (2007), p. 025012. DOI: 10.1103/PhysRevD.75.025012.

[79]   R. Alkofer, M. Q. Huber and K. Schwenzer.
       'Infrared singularities in Landau gauge Yang-Mills theory'.
       Phys. Rev. D81 (2010), p. 105010. DOI: 10.1103/PhysRevD.81.105010.

[80]   C. S. Fischer and J. M. Pawlowski. 'Uniqueness of infrared asymptotics in
       Landau gauge Yang- Mills theory II'. *Phys. Rev.* D80 (2009), p. 025023.
       DOI: 10.1103/PhysRevD.80.025023.

[81]   A. C. Aguilar, D. Binosi and J. Papavassiliou.
       'Gluon and ghost propagators in the Landau gauge: Deriving lattice
       results from Schwinger-Dyson equations'. *Phys. Rev.* D78 (2008), p. 025010.
       DOI: 10.1103/PhysRevD.78.025010.

[82]   P. Boucaud et al.
       'On the IR behaviour of the Landau-gauge ghost propagator'.
       JHEP 06 (2008), p. 099. DOI: 10.1088/1126-6708/2008/06/099.

[83]   D. F. Litim. 'Optimization of the exact renormalization group'.
       Phys.Lett. B486 (2000), pp. 92–99.
       DOI: 10.1016/S0370-2693(00)00748-6.

[84]   C. S. Fischer, A. Maas and J. M. Pawlowski.
       'On the infrared behavior of Landau gauge Yang-Mills theory'.
       Annals Phys. 324 (2009), pp. 2408–2437.
       DOI: 10.1016/j.aop.2009.07.009.

[85]   U. Ellwanger. 'Flow equations and BRS invariance for Yang-Mills theories'.
       Phys. Lett. B335 (1994), pp. 364–370.
       DOI: 10.1016/0370-2693(94)90365-4.

[86]   M. Q. Huber and J. Braun. 'Algorithmic derivation of functional
       renormalization group equations and Dyson-Schwinger equations'.
       Comput.Phys.Commun. 183 (2012), pp. 1290–1320.
       DOI: 10.1016/j.cpc.2012.01.014.

[87]   A. K. Cyrol, M. Mitter and N. Strodthoff.
       'FormTracer - A Mathematica Tracing Package Using FORM'.
       Comput. Phys. Commun. C219 (2017), pp. 346–352.
       DOI: 10.1016/j.cpc.2017.05.024.

[88]   J. Vermaseren. 'New features of FORM' (2000).

[89] J. Kuipers, T. Ueda and J. A. M. Vermaseren. 'Code Optimization in FORM'. *Comput. Phys. Commun.* 189 (2015), pp. 1–19. DOI: 10.1016/j.cpc.2014.08.008.